Aus der Klinik für Neurologie
der Medizinischen Fakultät Charité – Universitätsmedizin Berlin

DISSERTATION

Magnetresonanztomographische Darstellung neuroinflammatorischer Prozesse in einem Mausmodell der Multiplen Sklerose

zur Erlangung des akademischen Grades
Doctor medicinae (Dr. med.)

vorgelegt der Medizinischen Fakultät
Charité – Universitätsmedizin Berlin

von

Eva-Kristin Würfel, geb. Tysiak

aus Siegen

Gutachter: 1. Prof. Dr. med. K. M. Einhäupl

2. Prof. Dr. med. D. Petersen

3. Prof. Dr. med. J. Gärtner

Datum der Promotion: 04.02.2011

Inhaltsverzeichnis

Zusammenfassung 4

Einleitung und Zielstellung 5

Material und Methoden 6

- Kontrastmittel 6
- Tiermodell 7
- MRT-Messungen 7
- Histologie 8
- Datenanalyse 8

Ergebnisse 9

- EAE-Verlauf nach Transfer PLP-spezifischer T-Zellen 9
- Läsionsverteilung im EAE-Modell 9
- MRT mit Gf im EAE-Modell 10
- MRT mit VSOP im EAE-Modell 11
- MRT nach Transfer von OVA-spezifischen T-Zellen 12

Diskussion 13

Literaturverzeichnis 16

Anteilserklärung. 20

Ausgewählte Publikationen 21

- „Mouse model mimics multiple sclerosis in the clinico-radiological paradox“..... 22
- „Beyond blood brain barrier breakdown – in vivo detection of occult neuroinflammatory foci by magnetic nanoparticles in high field MRI“ 31
- „CNS-irrelevant T-cells enter the brain, cause blood-brain barrier disruption but no glial pathology“ 39

Curriculum vitae 51

Publikationsliste 52

Selbstständigkeitserklärung 54

Danksagung 55

Zusammenfassung

Die kraniale und spinale Bildgebung mittels Magnetresonanztomographie (MRT) hat in den vergangenen Jahren einen zentralen Stellenwert zur Diagnosestellung, Verlaufs- und Therapiekontrolle der Multiplen Sklerose (MS) erlangt. Jedoch besteht trotz hoher Sensitivität der kontrastmittelgestützten MRT bei der Darstellung von entzündlichen Läsionen des zentralen Nervensystems (ZNS) noch immer eine Diskrepanz zwischen den klinischen Symptomen des Patienten und den Befunden der Bildgebung, bekannt als „klinisch-radiologisches Paradox“ der MS.

Zielsetzung dieser Studie war eine differenziertere Visualisierung einzelner Teilaspekte der Pathophysiologie der MS mittels MRT. Dazu wurden in einem Tiermodell für MS, der experimentellen autoimmunen Enzephalomyelitis, zwei experimentelle MRT Kontrastmittel, die paramagnetischen Nanopartikel VSOP und das Gadoliniumderivat Gadofluorin M (Gf), im Vergleich zu dem herkömmlichen Kontrastmittel Gadopentetat-Dimeglumin (Gd-DTPA) untersucht. SJL/J Mäuse wurden nach Transfer von Proteolipid-spezifischen, enzephalitogenen T-Zellen, bzw. Ovalbumin-spezifischen, ZNS-irrelevanten T-Zellen in einer Subgruppe, zu verschiedenen Zeitpunkten während des Krankheitsverlaufs mit einem 7 Tesla Kleintier MRT vor und nach Kontrastmittelgabe untersucht. Die MRT Schnittsequenzen wurden mit konventionell histologischen und immunhistochemisch gefärbten Gewebeschnitten korreliert.

Beide experimentelle Kontrastmittel stellten zusätzliche Läsionen dar, die mit Gd-DTPA nicht detektiert werden konnten. Die Verteilung der Läsionen umfasste das gesamte ZNS und ähnelte dem Läsionsmuster beschrieben bei MS. Gf zeigte sich besonders geeignet für die Visualisierung entzündlicher Hirnnervenveränderungen, z.B. des Nervus opticus. Zudem wurde eine ausgeprägte Kontrastmittelanreicherung im Plexus choroideus und anderen zirkumventrikulären Organen von erkrankten Mäusen festgestellt. VSOP erwies sich ausgesprochen sensitiv in der Darstellung von Bluthirnschrankenveränderungen und fungierte gleichzeitig als zellulärer Marker für aktivierte Makrophagen/Mikroglia.

Durch Anwendung von VSOP und Gf konnten verschiedene zelluläre, parenchymatöse und vaskuläre Veränderungen während einer entzündlichen Erkrankung des zentralen Nervensystems *in vivo* mittels MRT beobachtet werden, die der konventionellen Bildgebung bislang verborgen blieben.

Einleitung und Zielsetzung

Die Multiple Sklerose (MS) ist eine immunvermittelte demyelinisierende Erkrankung des zentralen Nervensystems (ZNS) mit vergleichsweise hoher Prävalenz unter jungen Erwachsenen. Die Erkrankung verläuft überwiegend schubförmig progredient und führt zu bleibenden Behinderungen während des späteren Krankheitsverlaufes [1, 2]. In den vergangenen Jahren wuchs der Stellenwert der Magnetresonanztomographie (MRT) als nicht-invasive Methode zur Diagnosesicherung und Verlaufsbeurteilung der MS. Konventionelle MRT-Techniken wie T2- und T1-gewichtete Sequenzen, letztere auch nach intravenöser Gabe des Kontrastmittels Gadopentetat-Dimeglumin (Gd-DTPA), bewiesen eine hohe Spezifität für die Darstellung fokaler MS-typischer zerebraler und spinaler Läsionen. In Konsequenz wurde die MRT zunehmend berücksichtigt in den Leitlinien zur Diagnosestellung der MS und fand als paraklinisches Messwerkzeug Eingang in Studien zur Erfolgsevaluation neuer Pharmakotherapien [3-6].

Trotz dieser Schlüsselstellung der Bildgebung mittels MRT bei MS besteht eine Diskrepanz zwischen der Läsionslast und der Aktivität einzelner Läsionen im MRT auf der einen Seite und den klinischen Symptomen sowie der Prognose des Patienten auf der anderen Seite, ein Phänomen beschrieben als „klinisch-radiologisches Paradox“ [7]. So bleibt ein Großteil aller in der MRT detektierbaren Läsionen klinisch inapparent [8], während verborgene Krankheitsherde in funktionell relevanten Hirnregionen Ursache lebenseinschränkender Funktionsausfälle für den Patienten sein können.

Damit besteht die Notwendigkeit zur Weiterentwicklung jetziger Bildgebungsmethoden mit dem Ziel, bisher okkulte Pathologie zu detektieren und neue Methoden zur selektiven Darstellung von einzelnen Krankheitskomponenten, wie z.B. der Demyelinisierung oder der Einwanderung von Immunzellen ins ZNS, zu entwickeln. Neben einer besseren Korrelation zum klinischen Erkrankungsgrad erhofft man sich dadurch zusätzlich die Möglichkeit, den Krankheitsverlauf verlässlicher zu prognostizieren, um den individuellen Patienten personalisiert entsprechend seines Risikoprofils beraten und therapieren zu können.

Ein Forschungsschwerpunkt der vergangenen Jahre lag im Bereich der Entwicklung neuer MRT-Kontrastmittel. Während der Einsatz von Gd-DTPA seit längerem Goldstandard zur Darstellung von Bluthirnschrankenstörungen ist und bislang der einzige *in vivo* Marker zur Bestimmung von akuter Krankheitsaktivität war, konnten durch die Verwendung paramagnetischer Nanopartikel erstmals Makrophagen und andere Immunzellen *in vivo* dargestellt werden, mit aussichtsreicher

Evaluation in ersten humanen Studien [7, 9, 10]. Gadofluorin M (Gf), ein chemisch modifiziertes Gadoliniumderivat, wurde im Tiermodell als Kontrastmittel erprobt, um De- und Remyelinisierungsprozesse mittels MRT sichtbar zu machen [11, 12].

In der vorliegenden Arbeit wurden mit Gf und den paramagnetischen Nanopartikeln „very small superparamagnetic iron oxide particles“ (VSOP), zwei neuartige experimentelle MRT-Kontrastmittel in einem Mausmodell für MS, der experimentellen autoimmunen Enzephalomyelitis (EAE), angewendet. Zielsetzung der Arbeit war

1.) die Darstellung der Läsionsverteilung nach Applikation von Gf bzw. VSOP im Vergleich zum herkömmlichen Kontrastmittel Gd-DTPA,
2.) die Identifikation kontrastmittelspezifischer Besonderheiten und eventueller Vorteile für die Visualisierung von Teilaspekten der Pathologie der MS durch Korrelation mit histologischen Untersuchungen und den klinischen Symptomen der Versuchstiere,
3.) sowie die Einsicht in noch ungeklärte Aspekte der Pathophysiologie der EAE bzw. MS durch longitudinale Verlaufsbeobachtungen mittels *in vivo* MRT.

Material und Methoden

Kontrastmittel

Gf (Gadofluorin M, Bayer-Schering AG, Berlin) ist ein amphiphiler Gadoliniumkomplex mit einem Molekulargewicht von ca. 1,53 g/mol, synthetisiert durch Anhängen einer Perfluoroctylkette an eine gadoliniumhaltige Ringstruktur. In wässrigen Lösungen formt es Mizellen und verhält sich daher lipophiler als konventionelles Gd-DTPA. Im Blut wird es vorwiegend proteingebunden transportiert [11, 13]. Für immunfluoreszenzhistologische Untersuchungen wurde Gf gekoppelt mit einem roten Fluoreszenzmarker verwendet (Gf-Cy3.5).
VSOP (very small superparamagnetic iron oxide particels, Ferropharm, Teltow) sind magnetische Nanopartikel mit einer elektrostatisch stabilisierten Zitrathülle. Mit einem Kerndurchmesser von nur 5 nm zeigten sie sich besser geeignet zur Beladung von z.B. Phagozyten als größere, dextranbehüllte Nanopartikel [14].

Tiermodell

Weibliche sechs bis acht Wochen alte SJL/J Mäuse, bezogen von Charles River (Sulzfeld, Deutschland), wurden in einem spezifiziert pathogenfreien Tierstall in klimatisierten Käfigen gehalten mit Futter und Wasser *ad libitum*. Alle Experimente wurden durch das Landesamt für Arbeitsschutz, Gesundheitsschutz und technische Sicherheit, Berlin, genehmigt. Für den Transfer von antigenspezifischen T-Zellen wurden Mäuse immunisiert mit 250 µg Proteolipid Protein (PLP, murines Proteolipid Protein p139-151; Reinheit > 95 %, Pepceutical, Leicester, Groß-Britannien) bzw. Ovalbumin (OVA, Sigma-Aldrich, Hamburg) gelöst in 100 µl Emulsion aus gleichen Anteilen Phosphatpuffers (PBS) und Adjuvants (Complete Freunds Adjuvant, Difco Laboratories Detroit, USA) sowie 4 mg/ml Mycobacterium Tuberculosis H37Ra (Difco Laboratories Detroit, USA) [15]. Nach Ablauf von zehn Tagen wurden die drainierenden Lymphknoten entnommen, die Zellen daraus isoliert und restimuliert mit 12,5 µg/ml PLP oder OVA in Zellkulturmedium (RPMI 1640 supplementiert mit 2 mM L-Glutamin, 100 U/ml Penicillin, 100 µg/ml Streptomycin und 10 % fetalem Kälberserum) für vier Tage bei 37 °C. Die so gewonnenen antigenspezifischen T-Zell-Blasten wurden intraperitoneal in syngene Rezipienten injiziert (8 - 12 x 10^6 Zellen pro Maus).

Die Versuchstiere wurden täglich gewogen und auf EAE Krankheitssymptome hin untersucht nach folgender Stadieneinteilung [15]: 0, nicht betroffen; 1, Reduzierter Schwanztonus oder beeinträchtigter Aufrichtreflex; 2, Paraparese; 3, Paraplegie; 4, Paraplegie mit Schwäche der Vorderpfoten oder komplette Paralyse. Bei einem Stadium > 4 wurden die Tiere euthanasiert.

MRT-Messungen

Die Studien wurden in einem 7 Tesla Kleintier MRT (Pharmascan 70/16AS, Bruker Biospin, Ettlingen) durchgeführt. Die Versuchstiere erhielten eine Inhalationsnarkose mit 1,5 - 2,0 % Isofluran (Forene, Abbot, Wiesbaden) unter Maskenbeatmung mit 100 % O_2 (0,6 l/min) und Überwachung von Respiration und Körpertemperatur (Bio Trig System, SA Instruments, Inc., Stony Brook, USA).

Axiale und koronare T1-gewichtete Sequenzen (MSME; TE 10,5 ms, TR 322 ms, 0,5 mm Schichtdicke, Matrix 256 x 256, field of view (FOV) 2,8 cm, achtfach gemittelt), fettunterdrückte Turbo Spin Echo T2 bzw. protonendichtegewichtete Sequenzen (RARE; TE1 14,5 ms, TE2 65,5 ms, TR 4500 ms, 0,5 mm Schichtdicke, Matrix 256 x 256, FOV 2,8 cm, achtfach gemittelt) und T2*-gewichtete Sequenzen (GEFI; TE 5,6 ms, TR 1200 ms, flip angle 35°, 0,5 mm Schichtdicke, Matrix 256 x 256, FOV 2,8 cm, vierfach gemittelt) wurden vor und

nach intravenöser Kontrastmittelgabe erstellt. Bluthirnschrankenstörungen wurden dargestellt mittels MRT Akquisition unmittelbar nach intravenöser Injektion von 0,2 mmol/kg Körpergewicht Gd-DTPA (Magnevist, Schering AG, Berlin). Bei Nachweis einer Kontrastmittelanreicherung bekamen die Tiere 0,2 mmol/kg Körpergewicht VSOP oder 0,1 mmol/kg Körpergewicht Gf intravenös gespritzt und wurden nach 24 h erneut kernspintomographisch untersucht. Entsprechend spezifischer Fragestellungen wurde dieses Messprotokoll variiert.

Histologie

Für die histologische Aufarbeitung wurden die Mäuse letal narkotisiert (Xylazinhydrochlorid, Rompun 2 %, Bayer, Leverkusen; und Ketamin, CuraMED Pharma, Karlsruhe) und intrakardial perfundiert mit 4 % Paraformaldehyd in PBS. Gehirn und Rückenmark wurden präpariert, dann zur Kryoprotektion in 30 % Sukrose dehydriert und anschließend eingefroren bei -80 °C. Axiale Kryoschnitte wurden Hämatoxylin und Eosin (H&E) gefärbt zur Darstellung entzündlicher Zellinfiltration, oder Berliner Blau gefärbt nach Perls Methode [16], zum Nachweis von VSOP.
Zum immunhistochemischen Nachweis von Makrophagen und Mikroglia wurden weitere Gewebsschnitte mit rabbit anti-IBA-1 Antikörper (1:1000, Wako Chemikalien, Neuss) über Nacht bei 4 °C inkubiert, und anschließend ein Zweitantikörper (anti-rabbit Cy2, Amersham, München) für 1 h bei Raumtemperatur appliziert. Die Schnitte wurden gefärbt mit Hoechst-33258 (Molecular Probes, Leiden, Niederlande) zur Darstellung von Zellkernen, sowie mit Rhodamin Phalloidin (Molecular Probes, Leiden, Niederlande), um vaskuläre Strukturen zu identifizieren. Ausgesuchte Schnitte wurden mittels Fluoreszenzmikroskopie untersucht und digital photographiert (Olympus BX-51, Hamburg).

Datenanalyse

Die MRT Daten wurden manuell koregistriert und Magnetfeldinhomogenitäten korrigiert mit MIPAV 6.1 (Center for Information Technology, National Institutes of Health, Bethesda, MD, USA). Statistische Analysen wurden mit GraphPad Prism 4.0c (GraphPad Software, Inc., San Diego, CA, USA) durchgeführt.

EAE-Verlauf nach Transfer PLP-spezifischer Zellen

Nach Transfer PLP-spezifischer, enzephalitogener T-Zellen entwickelten 29 von 32 untersuchten Mäusen EAE-typische Krankheitssymptome zwischen dem sechsten und dem vierzehnten Tag (Mittelwert 9,55 ± 1,88 Tage Standardabweichung). Die Krankheit verlief unterschiedlich stark progredient mit maximalen EAE Scores von 1 bis 4 (Mittelwert 2,47 ± 1,06) in den verschiedenen Versuchstieren.

Läsionsverteilung im EAE-Modell

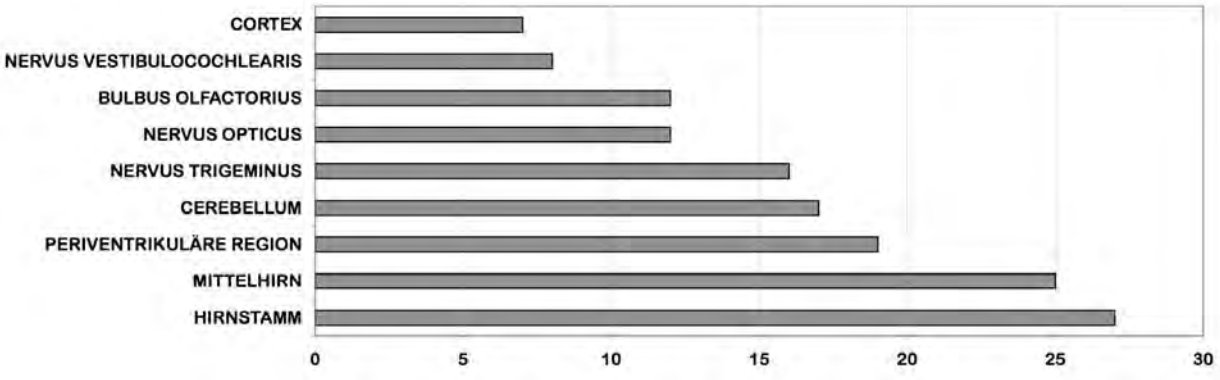

Abbildung 1: Verteilung aller mittels MRT detektierten Läsionen (Gd-DTPA, VSOP und Gf) in 32 EAE Tieren. Identische Läsionen, die mit mehreren Kontrastmitteln dargestellt werden konnten, wurden nur einfach gezählt.

Kontrastmittelanreichernde Läsionen waren zahlreich und in verschiedenen Gehirnregionen nachweisbar (Abb. 1, Publikation 1). Am Häufigsten betroffen war der Hirnstamm gefolgt von Läsionen im Mittelhirn, periventrikulären Arealen und dem Cerebellum. Des Weiteren konnte eine Hirnnervenbeteiligung des Nervus oculomotorius, des Nervus trigeminus, des Nervus vestibulocochlearis bzw. entsprechender Kerngebiete und des Bulbus olfactorius dargestellt werden. In 17 Mäusen kam es zum Übertritt von Kontrastmittel in das Ventrikelsystem.

In zehn Mäusen konnten kontrastmittelanreichernde Läsionen schon vor klinisch manifester Erkrankung detektiert werden. Bei drei Mäusen, die klinisch nicht erkrankten, konnte ein subklinischer Verlauf der EAE durch Nachweis kontrastmittelanreichernder Läsionen mittels MRT gezeigt werden.

MRT mit Gf im EAE-Modell

Kontrastmittelanreicherungen nach Gf erschienen hyperintens in T1-gewichteten Sequenzen mit maximaler Ausprägung nach 24 h. Die Anwendung von Gf erhöhte die Nachweisbarkeit entzündlicher Läsionen im Vergleich zu Gd-DTPA (Abb. 2, Publikation 1). So konnten bei 15 Mäusen, die mit Gd-DTPA und Gf untersucht wurden, 26 von insgesamt 61 Läsionen exklusiv mit Gf dargestellt werden. Besonders die Darstellung inflammatorischer Veränderungen des Nervus opticus und anderer Hirnnerven wurde durch Gf verbessert. In der histologischen Untersuchung zeigte sich 24 h nach Gf Applikation eine diffuse, extrazelluläre Akkumulation von Gf im Gewebe in der Umgebung von entzündlichen Plaques (Abb. 3 A). Nach 72 h konnte die Aufnahme von Gf in Makrophagen/Mikroglia nachgewiesen werden (Abb. 3 B1).

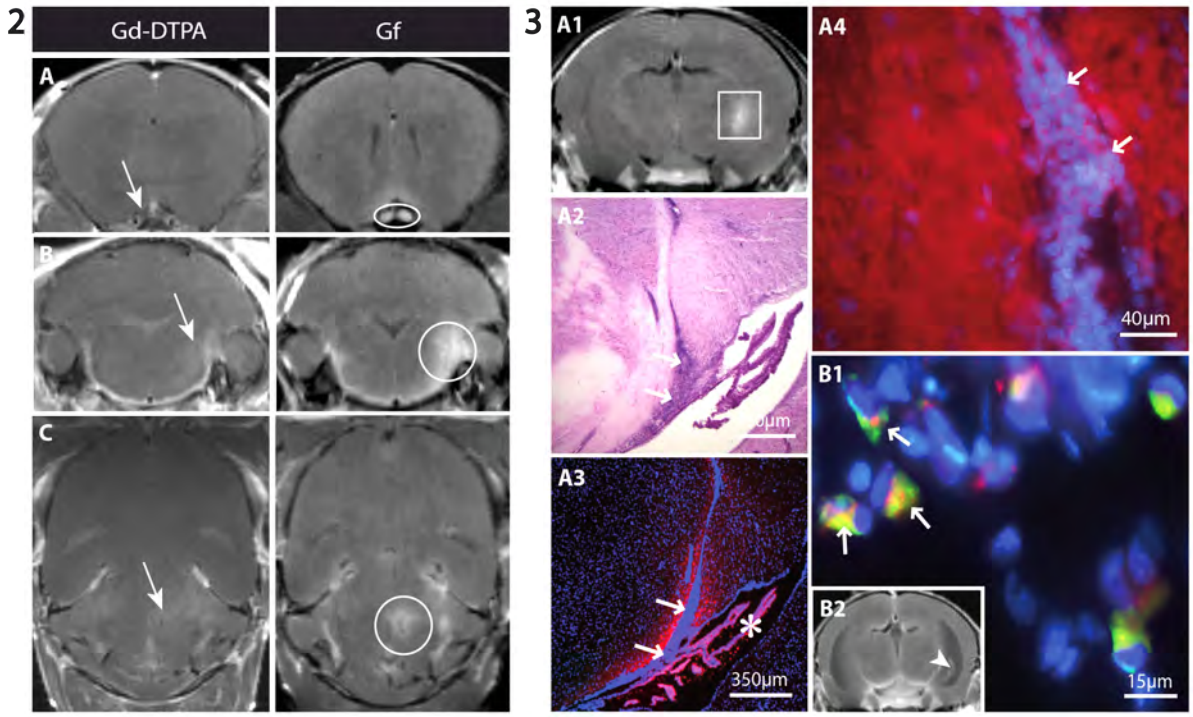

Abbildung 2: Gf verbesserte die Darstellung entzündlicher Läsionen im Verlauf von Hirnnerven (A: Nervus opticus, B: Nervus trigeminus) und zeigte Läsionen, die nach Gd-DTPA Gabe nicht abgrenzbar waren (C: Mittelhirn). Gezeigt sind koronare (A, B) und axiale (C) T1-gewichtete Schnittbilder unmittelbar nach Gd-DTPA Gabe (linke Spalte, Pfeile) und 24 h nach Gf Injektion (rechte Spalte, Kreise).

Abbildung 3: Die Gewebeverteilung von Gf wurde histologisch zu zwei Zeitpunkten untersucht, 24 h (A) und 72 h (B) nach intravenöser Injektion, und mit der Gf Anreicherung in T1-gewichteten MRT-Bildern korreliert (A1, B2). Dargestellt sind entzündliche Zellinfiltrate (Pfeile) in der parahippocampalen Fissur mit diffuser Gf Anreicherung im benachbarten Gewebe (A2: H&E-Färbung; A3, A4: rot → Gf; blau → Hoechst 33258, Zellkerne). Nach 72 h konnte die Inkorporation von Gf in Makrophagen nachgewiesen werden (B1: Plexus choroideus: rot → Gf; grün → IBA-1, Mikroglia/ Makrophagen; blau → Hoechst 33258).

Des Weiteren fiel eine Anreicherung von Gf im Plexus choroideus (Abb. 3 B2) und anderen zirkumventrikulären Organen auf. Eine vergleichende Analyse mit gesunden Kontrollmäusen zeigte, dass die Gf Anreicherung im Plexus choroideus, im subfornikulären Organ der Lamina terminalis sowie in der Area postrema bei EAE Mäusen signifikant gesteigert war ($p < 0,05$) (*Daten noch unveröffentlicht*).

MRT mit VSOP im EAE-Modell

VSOP war unmittelbar nach Injektion im Blutpool nachweisbar und akkumulierte innerhalb von 6 h im Hirngewebe in Regionen mit gestörter Bluthirnschranke mit maximalem Signal nach 24 h. VSOP Anreicherungen erschienen hypointens in T2- und T2*-gewichteten Sequenzen. Durch VSOP Applikation konnten Läsionen dargestellt werden, die mit Gd-DTPA nicht detektiert wurden. In 14 Mäusen, die mit Gd-DTPA und VSOP untersucht wurden, konnten 55 kontrastmittelanreichernde Läsionen gezählt werden, von denen 13 ausschließlich VSOP anreicherten. Insbesondere Läsionen in eher EAE-untypischen Lokalisationen wie im Bereich des Cortex und des Bulbus olfactorius wurden oft nur nach VSOP Gabe dargestellt. Generell waren die Läsionen nach VSOP Gabe besser abgrenzbar im Vergleich zur eher diffusen Gd-DTPA Anreicherung (Abb. 4, Publikation 2).

In den histologischen Untersuchungen konnten mittels Berliner Blau Färbung zwei Verteilungsmuster des Kontrastmittels im Parenchym unterschieden werden (Abb. 5). Die Verteilung im Gewebe korrelierte mit den Kontrastmittelanreicherungen in der MRT. Zum Einen fand sich eine verstreute Anreicherung von VSOP im extrazellulären Gewebe. Des Weiteren ließ sich VSOP intrazellulär mit einer Verteilung nachweisen, die eine vesikuläre Aufnahme und Speicherung der Nanopartikel durch phagozytierende Zellen suggerierte. Diese Zellen entsprachen morphologisch in der Kolokalisation Makrophagen/Mikroglia, die mittels immun-histochemischer Fluoreszenzfärbung identifiziert wurden.

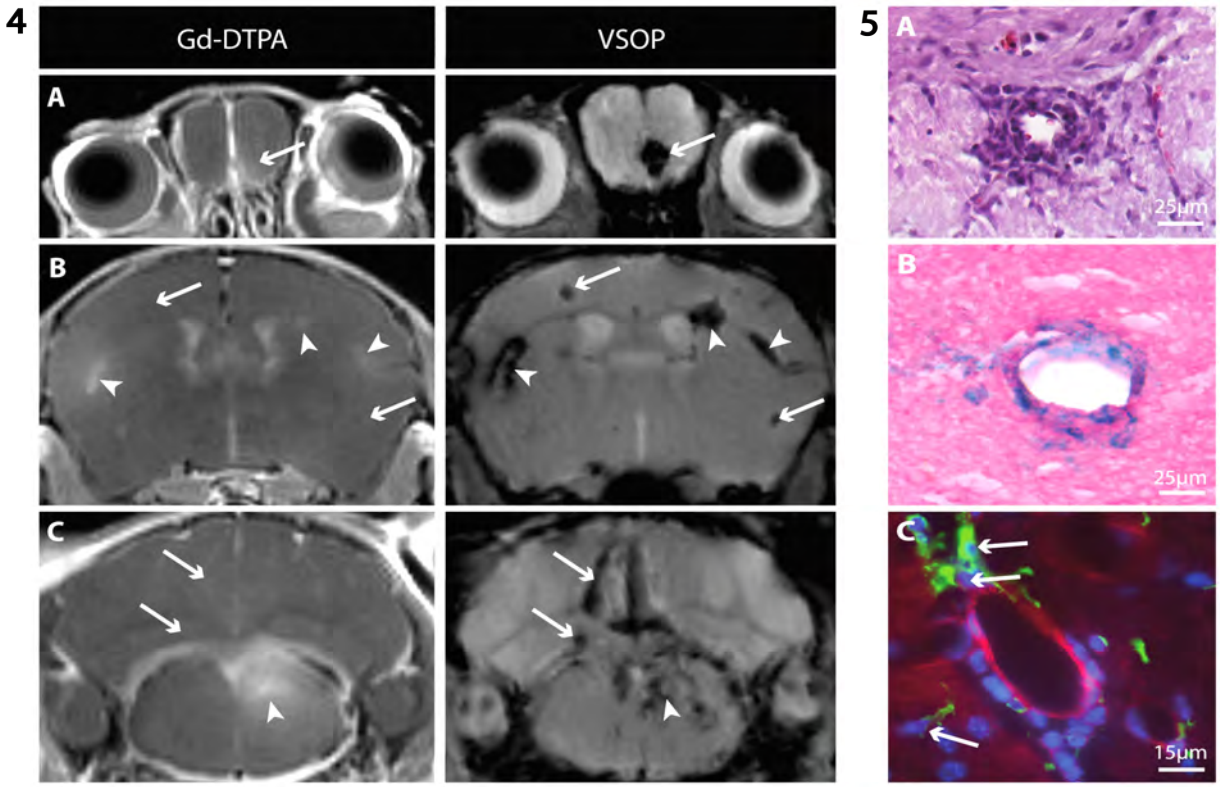

Abbildung 4: VSOP verbesserte den Nachweis entzündlicher Veränderungen im Bulbus olfactorius (A) und die Detektion kortikaler Läsionen (B). Zahlreiche Läsionen konnten nur mit VSOP dargestellt werden und nicht mit Gd-DTPA (A-C, Pfeile) bzw. waren besser abgrenzbar nach VSOP Gabe (Pfeilspitzen). Gezeigt sind koronare T1-gewichtete Schnittbilder unmittelbar nach Gd-DTPA Gabe (linke Spalte) und T2*-gewichtete Bilder 24 h nach VSOP Injektion (rechte Spalte).

Abbildung 5: Darstellung eines EAE-typischen perivaskulären, entzündlichen Plaques mit gesteigerter Extravasation von Immunzellen ins Gewebe (A: H&E-Färbung). In der Berliner Blau Färbung sind intra- und extrazelluläre VSOP-Anreicherungen nachweisbar (B), deren Verteilung kolokalisiert mit immunhistochemisch nachgewiesenen Makrophagen/Mikroglia (C: grün → IBA-1, Mikroglia/Makrophagen; blau → Hoechst 33258, Zellkerne; rot → Rhodamin Phalloidin, vaskuläre Strukturen).

MRT nach Transfer von OVA-spezifischen T-Zellen

Sechs Tiere, die OVA-spezifische und somit nicht-enzephalitogene T-Zellen transferiert bekamen, entwickelten keine EAE-typischen Symptome, sondern blieben während des gesamten Beobachtungszeitraums klinisch gesund. Die Tiere wurden zwischen dem ersten und dem 25. Tag nach T-Zell Transfer mittels MRT vor und nach intravenöser Gabe von Gd-DTPA untersucht (Publikation 3). Es wurden keine intraparenchymatösen Kontrastmittel-anreicherungen gefunden. Jedoch kam es zu einem diffusen, a.e. perivaskulärem Enhancement des Plexus choroideus und anderer zirkumventrikulärer Organe (Abb. 6), deutlich ausgeprägter als bei gesunden Kontrolltieren.

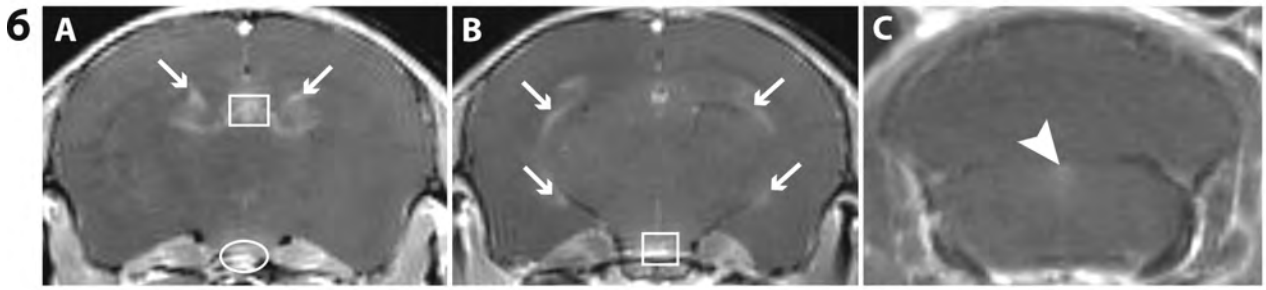

Abbildung 6: Nach Transfer von OVA-spezifischen T-Zellen kam es zu deutlichem Kontrastmittelenhancement im Plexus choroideus (A und B: Pfeile) und weiteren zirkumventrikulären Organen. Dargestellt sind das Subfornikuläre Organ (A, Rechteck), das Organum vasculosum der Lamina terminalis (A, Oval), die Eminencia mediana (B, Quadrat) und die Area postrema (C, Pfeilspitze).

Diskussion

In dieser Arbeit konnten unter Anwendung zweier neuartiger Kontrastmittel, Gf und VSOP, in einem Tiermodell der MS inflammatorische Läsionen magnetresonanztomographisch nachgewiesen werden, die der konventionellen MRT-Bildgebung verborgen blieben. Dies gelang an erster Stelle durch eine sensitivere Detektion von Bluthirnschrankenveränderungen. Zusätzlich wurden weitere entzündungspezifische Korrelate für Kontrastmittelanreicherungen identifiziert, wie eingewanderte Immunzellen sowie Veränderungen der extrazellulären Matrix im Bereich von inflammatorischen Plaques.

EAE, das hier verwendete Tiermodell der MS, geriet in den letzten Jahren als unzureichendes Modellsystem teils unter Kritik, u. a. da in der EAE entwickelte Therapieansätze nur bedingt auf den Menschen übertragbar waren [17, 18]. Die hier durchgeführten MRT Untersuchungen mit sehr guter Bildauflösung durch hohe Magnetfeldstärke unter Verwendung experimenteller Kontrastmittel zeigten zahlreiche pathophysiologische Charakteristika, die die Ähnlichkeit der EAE mit MS unterstreichen. Zum Einen bestätigte sich das „klinisch-radiologische Paradox“ der MS auch in der EAE: Der Nachweis kontrastmittelanreichernder Läsionen erwies sich als sensitiveres Mittel verglichen mit der klinischen Beurteilung der Mäuse, um die Erkrankung nachzuweisen. So wurden in zehn Tieren Läsionen bis zu drei Tage vor Beginn klinischer Symptome detektiert, bzw. die Tiere erkrankten nur subklinisch. Zum Anderen entsprach die

Verteilung der Läsionen in der EAE näher dem Verteilungsmuster bei MS als dies aus früheren histologischen Untersuchungen erwartet wurde. Die entzündlichen Veränderungen bei EAE wurden im klassischen Rattenmodell als „aufsteigend“ beschrieben mit Beginn im lumbalen Rückenmark und weiteren Prädilektionsstellen im höheren Rückenmark und Hirnstamm [19]. In den hier präsentierten MRT Untersuchungen ließen sich jedoch kontrastmittelanreichernde Läsionen weit verteilt im gesamten ZNS nachweisen. Das Rückenmark der Mäuse wurde bei technischen Schwierigkeiten u. a. aufgrund von Atmungsartefakten nicht systematisch in der MRT untersucht.

Interessant hinsichtlich der Parallelität zur MS war die Häufigkeit von Konstrastmittel-anreicherungen von Hirnnerven, insbesondere des Nervus opticus. Die Darstellung dieser profitierte besonders von der Anwendung des Kontrastmittels Gf. So konnten in einer Gruppe von 15 Mäusen, die mit Gd-DTPA und Gf untersucht wurden, 90% aller Läsionen des Nervus opticus, 60% des Nervus vestibulocochlearis und 40% des Nervus trigeminus exklusiv mittels Gf dargestellt werden. Gf bindet an Serumalbumin und Komponenten der extrazellulären Matrix [13]. In verschiedenen Modellen peripherer Nervendegeneration wurde die Eignung von Gf als Marker für De- und Remyelinisierung postuliert [11, 12]. In dieser Studie konnte 24 h nach Gf Injektion eine diffuse, extrazelluläre Anreicherung des Kontrastmittels in der Umgebung von inflammatorischen Plaques nachgewiesen werden. Diese Gewebeakkumulation ist a.e. zurückzuführen auf eine Kontrastmittelextravasation bei geschädigter Bluthirnschranke und anschließende Bindung an Proteine der extrazellulären Matrix, die durch die entzündlichen Degradationsprozesse exponiert werden [20]. Ein direkter Zusammenhang zwischen Demyelinisierung und Gf Anreicherung ließ sich trotz Anwendung verschiedener histologischer Myelinfärbungen nicht belegen. Das Transfer EAE Modell, das in dieser Studie verwendet wurde, weist allerdings bekanntermaßen in der akuten Phase nur geringgradige Demyelinisierungen auf [18].

Neben der sensitiveren Darstellung vieler Läsionen besonders im Verlauf von Hirnnerven fiel eine frühe Anreicherung von Gf im Plexus choroideus sowie anderen zirkumventrikulären Organen auf. Zirkumventrikuläre Organe sind Regionen im ZNS, gelegen entlang des Ventrikelsystems, die sich durch eine physiologisch erhöhte Durchlässigkeit der Bluthirnschranke auszeichnen [21, 22]. Dadurch wird regional ein kontinuierlicher Austausch von Molekülen und Immunzellen zwischen ZNS und dem Blutkreislauf ermöglicht [23]. Innerhalb des Immunprivilegs des ZNS, das sich auszeichnet durch ein restriktives Immunsystem, kommt den zirkumventrikulären Organen somit die Sonderstellung eines „Tors“ zum Gehirn zu. In den MR Untersuchungen nach Gf Gabe zeigte sich in EAE-Mäusen im Vergleich zu gesunden

Kontrollmäusen eine signifikant gesteigerte Kontrastmittelanreicherung im Plexus choroideus, dem Subfornikulären Organ und der Area postrema. Histologisch ließ sich eine Inkorporation von Gf in Makrophagen/Mikroglia nachweisen mit hoher Zelldichte im Plexus choroideus. Interessanterweise kam es auch nach dem Transfer von OVA-spezifischen und somit nicht-enzephalitogenen Zellen zu einer Kontrasmittelanreicherung im Bereich der zirkumventrikulären Organe. Unsere *in vivo* Beobachtungen unterstützen die bisherigen Hinweise für eine Schlüsselstellung der zirkumventrikulären Organe in der Immunregulation des ZNS unter physiologischen [24] und pathologischen Bedingungen [25, 26] und befürworten Folgestudien unter Verwendung von Gf.

Zur Visualisierung von Immunzellen in der MRT wurde in dieser Studie zusätzlich das neuartige paramagnetische Kontrastmittel VSOP verwendet. Paramagnetische Nanopartikel wurden in den vergangenen Jahren vermehrt eingesetzt zur Markierung verschiedener Zelltypen für die MR Bildgebung [27, 28]. Besonders erfolgreich gelang dies für die Darstellung primär phagozytierender Zellen, da diese die Nanopartikel bereitwillig inkorporieren. So konnten im Blutkreislauf zirkulierende Makrophagen u. a. in EAE Studien [29-31] und Tiermodellen für Schlaganfall [32] nach intravenöser Injektion markiert werden und in Folge im ZNS nachgewiesen werden. Die hier verwendeten VSOP unterscheiden sich von herkömmlichen Nanopartikel durch eine elektrostatisch stabilisierte Zitrathülle und einen sehr kleinen Durchmesser von ca. 5 nm [33]. Sie wurden bislang erfolgreich zur Markierung von Stammzellen [34, 35], neuronalen Präkursorzellen [36] und monozytären Zellen [37] eingesetzt. Hier wurden VSOP erstmals zur *in vivo* Markierung von Makrophagen im EAE Modell erprobt. In einer Gruppe von 14 Mäusen, die mit Gd-DTPA und mit VSOP untersucht wurden, ließen sich 13 von 55 Läsionen nur nach VSOP Gabe darstellen. Besonders kleine, kortikale Läsionen und solche im Bereich des Bulbus olfactorius waren besser abgrenzbar mit VSOP. Die Ausbreitung der durch VSOP hervorgerufenen Hypointensitäten war am größten in T2*-gewichteten Sequenzen. Diese sind hochsensitiv für magnetische Suszeptibilitätsveränderungen hervorgerufen durch paramagnetische Nanopartikel [28], was eine mögliche Ursache für die verbesserte Darstellbarkeit kleiner Läsionen im Vergleich zu Gd-DTPA ist. In der histologischen Analyse wurde VSOP sowohl extrazellulär im Parenchym als auch intrazellulär in phagozytierenden Zellen nachgewiesen. Dieses divergente Verteilungsmuster impliziert, dass paragmagnetische Nanopartikel nicht nur wie ursprünglich hypothetisiert nach Inkorporation durch Makrophagen ins ZNS transportiert werden, sondern VSOP aufgrund der kleinen Partikelgröße bei gestörter Bluthirnschranke zusätzlich zellunabhängig im Hirngewebe akkumuliert. Unterstützt wird diese Schlussfolgerung durch Untersuchungen zur Kinetik, mit der sich kontrastmittelanreichernde Läsionen nach VSOP

Injektion ausbreiteten: So konnte schon innerhalb der ersten 6 h nach Kontrastmittelapplikation eine Extravasation und die intraparenchymatöse VSOP Akkumulation beobachtet werden. Diese histologischen und kernspintomographischen Beobachtungen unterscheiden VSOP von herkömmlichen, dextranumhüllten Nanopartikeln, die eine gestörte Bluthirnschranke mutmaßlich nicht überschreiten [29, 31].

Zusammenfassend gelang es in dieser Arbeit, bislang verborgene pathophysiologische Aspekte einer entzündlichen Erkrankung des ZNS mit Hilfe der MRT nicht-invasiv sichtbar zu machen. So konnten Entzündungsprozesse im Verlauf von Hirnnerven mit Gf sensitiv detektiert werden. Des Weiteren zeigten sich Hinweise auf eine immunvermittelnde Funktion der zirkumventrikulären Organe. Anreicherungen der paramagnetische Nanopartikel, VSOP, lagen pathophysiologisch sowohl eingewanderte Makrophagen/Mikroglia als auch Bluthirnschranken-veränderungen zu Grunde. VSOP waren besonders geeignet für die Visualisierung kleiner, kortikaler Läsionen. Die hier mittels MRT gezeigte Läsionsverteilung bestätigt die Relevanz des EAE Modells für die MS Forschung.

Literaturverzeichnis

1 Noseworthy JH, Lucchinetti C, Rodriguez M, Weinshenker BG. Multiple sclerosis. N Engl J Med 2000;343:938-952

2 Trapp BD, Nave KA. Multiple sclerosis: an immune or neurodegenerative disorder? Annu Rev Neurosci 2008;31:247-269

3 Bakshi R, Thompson AJ, Rocca MA et al. MRI in multiple sclerosis: current status and future prospects. Lancet Neurol 2008;7:615-625

4 Rashid W, Miller DH. Recent advances in neuroimaging of multiple sclerosis. Semin Neurol 2008;28:46-55

5 Bar-Zohar D, Agosta F, Goldstaub D, Filippi M. Magnetic resonance imaging metrics and their correlation with clinical outcomes in multiple sclerosis: a review of the literature and future perspectives. Mult Scler 2008;14:719-727

6 Sormani MP, Bonzano L, Roccatagliata L, Cutter GR, Mancardi GL, Bruzzi P. Magnetic resonance imaging as a potential surrogate for relapses in multiple sclerosis: a meta-analytic approach. Ann Neurol 2009;65:268-275

7 Neema M, Stankiewicz J, Arora A, Guss ZD, Bakshi R. MRI in multiple sclerosis: what's inside the toolbox? Neurotherapeutics 2007;4:602-617

8 McFarland HF, Stone LA, Calabresi PA, Maloni H, Bash CN, Frank JA. MRI studies of multiple sclerosis: implications for the natural history of the disease and for monitoring effectiveness of experimental therapies. Mult Scler 1996;2:198-205

9 Dousset V, Brochet B, Deloire MS et al. MR imaging of relapsing multiple sclerosis patients using ultra-small-particle iron oxide and compared with gadolinium. AJNR Am J Neuroradiol 2006;27:1000-1005

10 Vellinga MM, Oude Engberink RD, Seewann A et al. Pluriformity of inflammation in multiple sclerosis shown by ultra-small iron oxide particle enhancement. Brain 2008;131:800-807

11 Bendszus M, Wessig C, Schutz A et al. Assessment of nerve degeneration by gadofluorine M-enhanced magnetic resonance imaging. Ann Neurol 2005;57:388-395

12 Stoll G, Wessig C, Gold R, Bendszus M. Assessment of lesion evolution in experimental autoimmune neuritis by gadofluorine M-enhanced MR neurography. Exp Neurol 2006;197:150-156

13 Meding J, Urich M, Licha K et al. Magnetic resonance imaging of atherosclerosis by targeting extracellular matrix deposition with Gadofluorine M. Contrast Media Mol Imaging 2007;2:120-129

14 Fleige G, Seeberger F, Laux D et al. In vitro characterization of two different ultrasmall iron oxide particles for magnetic resonance cell tracking. Invest Radiol 2002;37:482-488

15 Aktas O, Smorodchenko A, Brocke S et al. Neuronal damage in autoimmune neuroinflammation mediated by the death ligand TRAIL. Neuron 2005;46:421-432

16 Perl DP, Good PF. Comparative techniques for determining cellular iron distribution in brain tissues. Ann Neurol 1992;32 Suppl:S76-81

17 Sriram S, Steiner I. Experimental allergic encephalomyelitis: a misleading model of multiple sclerosis. Ann Neurol 2005;58:939-945

18 Gold R, Linington C, Lassmann H. Understanding pathogenesis and therapy of multiple sclerosis via animal models: 70 years of merits and culprits in experimental autoimmune encephalomyelitis research. Brain 2006;129:1953-1971

19 Oldendorf WH, Towner HF. Blood-brain barrier and DNA changes during the evolution of experimental allergic encephalomyelitis. J Neuropathol Exp Neurol 1974;33:616-631

20 van Horssen J, Bo L, Dijkstra CD, de Vries HE. Extensive extracellular matrix depositions in active multiple sclerosis lesions. Neurobiol Dis 2006;24:484-491

21 Johnson AK, Gross PM. Sensory circumventricular organs and brain homeostatic pathways. Faseb J 1993;7:678-686

22 Ganong WF. Circumventricular organs: definition and role in the regulation of endocrine and autonomic function. Clin Exp Pharmacol Physiol 2000;27:422-427

23 Ransohoff RM, Kivisakk P, Kidd G. Three or more routes for leukocyte migration into the central nervous system. Nat Rev Immunol 2003;3:569-581

24 Kivisakk P, Mahad DJ, Callahan MK et al. Human cerebrospinal fluid central memory CD4+ T cells: evidence for trafficking through choroid plexus and meninges via P-selectin. Proc Natl Acad Sci U S A 2003;100:8389-8394

25 Engelhardt B, Wolburg-Buchholz K, Wolburg H. Involvement of the choroid plexus in central nervous system inflammation. Microsc Res Tech 2001;52:112-129

26 Schulz M, Engelhardt B. The circumventricular organs participate in the immunopathogenesis of experimental autoimmune encephalomyelitis. Cerebrospinal Fluid Res 2005;2:8

27 Arbab AS, Liu W, Frank JA. Cellular magnetic resonance imaging: current status and future prospects. Expert Rev Med Devices 2006;3:427-439

28 Modo M, Hoehn M, Bulte JW. Cellular MR imaging. Mol Imaging 2005;4:143-164

29 Dousset V, Ballarino L, Delalande C et al. Comparison of ultrasmall particles of iron oxide (USPIO)-enhanced T2-weighted, conventional T2-weighted, and gadolinium-enhanced T1-weighted MR images in rats with experimental autoimmune encephalomyelitis. AJNR Am J Neuroradiol 1999;20:223-227

30 Berger C, Hiestand P, Kindler-Baumann D, Rudin M, Rausch M. Analysis of lesion development during acute inflammation and remission in a rat model of experimental autoimmune encephalomyelitis by visualization of macrophage infiltration, demyelination and blood-brain barrier damage. NMR Biomed 2006;19:101-107

31 Floris S, Blezer EL, Schreibelt G et al. Blood-brain barrier permeability and monocyte infiltration in experimental allergic encephalomyelitis: a quantitative MRI study. Brain 2004;127:616-627

32 Rausch M, Baumann D, Neubacher U, Rudin M. In-vivo visualization of phagocytotic cells in rat brains after transient ischemia by USPIO. NMR Biomed 2002;15:278-283

33 Wagner S, Schnorr J, Pilgrimm H, Hamm B, Taupitz M. Monomer-coated very small superparamagnetic iron oxide particles as contrast medium for magnetic resonance imaging: preclinical in vivo characterization. Invest Radiol 2002;37:167-177

34 Heymer A, Haddad D, Weber M et al. Iron oxide labelling of human mesenchymal stem cells in collagen hydrogels for articular cartilage repair. Biomaterials 2008;29:1473-1483

35 Stroh A, Faber C, Neuberger T et al. In vivo detection limits of magnetically labeled embryonic stem cells in the rat brain using high-field (17.6 T) magnetic resonance imaging. Neuroimage 2005;24:635-645

36 Focke A, Schwarz S, Foerschler A et al. Labeling of human neural precursor cells using ferromagnetic nanoparticles. Magn Reson Med 2008;60:1321-1328

37 Stroh A, Zimmer C, Werner N et al. Tracking of systemically administered mononuclear cells in the ischemic brain by high-field magnetic resonance imaging. Neuroimage 2006;33:886-897

Anteilserklärung

Eva-Kristin Würfel, geb. Tysiak, hatte folgenden Anteil an den vorgelegten Publikationen:

Publikation 1: 60 %
E. Tysiak, J. Wuerfel, T. Prozorowski, M. Smyth, S. Mueller, J. Schnorr, M. Taupitz, F. Zipp. Mouse model mimics multiple sclerosis in the clinico-radiological paradox.
European Journal of Neuroscience 2007, Jul; 26(1):190-198.

Beitrag im Einzelnen:
- Durchführung des tierexperimentellen Teils: Induktion des Tiermodells; klinische Beurteilung, Anästhesie und Perfusion der Mäuse.
- Durchführung der Histologie: Organextraktion, Gewebefixierung, Schnitte, konventionelle und immunhistochemische Färbungen.
- Anteilige Durchführung der MRT Messungen.
- Entwurf des Manuskripts, Bildbearbeitung und Statistik.

Publikation 2: 70 %
E. Tysiak, P. Asbach, O. Aktas, H. Waiczies, M. Smyth, J. Schnorr, M. Taupitz, J. Wuerfel. Beyond blood brain barrier breakdown – in vivo detection of occult neuroinflammatory foci by magnetic nanoparticles.
Journal of Neuroinflammation 2009, Aug 6;6:20.

Beitrag im Einzelnen:
- Durchführung des tierexperimentellen Teils: Induktion des Tiermodells; klinische Beurteilung, Anästhesie und Perfusion der Mäuse.
- Durchführung der Histologie: Organextraktion, Gewebefixierung, Schnitte, konventionelle und immunhistochemische Färbungen.
- Anteilige Durchführung der MRT Messungen.
- Entwurf des Manuskripts, Bildbearbeitung und Statistik.

Publikation 3: 20 %
J. Wuerfel, A. Smorodchenko, E. Pohl, J. Vogt, E. Tysiak, R. Glumm, S. Hendrix, R. Nitsch, F. Zipp, C. Infante-Duarte. CNS-irrelevant T cells enter the brain, cause blood-brain barrier disruption but no glial pathology.
European Journal of Neuroscience 2007, Sept; 26(6):1387-98.

Beitrag im Einzelnen:
- Durchführung der quantitativ stereologischen Auswertung der T-Zell Infiltration ins Rückenmark der Modell- und Kontrollmäuse.
- Anteilige Durchführung der MRT Messungen.
- Mitarbeit am Manuskript.

Prof. Dr. Karl Max Einhäupl	Eva-Kristin Würfel
Betreuer der Promotion	Promotionsanwärterin

Ausgewählte Publikationen

1.) E. Tysiak, J. Wuerfel, T. Prozorowski, M. Smyth, S. Mueller, J. Schnorr, M. Taupitz, F. Zipp. Mouse model mimics multiple sclerosis in the clinico-radiological paradox. European Journal of Neuroscience 2007, Jul; 26(1):190-198.

2.) E. Tysiak, P. Asbach, O. Aktas, H. Waiczies, M. Smyth, J. Schnorr, M. Taupitz, J. Wuerfel. Beyond blood brain barrier breakdown – in vivo detection of occult neuroinflammatory foci by magnetic nanoparticles.
Journal of Neuroinflammation 2009, Aug 6;6:20.

3.) J. Wuerfel, A. Smorodchenko, E. Pohl, J. Vogt, E. Tysiak, R. Glumm, S. Hendrix, R. Nitsch, F. Zipp, C. Infante-Duarte. CNS-irrelevant T cells enter the brain, cause blood-brain barrier disruption but no glial pathology.
European Journal of Neuroscience 2007, Sept; 26(6):1387-98.

European Journal of Neuroscience, Vol. 26, pp. 190–198, 2007 doi:10.1111/j.1460-9568.2007.05644.x

Mouse model mimics multiple sclerosis in the clinico-radiological paradox

Jens Wuerfel,[1,*] Eva Tysiak,[1,*] Timour Prozorovski,[1] Maureen Smyth,[1] Susanne Mueller,[2] Joerg Schnorr,[3] Matthias Taupitz[3] and Frauke Zipp[1]
[1]Cecilie-Vogt-Clinic for Molecular Neurology, Charité – University Medicine Berlin, and Max-Delbrueck-Center for Molecular Medicine, Germany
[2]Berlin Neuro Image Center, Charité – University Medicine Berlin, Germany
[3]Department of Radiology, Neuroscience Research Center, Charité – University Medicine Berlin, Germany

Keywords: blood–brain barrier, cranial nerve, EAE, multiple sclerosis

Abstract

The value of experimental autoimmune encephalomyelitis (EAE), an animal model of multiple sclerosis, in deriving novel diagnostic and therapeutic input has been subject to recent debate. This study is the first to report a disseminated distribution of plaques including cranial nerves, prior to or at early stages of disease in murine adoptive transfer EAE, irrespective of the development of clinical symptoms. We induced EAE by adoptive proteolipid protein-specific T-cell transfer in 26 female SJL/J mice, and applied high-field-strength magnetic resonance imaging (MRI) scans longitudinally, assessing blood–brain barrier (BBB) disruption by gadopentate dimeglumine enhancement. We visualized inflammatory nerve injury by gadofluorine M accumulation, and phagocytic cells in inflamed tissue by very small anionic iron oxide particles (VSOP-C184). MRI was correlated with immunohistological sections. In this study, we discovered very early BBB breakdown of white and grey brain matter in 25 mice; one mouse developed exclusively spinal cord inflammation. Widely disseminated contrast-enhancing lesions preceded the onset of disease in 10 animals. Such lesions were present despite the absence of any clinical disease formation in four mice, and coincided with the first detectable symptoms in others. Cranial nerves, predominantly the optic and trigeminal nerves, showed signal intensity changes in nuclei and fascicles of 14 mice. At all sites of MRI lesions we detected cellular infiltrates on corresponding histological sections. The discrepancy between the disease burden visualized by MRI and the extent of disability indeed mimics the human clinico-radiological paradox. MRI should therefore be implemented into evaluational *in vivo* routines of future therapeutic EAE studies.

Introduction

Experimental autoimmune encephalomyelitis (EAE) is an animal model that contributes to our present knowledge of multiple sclerosis (MS), a chronic inflammatory disease of the CNS. Although the precise sequence of events leading to plaque formation is not completely understood, either in the human disease or in EAE, the disruption of the blood–brain barrier (BBB) is seen as a critical stage in the evolution of brain lesions (McFarland *et al*., 1992; Wuerfel *et al*., 2004). The focal inability of the BBB to protect the CNS by preventing intravascular macromolar substances from entering the brain parenchyma can be visualized with gadopentate dimeglumine (Gd-DTPA)-enhanced magnetic resonance imaging (MRI), which is today's gold standard for defining disease activity in patients with MS paraclinically. However, BBB disruption does not necessarily reflect clinical disability. As early as 1868, J.M. Charcot noted a discrepancy between the visible pathology and the clinical symptoms reported by an individual patient (Charcot, 1868), a phenomenon described today as the clinico-radiological paradox with respect to MRI-detectable lesions (Barkhof, 2002). To further elucidate the pathomechanism, that leads to acute BBB breakdown and drives inflammation, *in vivo* studies with histopathological correlations are necessary. These can be investigated in animal models, but are not accessible to human *post mortem* studies that display a single time point only (Nijeholt *et al*., 2001). EAE has proven to be a valuable tool in understanding T-cell-mediated immune damage of the CNS, and the model has led directly to the development of therapies approved for use in MS today. Nevertheless, the merits and demerits of EAE research have recently been subject to heated debate (Sriram & Steiner, 2005; Gold *et al*., 2006; Steinman & Zamvil, 2006). Although MRI is more sensitive in detecting disease severity compared with clinical examination, which in rodents predominantly assesses spinal cord pathology, in the past *in vivo* MR studies of the animal model were hampered by technical limitations such as insufficient spatial resolution. The development of high-resolution MR sequences using high-magnetic-field strength in dedicated rodent scanner systems prompted us to systematically investigate the kinetics of BBB breakdown in SJL/J mice after transfer of pathogenic T-cells, a model for diagnostic as well as therapeutic strategies in MS (Aktas *et al*., 2005). Different MR contrast agents were applied to visualize BBB disruption, nerve injury and phagocytic cells in inflammatory plaques *in vivo*. Imaging results were confirmed by consecutive immunohistochemical and conventional histological evaluation.

Correspondence: Dr F. Zipp, as above.
E-mail: frauke.zipp@charite.de

*J.W. and E.T. contributed equally to this work.

Received 28 February 2007, revised 17 May 2007, accepted 21 May 2007

Materials and methods

Induction of EAE

Female SJL/J mice, 6–8 weeks old, were purchased from Charles River (Sulzfeld, Germany) and kept in a climate-controlled room, housed in sawdust-lined cages, receiving standard rodent chow and water *ad libitum*. All experiments were approved by the local animal welfare committee and conformed to the European Communities Council Directive (86/609/EEC). For adoptive transfer of murine proteolipid peptide (PLP; p139–151; purity >95%, Pepceuticals, Leicester, UK)-specific T-cells, mice were immunized subcutaneously (s.c.) with 250 μg PLP in 100 μL emulsion containing equal volumes of phosphate-buffered saline (PBS), complete Freunds adjuvant (Difco Laboratories, Detroit, USA) and 4 mg/mL mycobacterium tuberculosis H37Ra (Difco Laboratories), as previously described (Aktas *et al*., 2005). Animals were killed by cervical dislocation. On Day 10, draining lymph nodes were isolated and immune cells were restimulated with PLP (12.5 μg/mL) in cell culture medium (RPMI 1640 supplemented with 2 mM L-glutamine, 100 U/mL penicillin, 100 μg/mL streptomycin and 10% foetal calf serum) for 4 days at 37 °C. T-cell blasts ($8–12 \times 10^6$ cells/mouse) were injected intraperitoneally into 26 syngenic recipients. Activity and antigen specificity of injected cells were routinely monitored by proliferation assays (^{3}H-thymidine), and surface expression of CD25, CD44 and CD69 by

TABLE 1. MR contrast enhancement preceded the development of clinical symptoms in 10 mice

			MRI signs: Gd-DTPA enhancement (BBB breakdown)						
Mouse	Onset of MRI signs (days)*	Clinical onset (days)*	BS	MB	PV	CB	CN	CO	Score†
1	8	11	+		+	+	+	+	1
2	12	13		+		+	+	+	1
3	10	11	+	+	+		+		1
4	8	9	+		+		+		2
5	9	10	+	+	+	+	+		1
6	13	ND	+	+	+			+	0
7	14	ND					+		0
8	13	ND	+	+	+				0
9	9	13		+	+	+	+		2
10	9	ND	+	+	+				0
Mean	10.5	11.2							1.3

A widespread contrast leakage distribution was observed in the depicted regions (+). *Times of onset after immunization (days) of the BBB breakdown and of the first clinical signs are given. †Score, EAE score at disease onset. BS, brainstem; MB, midbrain; PV, periventricular area; CB, cerebellum; CN, cranial nerve; CO, cortex; ND, no detectable clinical symptoms up to end of study.

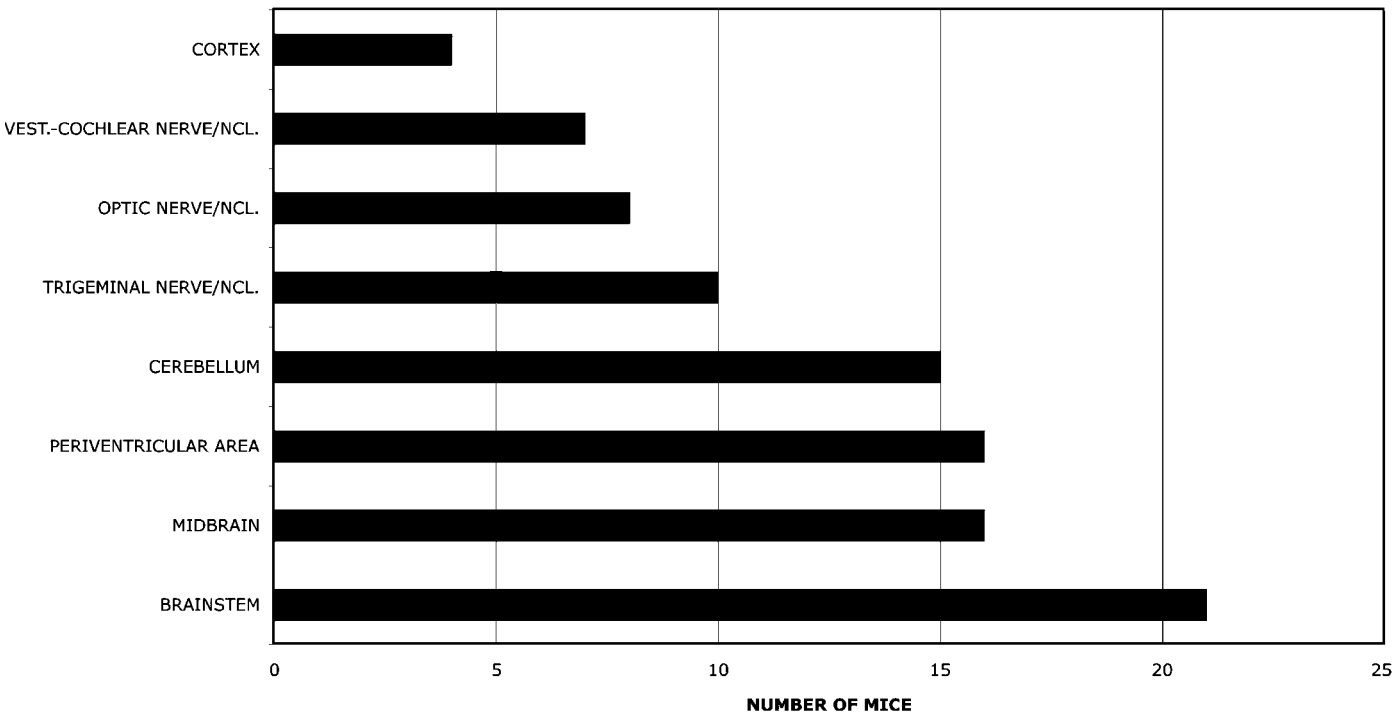

FIG. 1. Lesion distribution in 25 SJL/J EAE mice. Besides common lesion sites, e.g. brain stem and midbrain, we detected frequent cerebellar and cranial nerve involvement. Lesions that were taken into account typically had a size of 0.5–3 mm in diameter on MR images.

flow cytometry (BD Bioscience Pharmingen, Heidelberg, Germany), as reported elsewhere (Nitsch *et al.*, 2004).

Mice were weighed and scored for EAE daily as previously described (Aktas *et al.*, 2003): 0, unaffected; 1, tail weakness or impaired righting on attempt to roll over; 2, paraparesis; 3, paraplegia; 4, paraplegia with forelimb weakness or complete paralysis; score > 4, to be killed. Mice with a score of 4 received an intraperitoneal injection of 200 μL glucose (5%) daily.

MR imaging and analysis

Animals underwent MRI scans of the brain between 5 and 16 days after transfer of encephalitogenic T-cells. MRI was performed using a 7 Tesla rodent scanner (Pharmascan 70/16AS, Bruker BioSpin, Ettlingen, Germany) and a 20 mm RF-Quadrature-Volume head coil. Mice were placed on a heated circulating water blanket to ensure constant body temperature of 37 °C. Anaesthesia was induced with 3% and maintained with 1.5–2.0% isoflurane (Forene, Abbot, Wiesbaden, Germany) delivered in 0.6 L/min of 100% O_2 via a cemask under constant ventilation monitoring (Bio Trig System, SA Instruments, Stony Brook, New York, USA).

Axial and coronal T1-weighted [SME; TE 10.5 ms, TR 322 ms, 0.5 mm slice thickness, matrix 256 × 256, field of view (FOV) 2.8 cm, eight averages, 40 coronal slices, scan time 22 min, and 20 axial slices, scan time 16 min] fat-suppressed turbo spin echo T2-weighted (RARE; TE1 14.5 ms, TE2 65.5 ms, TR 4500 ms, 0.5 mm slice thickness, matrix 256 × 256, FOV 2.8 cm, eight averages, 40 coronal slices, scan time 28 min, and 20 axial slices, scan time 28 min) and T2*-weighted (GEFI; TE 5.6 ms, TR 1200 ms, flip angle 35 °, 0.5 mm slice thickness, matrix 256 × 256, FOV 2.8 cm, four averages, 40 coronal slices, scan time 20 min, and 20 axial slices, scan time 13 min) images were acquired before and after intravenous (i.v.) administration of contrast agent. Mice were investigated daily for BBB leakage directly after injection of 0.2 mmol/kg bodyweight Gd-DTPA (Magnevist, Schering AG, Berlin, Germany). If BBB breakdown was detected, we either applied 0.1 mmol/kg bodyweight gadofluorine M (Gf, Gd-GlyMe-DOTA-perfluorooctyl-mannose-conjugate; kindly provided by Drs M. Reinhardt and B. Misselwitz, Schering AG; Bendszus *et al.*, 2005) or 0.2 mmol/kg bodyweight very small iron oxide particle (VSOP)-C184 (VSOP, Ferropharm, Teltow, Germany; Fleige *et al.*, 2002). Out of 25 mice initially presenting with Gd-DTPA enhancement, 15 were immediately followed-up with Gf and five with VSOP. A subgroup of five animals was investigated after Gf injection and additionally with VSOP 24 h later. Because Gd-DTPA is quickly eliminated from the blood pool, it does not confound Gf-

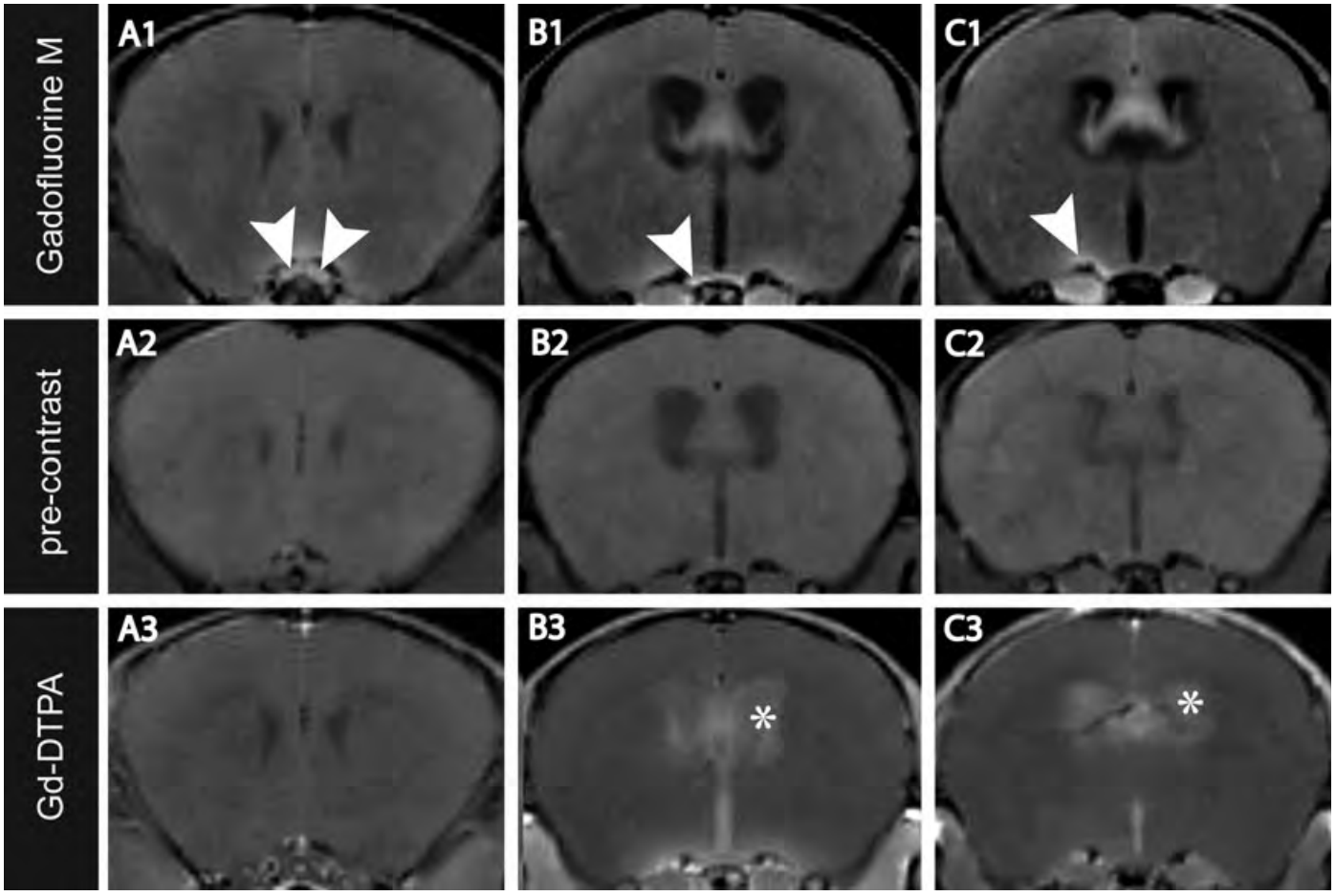

FIG. 2. Inflammation of the optic nerve could be observed in eight animals after gadofluorine M (Gf) or gadopentate dimeglumine (Gd-DTPA) application. Corresponding coronal T1-weighted images of three animals are given (A–C) after Gf enhancement (row 1); pre-contrast images (row 2) and Gd-DTPA-enhanced images (row 3) are shown for comparison. Gf accumulated in the optic nerve (A1), the optic chiasm (B1) or the optic tract (C1), and resulted in bright contrast enhancement (arrowheads). Enhancement after Gd-DTPA application was less pronounced (A3, B3) or absent (C3). Leakage of Gd-DTPA into the cerebrospinal fluid became visible in some animals (*, B3, C3).

or VSOP-enhanced signalling. On the other hand, to rule out iron oxide-related signal changes in T1, gadolinium-based imaging always preceded VSOP-enhanced investigations.

Gf is an amphiphilic gadolinium complex that forms large micelles in water and binds strongly to hydrophobic sites on proteins. It was recently reported to enable the detection of peripheral nerve inflammation and degeneration (Bendszus & Stoll, 2005). VSOP are novel electrostatically monomer-coated iron oxide nanoparticles with a hydrodynamic diameter of only 7 nm, that were originally designed for blood pool contrast (Taupitz *et al*., 2004). Their ability to label mononuclear cells was shown by Stroh *et al*. (2006). Identical slice positions were used for all sequences applied: coronal slices were aligned to the olfactory bulb/frontal lobe fissure and covered the entire brain up to the cervical spinal cord. Axial slices were positioned parallel to a plane through the most frontal tip of the olfactory bulb and the most rostral cerebellar part.

MRI data were analysed using the MEDx3.4.3 software package (Medical Numerics, Virginia, USA) on a LINUX workstation.

Histology

For histological analysis, mice were lethally anaesthetized (xylazin-hydrochloride, Rompun 2%, Bayer, Leverkusen, Germany, and ketamine, CuraMED Pharma, Karlsruhe, Germany) and intracardially perfused with 0.1 M PBS and fixed in 4% paraformaldehyde (PFA) in 0.1 M PBS. Brain and spinal cord were removed and postfixed in 4% PFA. The tissue was then dehydrated in 30% sucrose for cryoprotection and stored at −80 °C. Axial cryosections (Jung cryostat 2800 Frigocut-E, Cambridge Instruments, Nussloch, Germany) of the entire brain were stained either by standard haematoxylin and eosin (H&E) procedure (20 μm slice thickness) or by Prussian Blue staining according to Perl's method (Perl & Good, 1992) to detect VSOP C-184 (40 μm slice thickness). H&E staining was used to grade inflammation.

Immunohistochemistry

For further characterization of microglia/macrophages, 10 μm tissue sections were incubated with rabbit anti-IBA-1 antibodies (1 : 1000, Wako Chemicals, Neuss, Germany) in PBS overnight at 4 °C after preincubation in 10% normal goat serum (CALTAG, Invitrogen, Karlsruhe, Germany) to block non-specific binding, and then with a secondary antibody (anti-rabbit Cy2, Amersham, Muenchen, Germany) for 1 h at room temperature. Additionally, slices were counterstained with Hoechst-33258 (Molecular Probes, Leiden, the Netherlands) to visualize cell nuclei, and with rhodamine phalloidin (Molecular Probes) to identify vascular structures. Finally, all slices were washed three times in PBS and cover-sealed with fluorescence mounting medium (DAKO Deutschland GmbH, Germany). Images were taken with a filter (U-MNIBA, Olympus BX-51 microscope, Hamburg, Germany) using an Olympus digital camera. Images were assembled using Adobe Photoshop (Adobe Systems, San Jose, CA, USA).

Results

BBB breakdown precedes clinical development of EAE

After adoptive T-cell transfer, 22 of 26 immunized mice developed clinical signs of EAE. The first symptoms arose at Day 6, and progressed to an EAE score of 2.7 (1–4) at the peak of the disease. Clinical onset was typically preceded by loss of 10% bodyweight. In these 22 mice, disease started with a loss of tail tonus and/or impaired righting reflex. Animals were killed for histological analysis before clinical remission within 2–5 days after disease onset.

Lesion development was assessed by the presence of Gd-DTPA, Gf or VSOP in the brain parenchyma before, directly after and 24 h post-systemic contrast agent application. On MR images, lesions typically appeared at a size of 0.5–3 mm in diameter. Twenty-five animals developed intracranial lesions. In 10 animals, these preceded the first clinical signs of disease for 1–3 days, or were detectable despite the absence of neurological symptoms (Table 1). In the other mice, the initial detection of BBB breakdown coincided with clinical symptoms. Only one animal did not develop supraspinal contrast enhancement

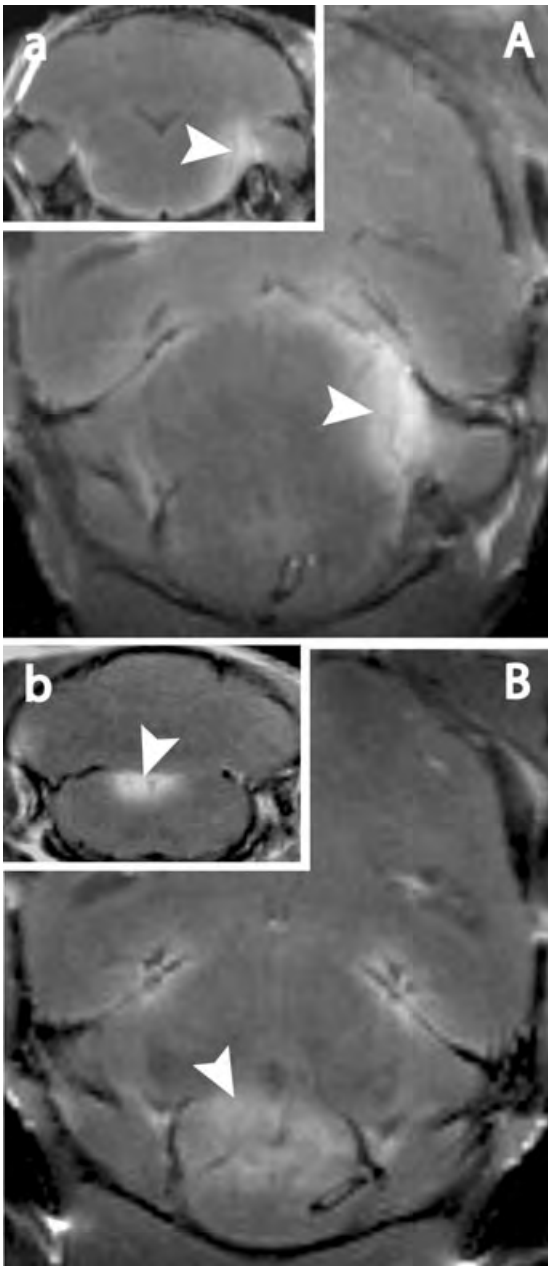

FIG. 3. Inflammation of cranial nerve fascicles and nuclei was a frequent finding. Axial (A, B) and coronal (a, b) T1-weighted images are presented post-Gf application. Contrast enhancement is visible at the left trigeminal nerve fascicle (A, a) and in the area of the vestibulo-cochlear nuclei (B, b).

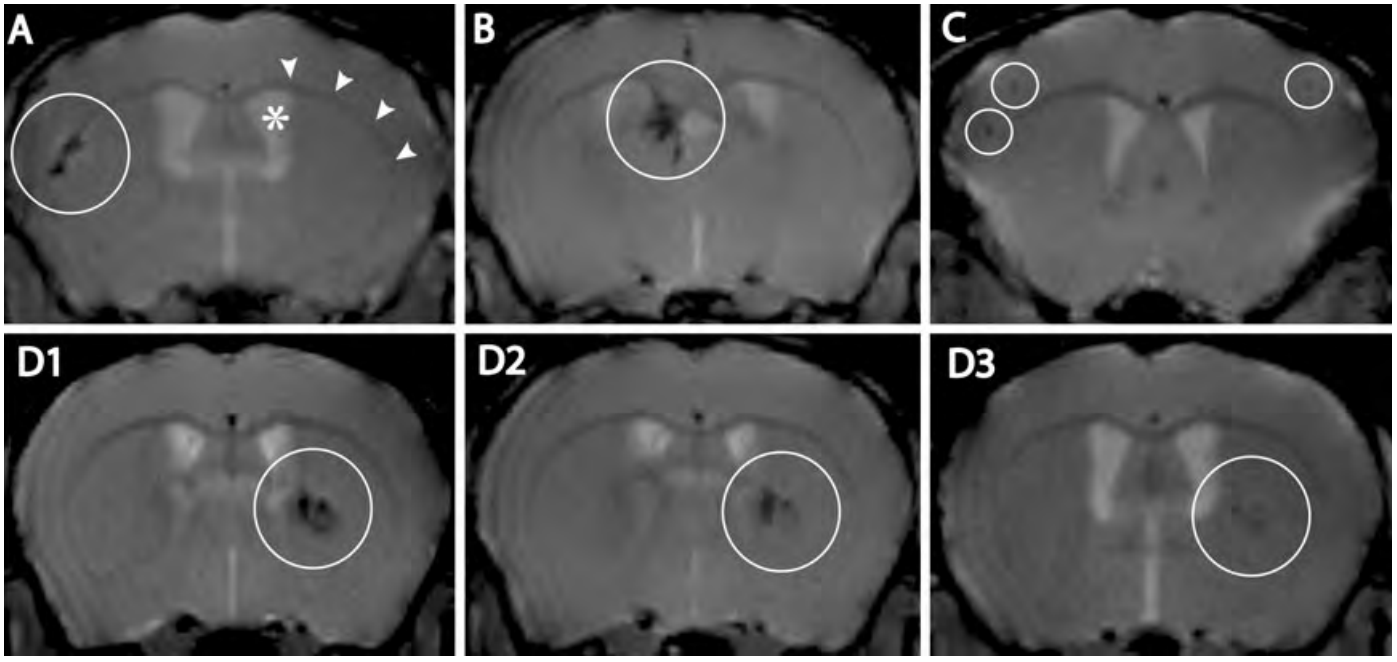

FIG. 4. Coronal T2*-weighted images 24 h post-VSOP administration. Marked signal extinctions are shown in the corpus callosum (A), in the periventricular white matter (B, D) and the cortex (C), all of which are lesion sites also common in MS. A typical time course of VSOP T2* signal extinction is depicted in (D) (D1: 6 h post-application; D2: 24 h post-application; D3: 10 days post-application). Arrowheads show as an example the corpus callosum; * marks the ventricular system (A1).

before the end of the study. In this mouse, the histological examination revealed pronounced lower spinal cord infiltrates in the absence of inflammatory activity in the brain. Six healthy control animals did not develop alterations in the BBB integrity.

Lesion distribution widely extends beyond expected areas, often includes central cranial nerves and cerebellum, and does not correlate with clinical symptoms

Contrast-enhancing lesions were widely disseminated in various regions of the brain. In most cases we were able to localize BBB leakage to the brain stem (84%), the periventricular area (64%), the midbrain (64%) and the cerebellum (40%). The regional distribution at onset is listed in Fig. 1. We noted frequent early central cranial nerve involvement. In 14 out of 25 animals (56%), lesions were at the site of single or multiple cranial nerve fascicles, ganglia or nuclei. Optic system involvement was visualized in eight mice. The most commonly affected structure of the optic system was the optic tract, but the chiasm and optic nerve were also affected (Fig. 2). Contrast enhancement of the trigeminal nuclei and fascicles on one or both sides was clearly discernable in 10 mice (Fig. 3A). Furthermore, in seven animals proximal parts of the vestibulo-cochlear nerves were visibly affected (Fig. 3B). As in patients, cortical BBB breakdown was a less frequent finding (16%), but still clearly identifiable in four animals (Fig. 4C).

Importantly, BBB disruption correlated only partially with clinical signs. In four animals, which remained without pathological clinical features until the termination of the study, we detected prominent contrast-enhancing lesions in various regions of the CNS. Contrast-enhanced MRI proved to be a more sensitive marker of acute inflammation than the assessment of clinical disability.

High-resolution MRI is sensitive in visualizing microglia and macrophages after endocytosis of VSOP

The novel superparamagnetic contrast agent VSOP can indirectly visualize phagocytic cells *in vivo*. VSOP is a very small citrate-coated iron oxide particle with dual function. It instantly shows BBB breakdown by extravasation (Fig. 4D), and in inflammatory plaques it is readily incorporated by microglia and infiltrating macrophages (Fig. 5). We established high-resolution T2*-weighted sequences with optimized signal-to-noise ratio to visualize even small amounts of incorporated VSOP in plaques (Fig. 4). Gradient echo T2*-weighted imaging is highly sensitive for magnetic susceptibility changes caused by such iron oxide particles, but also for signal extinctions derived from local field inhomogeneities or haemoglobin within intact vessels, which may obscure the signal from incorporated contrast agent. For the reduction of such artefacts and unspecific magnetic field inhomogeneities, very short echo times (TE) were applied (see Materials and methods). Additionally, in order to avoid potential

FIG. 5. MR images were correlated to histological sections (A1, A2). Contrast enhancement is shown in the area of the trigeminal nerve indicated by an arrowhead in a coronal T1-weighted image (A1). The same region is shown after VSOP application with Prussian Blue staining (A2, arrowhead). Higher magnifications of H&E staining are given in (A3, A4), and Prussian Blue staining in (A5, A6). Please note the broad immune cell infiltration (A3, A4). Additional erythrocytic extravasates indicate a largely disrupted BBB (A4, A6, indicated by *). After VSOP application, iron oxide particles were present in lesions shown by Prussian Blue staining (A5). An example of intracellular VSOP accumulation is given in (A6, circle). Microglia and macrophages identified by immunohistochemistry aligned with cells containing VSOP in Prussian Blue stainings: (B1–B6) A perivascular lesion located at the cerebellar brain stem border. Co-localization of mononuclear cell infiltrates in H&E (B1, B2), intracellular VSOP with Prussian Blue (B3, B4), and macrophages/microglia at the same localization detected by immunohistochemical staining (B5, B6; green: Iba-1-positive microglia/macrophages; red: f-actin-positive vessel walls; blue: Hoechst 33258-stained cell nuclei).

intrinsic blood oxygenation level-dependent effects of perfused blood vessels, 100% O_2 was administered within the inhalation gas during MR scanning, a method that has been described to reduce the T2* effect of blood vessels (Himmelreich *et al*., 2005), and which was well tolerated by all animals studied, even at prolonged experimental times.

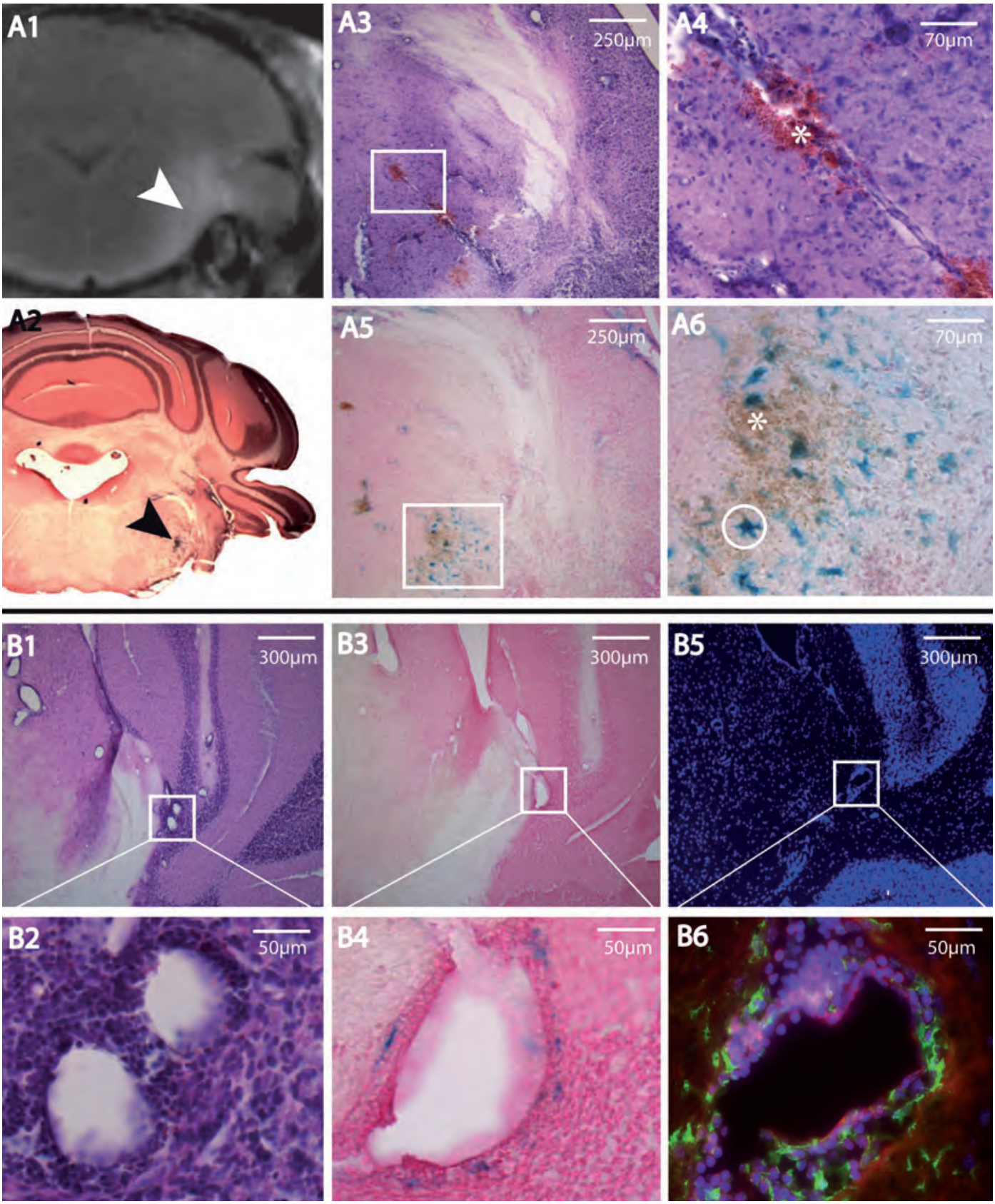

Directly after VSOP application, the cerebral vasculature and contrast-enhancing lesions appeared strongly hypointense on T2*-weighted images. In contrast to the blood pool, the signal intensity in lesions did not markedly decrease after 3–6 h, but remained hypointense (Fig. 4, D1). Although we noted a slight 'wash-out' of VSOP after 24 h, the signal intensity remained clearly visible for up to 10 days, indicating the endocytosis of VSOP by local microglia and macrophages invading neuroinflammatory plaques (Fig. 4, D3).

On histological examination, the presence of acute cellular infiltrates in each animal was confirmed for all sites of contrast enhancement in the MRI. An example is given in Fig. 5. In H&E stainings, delineated areas of intraparenchymal cell extravasation were typically 50–300 μm in diameter, forming a perivascular cuff. Some of these lesions extended into the surrounding parenchyma.

In areas of MR contrast enhancement, Iba-1 staining for macrophages/microglia co-localized in immunofluorescence microscopy to cells identified by H&E and Prussian Blue staining, demonstrating an uptake of VSOP by mononuclear immune cells activated or attracted to the foci of inflammation (Fig. 5). The number and extent of Prussian Blue-positive cells and disseminated Prussian Blue-positive particles in the tissue appeared less prominent histologically than had been expected on the basis of lesion size in the MRI. This might be due to the strongly enhancing 'blooming' effect of these particles in susceptible MR sequences, which leads to an overestimate of the iron content. However, it should be noted that a wash-out phenomenon during histological processing may contribute to the mismatch of appearance between MRI and histology.

Gf-enhanced MRI reveals cranial nerves inflammation

We also applied Gf, as this contrast agent was recently shown to enhance peripheral nerves after trauma (Bendszus *et al*., 2005). Gf gave rise to bright contrast enhancement on T1-weighted images and, in particular, facilitated the detection of cranial nerve inflammation (Figs 2 and 3). A strong signal increase was present in all regions previously showing Gd-DTPA leakage. In some cases, predominantly at sites of cranial nerve inflammation, we exclusively detected Gf-induced signal changes (Fig. 2, A1 and C1). Generally, Gd-DTPA enhancement appeared less prominent compared with Gf. Although the peak intensity developed delayed compared with Gd-DTPA (data not shown), Gf was present at the site of BBB breakdown for more than 24 h. The continuous lesional signal even after elimination of the contrast medium from the circulation enabled the unambiguous distinction between intravascular blood pool enhancement and actual tissue accumulation, which is of particular interest in models known for vessel-associated pathology, such as EAE.

Discussion

A critical stage in the development of an MS plaque is considered to be the disruption of the BBB (Harris *et al*., 1991; McFarland *et al*., 1992). This process is, at least in relapsing–remitting MS, believed to be initiated by autoreactive CD4+ lymphocytes, which migrate into the CNS and trigger an inflammatory response, leading to an increased cerebrovascular permeability and the infiltration of further immune cells. In the animal model EAE, neuropathological and radiolabelled receptor ligand-binding studies suggested an ascending nature of the disease arising at the sacral spinal cord, as described in guinea pigs and Lewis rats (Lassmann & Wisniewski, 1978; Mattner *et al*., 2005) and also reported in earlier MRI studies, although not convincingly (O'Brien *et al*., 1987; Hawkins *et al*., 1990, 1991). Here we demonstrate the widespread distribution of intracranial lesions already pre-onset or at onset of clinical symptoms in a murine EAE model. By transferring PLP-specific T-cells, we were able to omit adjuvants such as pertussis toxin (Hofstetter *et al*., 2002) or Freund's adjuvant (Rabchevsky *et al*., 1999), which may facilitate disease onset but also alter BBB integrity. The distinct lesion pattern including cerebellar and proximal cranial nerve inflammation, which we observed, and the presence of clinical silent lesions closely resemble the multifocal nature of the disease in patients with MS. No longer restrained by poor regional accuracy and a restriction to rat models (Namer *et al*., 1993; Morrissey *et al*., 1996), current MR technology allows for high-resolution *in vivo* imaging in murine EAE, as demonstrated here. Applying different contrast agents and high-resolution MRI, this study supports the relevance of adoptive transfer SJL/J EAE as a disease model of MS.

Superparamagnetic iron oxide particles have emerged as very promising new contrast agents, leading to increased signal intensity and opening up the possibility of cellular imaging (Xu *et al*., 1998; Dousset *et al*., 1999; Berger *et al*., 2006; Brochet *et al*., 2006). In earlier acute EAE studies, and in an ischaemic rat model, it was hypothesized that areas showing minor leakage of Gd-DTPA could be distinguished from areas enhanced by cells loaded with ultra-small superparamagnetic iron oxide (USPIO) particles, which actively penetrated the BBB (Rausch *et al*., 2002, 2003; Floris *et al*., 2004). These results were supported by a recent study on patients with MS reporting differential enhancement patterns after USPIO application compared with Gd-DTPA enhancement (Dousset *et al*., 2006). On applying a novel citrate-coated VSOP with a hydrodynamic diameter of only 7 nm we do not find major differences in its location compared with gadolinium-based contrast agents. Signal hypointensities in T2*-weighted images were present directly after application, suggesting that VSOP diffuses across the ruptured BBB and is subsequently taken up locally by resident or infiltrating phagocytozing cells. In contrast to Floris *et al*. (2004), who report on complete regression of the signal extinction 3 days after applying dextran-coated iron oxide particles – which they postulate as a result of the high turnover or influx of peripheral macrophages – the VSOP signal in our study remained visible for up to 10 days.

We additionally applied Gf, a novel amphiphilic contrast agent, which was recently tested in models of peripheral nerve degeneration and autoimmune neuritis (Bendszus & Stoll, 2005). Gf binds to albumin and, in the case of BBB disruption, to matrix proteins of the extravascular space or the parenchyma, providing a T1-positive MRI signal. The detailed mechanism leading to an accumulation in inflamed or injured tissue remains to be specified. Our study for the first time applied Gf in EAE. We detected areas with bright signal intensity after Gf application, which had not shown Gd-DTPA enhancement, e.g. inflamed regions of the optic and other cranial nerves. Our findings are concordant with an observation by Wessig *et al*. (2007), who reported on a T1-positive MRI enhancement exclusively after Gf injection in a model of focal demyelination of peripheral nerves. Therefore, Gf appears to facilitate the detection of BBB leakage and inflammatory foci in occult locations such as cranial nerves and fascicles, which have been neglected in previous EAE imaging studies.

To our knowledge, this is the first passive transfer EAE study in SJL/J mice systematically investigating early BBB disruption with different contrast agents in a high-resolution MR system accompanied by a detailed clinical, histological and immunofluorescence microscopy analysis. Despite the common notion that disease in EAE progresses from spinal cord to more rostral regions of the brain

(Oldendorf & Towner, 1974), we identified widespread BBB leakage in the brain already before clinical onset.

Early findings include the contrast enhancement of the cerebellum, coinciding with an impaired righting reflex in our clinical assessment. The righting reflex assesses the animal's capability to switch back to an upright position after being rolled on its back. This reflex tests spatial coordination and balance, features requiring an intact cerebellar functioning (Tonra, 2002). In a recent histological approach, the cerebellum was proposed to be particularly susceptible to an autoimmune-related BBB breakdown in active EAE, which may precede BBB disruption of the spinal cord (Muller *et al*., 2005). Furthermore, there is evidence for a differential susceptibility of cerebellar microvascular endothelial cells to loss of barrier properties in response to inflammatory stimuli, such as a reduced tight junction expression in the cerebellar BBB (Silwedel & Forster, 2006). Our corresponding MRI observations support these findings, using here an adoptive transfer model that is independent of unspecific adjuvant effects. We therefore suggest an immune-specific vulnerability of cerebellar vasculature

There has thus far been a reluctance to report or discuss the occurrence of optical, trigeminal or vestibular nerve affection in murine EAE. This may derive from the widely-held belief that inflammation in the spinal cord is the major clinical concern, but may also result from the shortcomings of the widely used EAE scoring system in assessing relevant symptoms. Our findings reveal that cranial nerve inflammation is a frequent feature in the EAE model, corresponding to symptoms well known in MS. Considering its clinical relevance, the assessment of cranial nerve impairment in EAE could provide a basis for future trials, e.g. by examining the integrity of the optic system by electrophysiological means (Martin *et al*., 2006) in combination with the MR imaging tools presented here, and by others (Song *et al*., 2003).

In this study, high-resolution MRI enhanced by novel contrast agents demonstrates widespread and early subclinical disease activity, which we confirmed by corresponding conventional and immunofluorescence microscopy. Our data support the notion that adoptive transfer EAE closely mimics MS. Technical advances have made murine MRI feasible, and ensure more reliable detection of disease activity than clinical assessment alone. MRI could therefore be included in future *in vivo* therapeutic and diagnostic EAE studies.

Acknowledgements

This work was supported by the Deutsche Forschungsgemeinschaft (SFB507), the Bundesministerium für Bildung und Forschung (BMBF), and by the Hertie Institut für MS-Forschung (IMSF) Göttingen. We thank Alistair Noon and Andrew Mason for reading this manuscript as native English speakers.

Abbreviations

BBB, blood–brain barrier; EAE, experimental autoimmune encephalomyelitis; FOV, field of view; Gd-DTPA, gadopentate dimeglumine; Gf, gadofluorine M, Gd-GlyMe-DOTA-perfluorooctyl-mannose-conjugate; H&E, haematoxylin and eosin; MRI, magnetic resonance imaging; MS, multiple sclerosis; PBS, phosphate-buffered saline; PLP, proteolipid peptide; USPIO, ultra-small superparamagnetic iron oxide; VSOP, very small iron oxide particle.

References

Aktas, O., Smorodchenko, A., Brocke, S., Infante-Duarte, C., Topphoff, U.S., Vogt, J., Prozorovski, T., Meier, S., Osmanova, V., Pohl, E., Bechmann, I., Nitsch, R. & Zipp, F. (2005) Neuronal damage in autoimmune neuroinflammation mediated by the death ligand TRAIL. *Neuron*, **46**, 421–432.

Aktas, O., Waiczies, S., Smorodchenko, A., Dorr, J., Seeger, B., Prozorovski, T., Sallach, S., Endres, M., Brocke, S., Nitsch, R. & Zipp, F. (2003) Treatment of relapsing paralysis in experimental encephalomyelitis by targeting Th1 cells through atorvastatin. *J. Exp. Med.*, **197**, 725–733.

Barkhof, F. (2002) The clinico-radiological paradox in multiple sclerosis revisited. *Curr. Opin. Neurol.*, **15**, 239–245.

Bendszus, M. & Stoll, G. (2005) Technology insight: visualizing peripheral nerve injury using MRI. *Nat. Clin. Pract. Neurol.*, **1**, 45–53.

Bendszus, M., Wessig, C., Schutz, A., Horn, T., Kleinschnitz, C., Sommer, C., Misselwitz, B. & Stoll, G. (2005) Assessment of nerve degeneration by gadofluorine M-enhanced magnetic resonance imaging. *Ann. Neurol.*, **57**, 388–395.

Berger, C., Hiestand, P., Kindler-Baumann, D., Rudin, M. & Rausch, M. (2006) Analysis of lesion development during acute inflammation and remission in a rat model of experimental autoimmune encephalomyelitis by visualization of macrophage infiltration, demyelination and blood–brain barrier damage. *NMR Biomed.*, **19**, 101–107.

Brochet, B., Deloire, M.S., Touil, T., Anne, O., Caille, J.M., Dousset, V. & Petry, K.G. (2006) Early macrophage MRI of inflammatory lesions predicts lesion severity and disease development in relapsing EAE. *Neuroimage*, **32**, 266–274.

Charcot, J.M. (1868) Histologie de la sclérose en plaques. *Gaz. Hôp.*, **41**, 554–555, 557–558, 566.

Dousset, V., Brochet, B., Deloire, M.S., Lagoarde, L., Barroso, B., Caille, J.M. & Petry, K.G. (2006) MR imaging of relapsing multiple sclerosis patients using ultra-small-particle iron oxide and compared with gadolinium. *AJNR Am. J. Neuroradiol.*, **27**, 1000–1005.

Dousset, V., Delalande, C., Ballarino, L., Quesson, B., Seilhan, D., Coussemacq, M., Thiaudiere, E., Brochet, B., Canioni, P. & Caille, J.M. (1999) In vivo macrophage activity imaging in the central nervous system detected by magnetic resonance. *Magn. Reson. Med.*, **41**, 329–333.

Fleige, G., Seeberger, F., Laux, D., Kresse, M., Taupitz, M., Pilgrimm, H. & Zimmer, C. (2002) In vitro characterization of two different ultrasmall iron oxide particles for magnetic resonance cell tracking. *Invest. Radiol.*, **37**, 482–488.

Floris, S., Blezer, E.L., Schreibelt, G., Dopp, E., van der Pol, S.M., Schadee-Eestermans, I.L., Nicolay, K., Dijkstra, C.D. & de Vries, H.E. (2004) Blood–brain barrier permeability and monocyte infiltration in experimental allergic encephalomyelitis: a quantitative MRI study. *Brain*, **127**, 616–627.

Gold, R., Linington, C. & Lassmann, H. (2006) Understanding pathogenesis and therapy of multiple sclerosis via animal models: 70 years of merits and culprits in experimental autoimmune encephalomyelitis research. *Brain*, **129**, 1953–1971.

Harris, J.O., Frank, J.A., Patronas, N., McFarlin, D.E. & McFarland, H.F. (1991) Serial gadolinium-enhanced magnetic resonance imaging scans in patients with early, relapsing-remitting multiple sclerosis: implications for clinical trials and natural history. *Ann. Neurol.*, **29**, 548–555.

Hawkins, C.P., Mackenzie, F., Tofts, P., du Boulay, E.P. & McDonald, W.I. (1991) Patterns of blood–brain barrier breakdown in inflammatory demyelination. *Brain*, **114**, 801–810.

Hawkins, C.P., Munro, P.M., MacKenzie, F., Kesselring, J., Tofts, P.S., du Boulay, E.P., Landon, D.N. & McDonald, W.I. (1990) Duration and selectivity of blood–brain barrier breakdown in chronic relapsing experimental allergic encephalomyelitis studied by gadolinium-DTPA and protein markers. *Brain*, **113**, 365–378.

Himmelreich, U., Weber, R., Ramos-Cabrer, P., Wegener, S., Kandal, K., Shapiro, E.M., Koretsky, A.P. & Hoehn, M. (2005) Improved stem cell MR detectability in animal models by modification of the inhalation gas. *Mol. Imaging*, **4**, 104–109.

Hofstetter, H.H., Shive, C.L. & Forsthuber, T.G. (2002) Pertussis toxin modulates the immune response to neuroantigens injected in incomplete Freund's adjuvant: induction of Th1 cells and experimental autoimmune encephalomyelitis in the presence of high frequencies of Th2 cells. *J. Immunol.*, **169**, 117–125.

Lassmann, H. & Wisniewski, H.M. (1978) Chronic relapsing EAE. Time course of neurological symptoms and pathology. *Acta Neuropathol. (Berl.)*, **43**, 35–42.

Martin, M., Hiltner, T.D., Wood, J.C., Fraser, S.E., Jacobs, R.E. & Readhead, C. (2006) Myelin deficiencies visualized in vivo: visually evoked potentials and T2-weighted magnetic resonance images of shiverer mutant and wild-type mice. *J. Neurosci. Res.*, **84**, 1716–1726.

Mattner, F., Katsifis, A., Staykova, M., Ballantyne, P. & Willenborg, D.O. (2005) Evaluation of a radiolabelled peripheral benzodiazepine receptor ligand in the central nervous system inflammation of experimental autoimmune encephalomyelitis: a possible probe for imaging multiple sclerosis. *Eur. J. Nucl. Med. Mol. Imaging*, **32**, 557–563.

McFarland, H.F., Frank, J.A., Albert, P.S., Smith, M.E., Martin, R., Harris, J.O., Patronas, N., Maloni, H. & McFarlin, D.E. (1992) Using gadolinium-enhanced magnetic resonance imaging lesions to monitor disease activity in multiple sclerosis. *Ann. Neurol.*, **32**, 758–766.

Morrissey, S.P., Stodal, H., Zettl, U., Simonis, C., Jung, S., Kiefer, R., Lassmann, H., Hartung, H.P., Haase, A. & Toyka, K.V. (1996) In vivo MRI and its histological correlates in acute adoptive transfer experimental allergic encephalomyelitis. Quantification of inflammation and oedema. *Brain*, **119**, 239–248.

Muller, D.M., Pender, M.P. & Greer, J.M. (2005) Blood–brain barrier disruption and lesion localisation in experimental autoimmune encephalomyelitis with predominant cerebellar and brainstem involvement. *J. Neuroimmunol.*, **160**, 162–169.

Namer, I.J., Steibel, J., Poulet, P., Armspach, J.P., Mohr, M., Mauss, Y. & Chambron, J. (1993) Blood–brain barrier breakdown in MBP-specific T cell induced experimental allergic encephalomyelitis. A quantitative in vivo MRI study. *Brain*, **116**, 147–159.

Nijeholt, G.J., Bergers, E., Kamphorst, W., Bot., J., Nicolay, K., Castelijns, J.A., van Waesberghe, J.H., Ravid, R., Polman, C.H. & Barkhof, F. (2001) Post-mortem high-resolution MRI of the spinal cord in multiple sclerosis: a correlative study with conventional MRI, histopathology and clinical phenotype. *Brain*, **124**, 154–166.

Nitsch, R., Pohl, E.E., Smorodchenko, A., Infante-Duarte, C., Aktas, O. & Zipp, F. (2004) Direct impact of T cells on neurons revealed by two-photon microscopy in living brain tissue. *J. Neurosci.*, **24**, 2458–2464.

O'Brien, J.T., Noseworthy, J.H., Gilbert, J.J. & Karlik, S.J. (1987) NMR changes in experimental allergic encephalomyelitis: NMR changes precede clinical and pathological events. *Magn. Reson. Med.*, **5**, 109–117.

Oldendorf, W.H. & Towner, H.F. (1974) Blood–brain barrier and DNA changes during the evolution of experimental allergic encephalomyelitis. *J. Neuropathol. Exp. Neurol.*, **33**, 616–631.

Perl, D.P. & Good, P.F. (1992) Comparative techniques for determining cellular iron distribution in brain tissues. *Ann. Neurol.*, **32** (Suppl.), S76–S81.

Rabchevsky, A.G., Degos, J.D. & Dreyfus, P.A. (1999) Peripheral injections of Freund's adjuvant in mice provoke leakage of serum proteins through the blood–brain barrier without inducing reactive gliosis. *Brain Res.*, **832**, 84–96.

Rausch, M., Baumann, D., Neubacher, U. & Rudin, M. (2002) In-vivo visualization of phagocytotic cells in rat brains after transient ischemia by USPIO. *NMR Biomed.*, **15**, 278–283.

Rausch, M., Hiestand, P., Baumann, D., Cannet, C. & Rudin, M. (2003) MRI-based monitoring of inflammation and tissue damage in acute and chronic relapsing EAE. *Magn. Reson. Med.*, **50**, 309–314.

Silwedel, C. & Forster, C. (2006) Differential susceptibility of cerebral and cerebellar murine brain microvascular endothelial cells to loss of barrier properties in response to inflammatory stimuli. *J. Neuroimmunol.*, **179**, 37–45.

Song, S.K., Sun, S.W., Ju, W.K., Lin, S.J., Cross, A.H. & Neufeld, A.H. (2003) Diffusion tensor imaging detects and differentiates axon and myelin degeneration in mouse optic nerve after retinal ischemia. *Neuroimage*, **20**, 1714–1722.

Sriram, S. & Steiner, I. (2005) Experimental allergic encephalomyelitis: a misleading model of multiple sclerosis. *Ann. Neurol.*, **58**, 939–945.

Steinman, L. & Zamvil, S.S. (2006) How to successfully apply animal studies in experimental allergic encephalomyelitis to research on multiple sclerosis. *Ann. Neurol.*, **60**, 12–21.

Stroh, A., Zimmer, C., Werner, N., Gertz, K., Weir, K., Kronenberg, G., Steinbrink, J., Mueller, S., Sieland, K., Dirnagl, U., Nickenig, G. & Endres, M. (2006) Tracking of systemically administered mononuclear cells in the ischemic brain by high-field magnetic resonance imaging. *Neuroimage*, **33**, 886–897.

Taupitz, M., Wagner, S., Schnorr, J., Kravec, I., Pilgrimm, H., Bergmann-Fritsch, H. & Hamm, B. (2004) Phase I clinical evaluation of citrate-coated monocrystalline very small superparamagnetic iron oxide particles as a new contrast medium for magnetic resonance imaging. *Invest. Radiol.*, **39**, 394–405.

Tonra, J.R. (2002) Cerebellar susceptibility to experimental autoimmune encephalomyelitis in SJL/J mice: potential interaction of immunology with vascular anatomy. *Cerebellum*, **1**, 57–68.

Wessig, C., Bendszus, M. & Stoll, G. (2007) In vivo visualization of focal demyelination in peripheral nerves by gadofluorine M-enhanced magnetic resonance imaging. *Exp. Neurol*, **204**, 14–19.

Wuerfel, J., Bellmann-Strobl, J., Brunecker, P., Aktas, O., McFarland, H., Villringer, A. & Zipp, F. (2004) Changes in cerebral perfusion precede plaque formation in multiple sclerosis: a longitudinal perfusion MRI study. *Brain*, **127**, 111–119.

Xu, S., Jordan, E.K., Brocke, S., Bulte, J.W., Quigley, L., Tresser, N., Ostuni, J.L., Yang, Y., McFarland, H.F. & Frank, J.A. (1998) Study of relapsing remitting experimental allergic encephalomyelitis SJL mouse model using MION-46L enhanced in vivo MRI: early histopathological correlation. *J. Neurosci. Res.*, **52**, 549–558.

Journal of Neuroinflammation

BioMed Central

Research

Open Access

Beyond blood brain barrier breakdown – *in vivo* detection of occult neuroinflammatory foci by magnetic nanoparticles in high field MRI

Eva Tysiak[1], Patrick Asbach[2], Orhan Aktas[1,3], Helmar Waiczies[1], Maureen Smyth[1], Joerg Schnorr[2], Matthias Taupitz[2] and Jens Wuerfel*[1]

Address: [1]Cecilie Vogt Clinic for Neurology, Charité – University Medicine Berlin, Germany, [2]Department of Radiology, Charité – University Medicine Berlin, Campus Mitte, Germany and [3]Department of Neurology, Heinrich-Heine-University, Duesseldorf, Germany

Email: Eva Tysiak - etysiak@med.uni-goettingen.de; Patrick Asbach - patrick.asbach@charite.de; Orhan Aktas - orhan.aktas@uni-duesseldorf.de; Helmar Waiczies - helmar@waiczies.de; Maureen Smyth - maureen.smyth@charite.de; Joerg Schnorr - joerg.schnorr@charite.de; Matthias Taupitz - matthias.taupitz@charite.de; Jens Wuerfel* - jens.wuerfel@charite.de

* Corresponding author

Published: 6 August 2009

Journal of Neuroinflammation 2009, **6**:20 doi:10.1186/1742-2094-6-20

Received: 21 March 2009
Accepted: 6 August 2009

This article is available from: http://www.jneuroinflammation.com/content/6/1/20

Abstract

Background: Gadopentate dimeglumine (Gd-DTPA) enhanced magnetic resonance imaging (MRI) is widely applied for the visualization of blood brain barrier (BBB) breakdown in multiple sclerosis and its animal model, experimental autoimmune encephalomyelitis (EAE). Recently, the potential of magnetic nanoparticles to detect macrophage infiltration by MRI was demonstrated. We here investigated a new class of very small superparamagnetic iron oxide particles (VSOP) as novel contrast medium in murine adoptive-transfer EAE.

Methods: EAE was induced in 17 mice via transfer of proteolipid protein specific T cells. MR images were obtained before and after application of Gd-DTPA and VSOP on a 7 Tesla rodent MR scanner. The enhancement pattern of the two contrast agents was compared, and correlated to histology, including Prussian Blue staining for VSOP detection and immunofluorescent staining against IBA-1 to identify macrophages/microglia.

Results: Both contrast media depicted BBB breakdown in 42 lesions, although differing in plaques appearances and shapes. Furthermore, 13 lesions could be exclusively visualized by VSOP. In the subsequent histological analysis, VSOP was localized to microglia/macrophages, and also diffusely dispersed within the extracellular matrix.

Conclusion: VSOP showed a higher sensitivity in detecting BBB alterations compared to Gd-DTPA enhanced MRI, providing complementary information of macrophage/microglia activity in inflammatory plaques that has not been visualized by conventional means.

Background

A fundamental pathologic feature of multiple sclerosis (MS) is the formation of multifocal plaques in the central nervous system (CNS), accompanied by a disruption of the blood brain barrier (BBB). Gadopentate dimeglumine (Gd-DTPA) does not cross an intact BBB and can thus be used to detect BBB leakage in acute inflammatory lesions by Gd-DTPA enhanced MRI [1]. Recently, iron-oxide based magnetic nanoparticles have evolved as a new class of MRI contrast agents [2-6], bearing the potential to

detect macrophage infiltrates into the CNS independently from BBB breakdown [7,8]. Macrophages play a pivotal role in the pathophysiology of MS, since they invade the CNS early during disease and act as effector cells in the inflammatory cascade, leading to persistent structural and functional tissue damage [9,10]. Dextran-coated magnetic nanoparticles have been applied in various animal models to visualize the migration of macrophages by MRI [2,7,8,11-15]. Two recent studies showed that the application of magnetic nanoparticles in MS patients resulted in a pattern that was distinct from BBB leakage visualized on Gd-DTPA enhanced images [16,17].

In this study, we investigated the capacity of novel, very small superparamagnetic iron oxide particles (VSOP) to detect neuroinflammatory foci in murine experimental autoimmune encephalomyelitis (EAE), an animal model of MS. VSOP are substantially smaller than conventional magnetic nanoparticles due to an electrostatically stabilized citrate coating [6], and therefore can also be used to detect BBB breakdown [18,19]. On the other hand, VSOP are very efficiently phagocytized [20] and were successfully applied for *in vivo* tracking of mononuclear cells in the past [21]. We analyzed the distribution pattern and kinetics of VSOP enhancement in adoptive-transfer EAE in comparison to conventional Gd-DTPA enhanced MRI and compared these findings with histopathological alterations.

Materials and methods

Adoptive-transfer EAE

Female SJL/J mice, six to eight weeks old, were purchased from Charles River (Sulzfeld, Germany). Animals were housed in sawdust-lined cages in a climate-controlled room and received standard rodent feed and water *ad libitum*. All experiments were approved by the local animal welfare committee and conformed to the European Communities Council Directive (86/609/EEC). For adoptive-transfer EAE, naïve donor mice were immunized with an emulsion containing 250 μg PLP (murine proteolipid peptide p139-151; purity > 95%, Pepceuticals, Leicester, UK) in equal volumes of phosphate buffered saline (PBS) and Complete Freund's Adjuvant (CFA, Difco Laboratories, Detroit, USA), and 4 mg/ml *Mycobacterium tuberculosis* H37Ra (Difco Laboratories, Detroit, USA), as previously described [22]. Ten days after immunization, cells were extracted from draining lymph nodes and restimulated with 12.5 μg PLP/ml in cell culture medium (RPMI 1640 supplemented with 2 mM L-glutamine, 100 U/ml penicillin, 100 μg/ml streptomycin and 10% fetal calf serum) for four days at 37°C. For adoptive transfer, 8–12 × 10^6 T-cell blasts in 100 μl PBS were injected intraperitoneally into 17 syngenic recipients.

Mice were weighed daily and scored for EAE [22]: 0, unaffected; 1, tail weakness or impaired righting on attempt to roll over; 2, paraparesis; 3, paraplegia; 4, paraplegia with forelimb weakness or complete paralysis; score > 4, to be sacrificed. Mice with a score of 4 received an intraperitoneal injection of 200 μl glucose (5%) daily.

MRI analysis

Cerebral MRI was performed on a 7 Tesla rodent MRI scanner (Pharmascan 70/16AS, Bruker BioSpin, Ettlingen, Germany), applying a 20 mm RF-Quadrature-Volume head coil. Animals received anesthesia via facemask induced with 3% and maintained with 1.5 – 2.0% isoflurane (Forene, Abbot, Wiesbaden, Germany) delivered in 100% O_2 under constant ventilation control (Bio Trig System, Bruker BioSpin, Ettlingen, Germany). Mice were placed on a heated circulating water blanket to keep up body temperature at 37°C.

Axial and coronal T1-weighted (MSME; TE 10.5 ms, TR 322 ms, 0.5 mm slice thickness, matrix 256 × 256, field of view (FOV) 2.8 cm, eight averages, 40 coronal slices, scan time 22 minutes, and 20 axial slices, scan time 16 min), fat-suppressed turbo spin echo T2-weighted (RARE; TE1 14.5 ms, TE2 65.5 ms, TR 4500 ms, 0.5 mm slice thickness, Matrix 256 × 256, FOV 2.8 cm, eight averages, 40 coronal slices, scan time 28 minutes, and 20 axial slices, scan time 28 minutes) and T2*-weighted (GEFI; TE 5.6 ms, TR 1200 ms, flip angle 35°, 0.5 mm slice thickness, Matrix 256 × 256, FOV 2.8 cm, four averages, 40 coronal slices, scan time 20 minutes, and 20 axial slices, scan time 13 minutes) images were acquired before and after intravenous (i.v.) administration of the respective contrast agent. Identical slice positions were used for all sequences applied: coronal slices were aligned to the olfactory bulb/frontal lobe fissure and covered the entire brain up to the cervical spinal cord. Axial slices were positioned parallel to a plane through the most frontal tip of the olfactory bulb and the most rostral cerebellar part. MRI data were analyzed using the MEDx3.4.3 software package (Medical Numerics, Virginia, USA) on a LINUX workstation.

Mice were investigated daily for the development of BBB breakdown beginning on the fifth day post T cell transfer with MRI immediately after injection of 0.2 mmol/kg bodyweight Gd-DTPA (Magnevist, Bayer-Schering Pharma AG, Berlin, Germany) into the tail vein. If parenchymal contrast enhancement was detected, animals received 0.2 mmol/kg bodyweight VSOP (VSOP C-184, Ferropharm, Teltow, Germany) and MR investigations were repeated after 24 h. Three animals with rapid onset received primarily VSOP and no Gd-DTPA.

Histology

For subsequent histological analysis, mice were lethally anaesthetized (Xylazinhydrochlorid, Rompun 2%, Bayer, Leverkusen, Germany, and Ketamin, CuraMED Pharma, Karlsruhe, Germany) and intracardially perfused with 0.1

M PBS and fixed in 4% paraformaldehyde (PFA) in 0.1 M PBS. Brain and spinal cord were removed and postfixed in 4% PFA. The tissue was then dehydrated in 30% sucrose for cryoprotection and stored at -80°C. Axial cryosections (Jung cryostat 2800 Frigocut-E, Cambridge Instruments, Nussloch, Germany) of the entire brain were stained either by standard hematoxylin and eosin (H&E) procedure to detect cellular inflammation or by Prussian Blue staining according to Perl's method [23] to detect VSOP.

For further characterisation of microglia/macrophages, tissue sections were incubated with rabbit anti-IBA-1 antibodies (1:1000, Wako Chemicals, Neuss, Germany) in PBS overnight at 4°C after preincubation in 10% normal goat serum (CALTAG, Invitrogen, Karlsruhe, Germany) to block non-specific binding, and then with a secondary antibody (anti-rabbit Cy2, Amersham, Munich, Germany) for 1 h at room temperature. Slices were counterstained with Hoechst-33258 (Molecular Probes, Leiden, the Netherlands) to visualize cell nuclei and with rhodamine phalloidin (Molecular Probes, Leiden, the Netherlands) to identify vascular structures. Finally, all slices were washed three times in PBS and cover-sealed with fluorescence mounting medium (DAKO Deutschland GmbH, Germany). Selected sections were examined by epifluorescence microscopy and digitally photographed (Olympus BX-51, Hamburg, Germany). Images were assembled using Adobe Photoshop (Adobe Systems, San Jose, CA, USA).

Results

Clinical EAE course

All mice developed EAE, presenting first clinical symptoms 7 – 14 (mean 9.9) days after the transfer of encephalitogenic T cells, most commonly initiated by an impaired tail motility and a delayed righting reflex after the animal was rolled on its back. The disease severity progressed to peak EAE scores between 1 and 4 (mean 2.5 ± 1.1) within several days, as illustrated in figure 1. Two animals were followed up longitudinally for three weeks until complete recovery.

VSOP enhanced MRI visualized inflammatory foci beyond BBB breakdown depicted by Gd-DTPA

Contrast enhanced MRI visualized 55 inflammatory plaques, most commonly in the brain stem and the periventricular area, but also disseminated throughout the remaining CNS (table 1). Areas of BBB breakdown appeared hyperintense on T1-weighted images after Gd-DTPA application or, respectively, hypointense on T2*-weighted images after VSOP enhancement (figure 2). The majority of the *in vivo* detected plaques were enhanced by both contrast agents (38 lesions), nevertheless, the enhancement pattern of Gd-DTPA and VSOP differed within the individual lesion, as demonstrated in figure 2

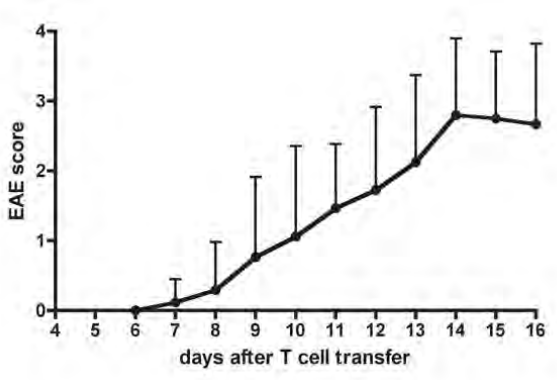

Figure 1
Clinical disease course. Clinical disease course in 17 mice after transfer (day 0) of proteolipid protein specific encephalitogenic T cells. Mean experimental autoimmune encephalomyelitis (EAE) scores and standard deviations are presented. Two animals were followed up until complete recovery (data for extended observation phase not shown).

(arrow heads). In general, Gd-DTPA enhanced lesions appeared more diffusely, gradually fading towards their edges, whereas VSOP hypointensities presented concise hypointense spots with clear margins towards the surrounding tissue.

Of note, 13 out of 55 inflammatory foci were exclusively visualized by VSOP, but could not be detected on Gd-DTPA enhanced T1-weighted images (table 1). Although these lesions did not show the conventional BBB breakdown characteristic defined by Gd-DTPA enhancement, they did not principally differ in terms of temporal or spatial MRI appearance in this study. Various examples are presented in figure 2 (small arrows). Vice versa, every Gd-DTPA enhancing lesions also clearly delineated by VSOP.

Histological correlation

Each Gd-DTPA or VSOP enhancing MRI lesion showed tissue pathology also on the corresponding histological slices. Perivascular and perimeningeal cell infiltrations were clearly demarked in H&E stainings (figure 3A). On Prussian Blue stained slices, iron depositions could be co-localized to these areas (figure 3B). VSOP was visualized within cellular compartments, suggesting their incorporation into cytoplasmatic vesicles (figure 3C). Furthermore, we detected extracellular magnetic nanoparticles accumulating diffusely within the brain parenchyma (figure 3D). Immunofluoresence stainings identified IBA-1 positive microglia/macrophages within perivascular lesions, which could be co-localized by their morphology to those cells exhibiting intravesicular VSOP on Prussian blue stainings (figure 3E,F).

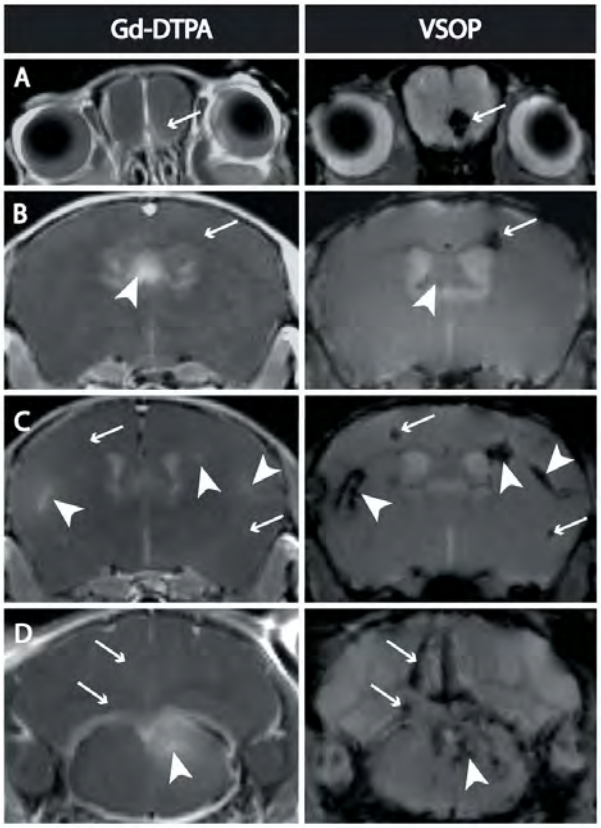

Figure 2
Comparison of contrast enhancing lesions. Comparison of coronal T1-weighted images immediately after Gd-DTPA administration versus T2*-weighted images 24 h after VSOP application. The majority of the lesions enhanced both, Gd-DTPA and VSOP, although shape differences within individual lesions were apparent (arrow heads). Furthermore, several plaques enhanced exclusively VSOP, but not Gd-DTPA (small arrows).

Kinetics and characterization of VSOP contrast

VSOP were strongly prominent in the blood pool as well as in areas of BBB breakdown within the first 6 h after application (figure 4). Figure 4 as an example depicts the typical signal void of inflammatory lesions 4–8 h post VSOP application in the diencephalon (A) and the cerebellum (B, C). In these early time points, regions with uniform Gd-DTPA enhancement did not appear accordingly evenly hypointense on co-localized T2*-weighted images after VSOP application, but these lesions were depicted clear-cut and more widespread in comparison (figure 4A, B). At later time points, i.e. after 18–24 h, parenchymal VSOP enhancement became most pronounced, when the non-specific blood pool contrast had completely vanished, and gradually ceased thereafter. Remarkably, some hypointense spots were still detectable 20 days after the initial application, despite complete clinical recovery of the animals at this time point (figure 5).

T2*-weighted sequences were most sensitive for the detection of magnetic nanoparticles, as illustrated in figure 6. None of the lesions could be differentiated prior to contrast agent administration in any of the investigated MRI sequences (T1-, T2-, T2*- or proton-density-weighted MRI), nor were lesions detectable in healthy control mice.

Discussion

In this study we investigated the capability of novel electrostatically stabilized magnetic nanoparticles, VSOP, to detect neuroinflammatory foci in murine adoptive transfer EAE, a disease model of MS. Although MRI revolutionized the diagnosis and management of MS patients [24], a persistent mismatch between clinical and MRI findings has remained [25,26]. Conventional MRI depicted hyperintense lesions on T2-weighted MRI as relatively unspecific traces of the disease and showed evidence of acutely disrupted BBB indicated by Gd-DTPA leakage into the parenchyma [27]. Both conventional imaging techniques correlated only weakly or moderately to disability and

Table 1: Distribution and number of contrast enhancing lesions (CEL).

Brain region	Exclusively VSOP enhancement	Gd-DTPA and VSOP enhancement	Total number of CEL
Brain stem	+++	+++++++++	12
Periventricular	++	++++++++++	12
Midbrain		+++++++++	9
Cerebellum	++	++++++	8
Olfactory bulb	+++	+++++	8
Cortex	+++	+++	6
	13	42	55

Data are given from 14 mice after Gd-DTPA and VSOP administration, respectively. Three mice received VSOP only and are not included in the table. Each + refers to an individual animal.

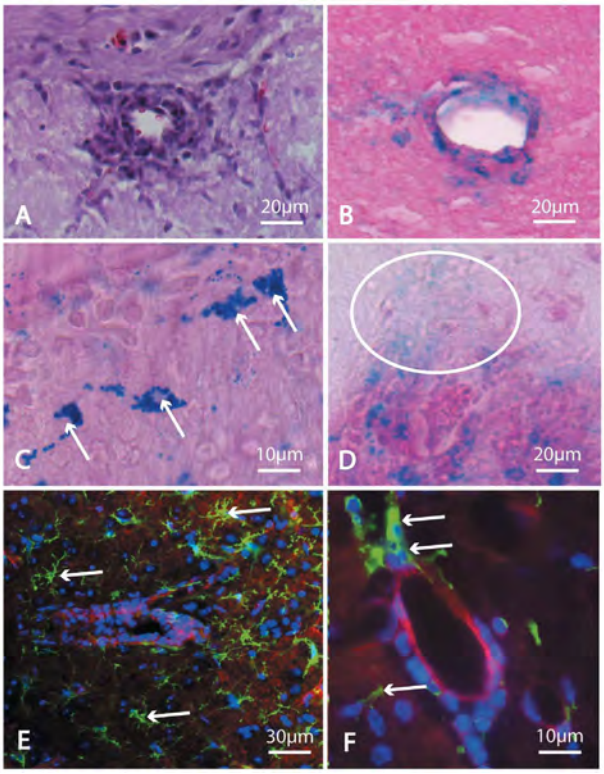

Figure 3
Histological findings. EAE-typical perivascular cell infiltrations were identified on Hematoxylin & Eosin stained slices (A). After Prussian Blue staining, VSOP was detected on corresponding sites (B). Two different distribution patterns of magnetic nanoparticles became evident: The incorporation of VSOP into cytoplasmatic vesicles within phagocytic cells (arrows in C), and a diffuse accumulation in the brain parenchyma (ellipse in D). IBA-1 positive macrophages/microglia were identified by immunofluorescent staining within perivascular plaques, colocalizing with Prussian Blue positive cells (arrows in E, and in higher magnification in F; green: anti-IBA-1, macrophages/microglia; blue: Hoechst 33258, cell nuclei; red: rhodamin phalloidin, vascular structures).

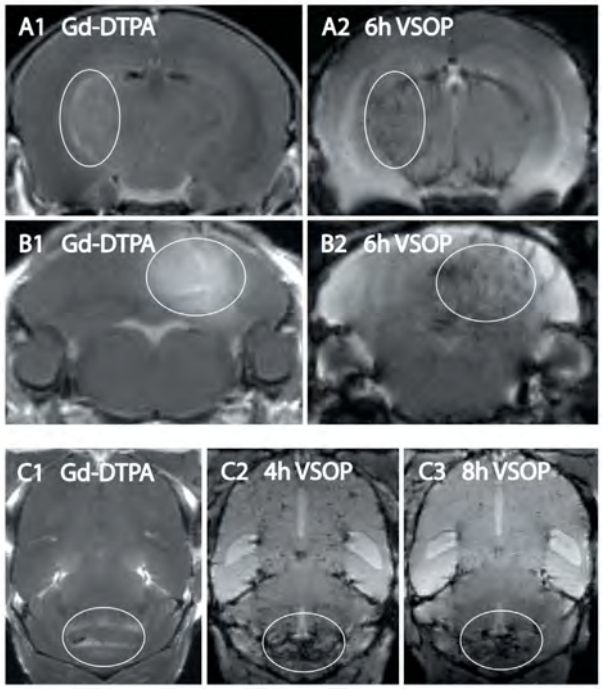

Figure 4
Early VSOP enhancement. In regions of blood brain barrier breakdown visualized by Gd-DTPA (A1, B1, C1), parenchymal VSOP leakage was detectable within the initial 6 h post application (A2, B2). Lesions became clearly distinguishable from the vasculature only after the blood pool contrast resolved. In C2, 4 h post application, intravascular VSOP is still visible. Eight hours after application, neuroinflammatory foci remain hypointense, where as intravascular signal decrease vanished (C3). Ellipses highlight contrast enhancing lesions.

clinical outcome of our patients [28]. Experimental contrast agents such as Gadofluorine M revealed blood brain barrier breakdown with higher sensitivity than conventional Gd-DTPA, but have not been applied to humans [18,29]. A new class of MRI contrast agents based on superparamagnetic iron oxide cores was recently developed and originally employed to visualize labeled cells [5,30-32]. In EAE, macrophages could be detected *in vivo* within inflammatory lesions after phagocytosis of magnetic nanoparticles [8,12,15,18,33]. Our finding of intracellular iron oxide, verified by Prussian Blue stained histology, is in line with these reports. Recent studies applying larger dextran-coated magnetic nanoparticles report their detection on MRI after a time delay of 24 h, presumably depending on the invasion of macrophages rather than on magnetic nanoparticles passively diffusing through the disrupted BBB barrier [4,8,12].

However, the extremely small VSOP investigated in this study became immediately visible after application as prominent T2*-hypointensity. Generally, VSOP detected lesions were in good spatial agreement to those areas that enhanced after Gd-DTPA application on T1-weighted MRI. Nevertheless, VSOP caused very distinct hypointense spots, whereas Gd-DTPA enhanced lesions appeared less clear cut on T1-weighted images. Most intriguingly, a subset of 13 out of 55 lesions became visible exclusively after VSOP injection, remaining unenhanced after concomitant Gd-DTPA application. In our study, these "VSOP-only" lesions did neither principally differ in space nor in time from those inflammatory plaques that simultane-

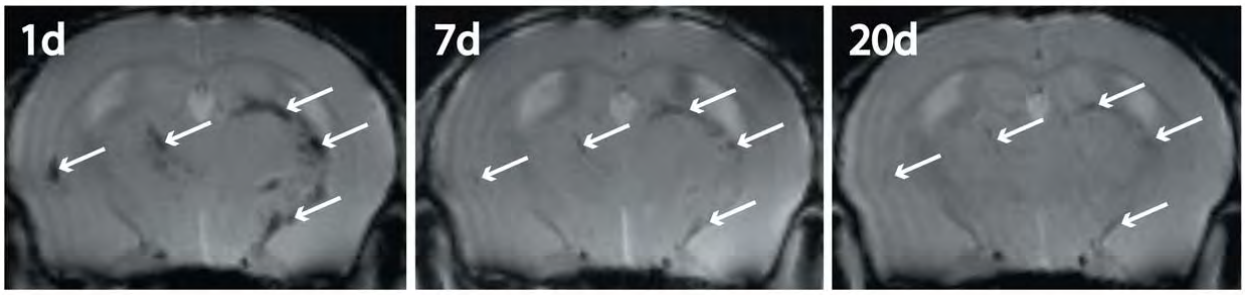

Figure 5
Time course of VSOP enhancement. In a longitudinal follow-up, T2*-hypointense lesions (arrows) were depicted at 24 h, 7 days and 20 days post VSOP application. Some hypointense plaques remained visible after 20 days.

ously enhanced both contrast agents, or on corresponding histology. Prussian-blue positive magnetic nanoparticles were present in vesicles within cells that were identified as macrophages/microglia on immunofluorescent stainings, and also as a diffuse extracellular accumulation within the connective tissue in vicinity to inflammatory plaques. Thus, VSOP enhanced MRI was capable of visualizing both, BBB disruption at high sensitivity as well as macrophage infiltration into neuroinflammatory lesions.

The occurrence of extracellular VSOP deposits in histology detected in regions without Gd-DTPA enhancement appears inscrutable at first sight. Two different underlying mechanisms have to be considered. First, BBB breakdown might be present but very subtle in these regions. Paramagnetic nanoparticles such as VSOP are characterized by a strong susceptibility effect in T2*-weighted imaging, possibly providing an augmented sensitivity for BBB alterations compared to Gd-DTPA. Secondly, presuming BBB integrity, VSOP might also accumulate in inflammatory foci due to a locally enhanced activity of transendothelial transport mechanisms during inflammation [34,35]. Nanoparticles were shown to facilitate drug delivery across the BBB [36]. Transport of transferrin into the CNS occurs via receptor-mediated transcytosis [37]. Which particular pathways might channel VSOP across an intact BBB remains to be determined.

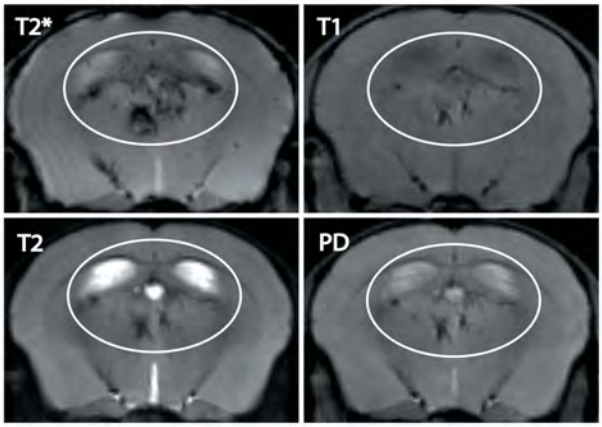

Figure 6
VSOP contrast in different MR sequences. Prominent contrast-enhancing periventricular lesions are depicted 24 h after VSOP injection on coregistered coronal T2*-, T2-, T1- and proton-density-weighted images (ellipse). T2*-weighted MRI was most sensitive in detecting magnetic nanoparticles. On T1-weighted images, very high VSOP concentrations became visible as hypointense spots at 7 Tesla.

Magnetic nanoparticles have already been applied in several human trials of cerebral ischemia [38,39] and in brain tumours [40]. In MS, two studies on magnetic nanoparticles were reported so far: In a prospective trial of Dousset et al. comprising ten MS patients with relapsing-remitting disease course, two patients presented enhancing lesions exclusively after administration of magnetic nanoparticles [17]. A very recent study by Vellinga et al. reported a mismatch of 144 out of 188 lesions in 14 patients, that could be visualized by dextran-coated magnetic nanoparticles (USPIO) enhanced MRI, but not by Gd-DTPA. Vice versa, of 59 Gd-DTPA positive lesions, 15 were USPIO negative in the same study [16]. Despite these encouraging initial experimental human trials, the exact specificity and sensitivity of different magnetic nanoparticles applied remains to be elucidated, since they obviously depict different aspects of pathology, as indicated by the data presented in this study.

VSOP has been investigated as a blood pool contrast agent in MR-angiography of the coronary arteries in a clinical phase 1B study, and was well tolerated [41]. Therefore, a future application also in MS seems feasible.

Conclusion

Here, we demonstrated that VSOP, due to their small size and special surface characteristics, uniquely combine the

advantages of an improved detection of occult BBB alterations, adding the capability of visualizing subtle macrophage infiltration into active neuroinflammatory plaques. Moreover, VSOP differ from other magnetic nanoparticles in their capability to exclusively image subtle BBB disruptions. Several lesions could be detected that enhanced solely VSOP, indicating the sensitivity for additional neuroinflammatory processes so far missed by conventional contrast media. Thus, novel magnetic nanoparticles may contribute to resolve the clinico-radiological paradox in future human trials.

Abbreviations

BBB: blood brain barrier; CNS: central nervous system; Gd-DPTA: gadopentate dimeglumine; MRI: magnetic resonance imaging; MS: multiple sclerosis; PBS: phosphate buffered saline; PFA: paraformaldehyde; USPIO: ultrasmall superparamagnetic iron oxide particles; VSOP: very small superparamagnetic nanoparticles.

Competing interests

The authors declare that they have no competing interests.

Authors' contributions

ET carried out animal experiments, histological analysis, MR imaging, and drafted the manuscript. PA established the MR imaging and revised the manuscript. OA instructed the animal experiments and revised the manuscript. MS participated in the animal experiments and MR imaging. JS designed and provided the contrast media and revised the manuscript. MT supervised MR imaging and revised the manuscript. JW designed the study, carried out the MR imaging and drafted the manuscript. All authors read and approved the final manuscript.

Acknowledgements

We thank M. Paetzel for proofreading this manuscript as a native English speaker, and F. Zipp for general support on this study. This work was supported by a Charité Individual Research Funding Grant, and by the Deutsche Forschungsgemeinschaft (SFB-TRR43) to OA.

References

1. Grossman RI, Braffman BH, Brorson JR, Goldberg HI, Silberberg DH, Gonzalez-Scarano F: **Multiple sclerosis: serial study of gadolinium-enhanced MR imaging.** *Radiology* 1988, **169:**117-122.
2. Dousset V, Ballarino L, Delalande C, Coussemacq M, Canioni P, Petry KG, Caille JM: **Comparison of ultrasmall particles of iron oxide (USPIO)-enhanced T2-weighted, conventional T2-weighted, and gadolinium-enhanced T1-weighted MR images in rats with experimental autoimmune encephalomyelitis.** *AJNR Am J Neuroradiol* 1999, **20:**223-227.
3. Arbab AS, Liu W, Frank JA: **Cellular magnetic resonance imaging: current status and future prospects.** *Expert Rev Med Devices* 2006, **3:**427-439.
4. Baeten K, Hendriks JJ, Hellings N, Theunissen E, Vanderlocht J, Ryck LD, Gelan J, Stinissen P, Adriaensens P: **Visualisation of the kinetics of macrophage infiltration during experimental autoimmune encephalomyelitis by magnetic resonance imaging.** *J Neuroimmunol* 2008, **195:**1-6.
5. Wu YJ, Muldoon LL, Varallyay C, Markwardt S, Jones RE, Neuwelt EA: **In vivo leukocyte labeling with intravenous ferumoxides/protamine sulfate complex and in vitro characterization for cellular magnetic resonance imaging.** *Am J Physiol Cell Physiol* 2007, **293:**C1698-1708.
6. Wagner S, Schnorr J, Pilgrimm H, Hamm B, Taupitz M: **Monomer-coated very small superparamagnetic iron oxide particles as contrast medium for magnetic resonance imaging: preclinical in vivo characterization.** *Invest Radiol* 2002, **37:**167-177.
7. Berger C, Hiestand P, Kindler-Baumann D, Rudin M, Rausch M: **Analysis of lesion development during acute inflammation and remission in a rat model of experimental autoimmune encephalomyelitis by visualization of macrophage infiltration, demyelination and blood-brain barrier damage.** *NMR Biomed* 2006, **19:**101-107.
8. Floris S, Blezer EL, Schreibelt G, Dopp E, Pol SM van der, Schadee-Eestermans IL, Nicolay K, Dijkstra CD, de Vries HE: **Blood-brain barrier permeability and monocyte infiltration in experimental allergic encephalomyelitis: a quantitative MRI study.** *Brain* 2004, **127:**616-627.
9. Bruck W, Sommermeier N, Bergmann M, Zettl U, Goebel HH, Kretzschmar HA, Lassmann H: **Macrophages in multiple sclerosis.** *Immunobiology* 1996, **195:**588-600.
10. Raivich G, Banati R: **Brain microglia and blood-derived macrophages: molecular profiles and functional roles in multiple sclerosis and animal models of autoimmune demyelinating disease.** *Brain Res Brain Res Rev* 2004, **46:**261-281.
11. Bendszus M, Stoll G: **Caught in the act: in vivo mapping of macrophage infiltration in nerve injury by magnetic resonance imaging.** *J Neurosci* 2003, **23:**10892-10896.
12. Dousset V, Gomez C, Petry KG, Delalande C, Caille JM: **Dose and scanning delay using USPIO for central nervous system macrophage imaging.** *Magma* 1999, **8:**185-189.
13. Rausch M, Baumann D, Neubacher U, Rudin M: **In-vivo visualization of phagocytotic cells in rat brains after transient ischemia by USPIO.** *NMR Biomed* 2002, **15:**278-283.
14. Rausch M, Hiestand P, Baumann D, Cannet C, Rudin M: **MRI-based monitoring of inflammation and tissue damage in acute and chronic relapsing EAE.** *Magn Reson Med* 2003, **50:**309-314.
15. Rausch M, Hiestand P, Foster CA, Baumann DR, Cannet C, Rudin M: **Predictability of FTY720 efficacy in experimental autoimmune encephalomyelitis by in vivo macrophage tracking: clinical implications for ultrasmall superparamagnetic iron oxide-enhanced magnetic resonance imaging.** *J Magn Reson Imaging* 2004, **20:**16-24.
16. Vellinga MM, Oude Engberink RD, Seewann A, Pouwels PJ, Wattjes MP, Pol SM van der, Pering C, Polman CH, de Vries HE, Geurts JJ, Barkhof F: **Pluriformity of inflammation in multiple sclerosis shown by ultra-small iron oxide particle enhancement.** *Brain* 2008, **131:**800-807.
17. Dousset V, Brochet B, Deloire MS, Lagoarde L, Barroso B, Caille JM, Petry KG: **MR imaging of relapsing multiple sclerosis patients using ultra-small-particle iron oxide and compared with gadolinium.** *AJNR Am J Neuroradiol* 2006, **27:**1000-1005.
18. Wuerfel J, Tysiak E, Prozorovski T, Smyth M, Mueller S, Schnorr J, Taupitz M, Zipp F: **Mouse model mimics multiple sclerosis in the clinico-radiological paradox.** *Eur J Neurosci* 2007, **26:**190-198.
19. Smorodchenko A, Wuerfel J, Pohl EE, Vogt J, Tysiak E, Glumm R, Hendrix S, Nitsch R, Zipp F, Infante-Duarte C: **CNS-irrelevant T-cells enter the brain, cause blood-brain barrier disruption but no glial pathology.** *Eur J Neurosci* 2007, **26:**1387-1398.
20. Fleige G, Seeberger F, Laux D, Kresse M, Taupitz M, Pilgrimm H, Zimmer C: **In vitro characterization of two different ultrasmall iron oxide particles for magnetic resonance cell tracking.** *Invest Radiol* 2002, **37:**482-488.
21. Stroh A, Zimmer C, Werner N, Gertz K, Weir K, Kronenberg G, Steinbrink J, Mueller S, Sieland K, Dirnagl U, *et al.*: **Tracking of systemically administered mononuclear cells in the ischemic brain by high-field magnetic resonance imaging.** *Neuroimage* 2006, **33:**886-897.
22. Aktas O, Smorodchenko A, Brocke S, Infante-Duarte C, Schulze Topphoff U, Vogt J, Prozorovski T, Meier S, Osmanova V, Pohl E, *et al.*: **Neuronal damage in autoimmune neuroinflammation mediated by the death ligand TRAIL.** *Neuron* 2005, **46:**421-432.
23. Perl DP, Good PF: **Comparative techniques for determining cellular iron distribution in brain tissues.** *Ann Neurol* 1992, **32(Suppl):**S76-81.

24. Bar-Zohar D, Agosta F, Goldstaub D, Filippi M: **Magnetic resonance imaging metrics and their correlation with clinical outcomes in multiple sclerosis: a review of the literature and future perspectives.** *Mult Scler* 2008, **14:**719-27.
25. Barkhof F: **The clinico-radiological paradox in multiple sclerosis revisited.** *Curr Opin Neurol* 2002, **15:**239-245.
26. Filippi M: **Predictive value of MRI findings in multiple sclerosis.** *Lancet Neurol* 2002, **1:**9.
27. McFarland HF, Frank JA, Albert PS, Smith ME, Martin R, Harris JO, Patronas N, Maloni H, McFarlin DE: **Using gadolinium-enhanced magnetic resonance imaging lesions to monitor disease activity in multiple sclerosis.** *Ann Neurol* 1992, **32:**758-766.
28. Goodin DS: **Magnetic resonance imaging as a surrogate outcome measure of disability in multiple sclerosis: have we been overly harsh in our assessment?** *Ann Neurol* 2006, **59:**597-605.
29. Bendszus M, Ladewig G, Jestaedt L, Misselwitz B, Solymosi L, Toyka K, Stoll G: **Gadofluorine M enhancement allows more sensitive detection of inflammatory CNS lesions than T2-w imaging: a quantitative MRI study.** *Brain* 2008, **131:**2341-2352.
30. Arbab AS, Yocum GT, Rad AM, Khakoo AY, Fellowes V, Read EJ, Frank JA: **Labeling of cells with ferumoxides-protamine sulfate complexes does not inhibit function or differentiation capacity of hematopoietic or mesenchymal stem cells.** *NMR Biomed* 2005, **18:**553-559.
31. Frank JA, Miller BR, Arbab AS, Zywicke HA, Jordan EK, Lewis BK, Bryant LH Jr, Bulte JW: **Clinically applicable labeling of mammalian and stem cells by combining superparamagnetic iron oxides and transfection agents.** *Radiology* 2003, **228:**480-487.
32. Stroh A, Faber C, Neuberger T, Lorenz P, Sieland K, Jakob PM, Webb A, Pilgrimm H, Schober R, Pohl EE, Zimmer C: **In vivo detection limits of magnetically labeled embryonic stem cells in the rat brain using high-field (17.6 T) magnetic resonance imaging.** *Neuroimage* 2005, **24:**635-645.
33. Corot C, Robert P, Idee JM, Port M: **Recent advances in iron oxide nanocrystal technology for medical imaging.** *Adv Drug Deliv Rev* 2006, **58:**1471-1504.
34. Lossinsky AS, Shivers RR: **Structural pathways for macromolecular and cellular transport across the blood-brain barrier during inflammatory conditions. Review.** *Histol Histopathol* 2004, **19:**535-564.
35. Pan W, Cain C, Yu Y, Kastin AJ: **Receptor-mediated transport of LIF across blood-spinal cord barrier is upregulated after spinal cord injury.** *J Neuroimmunol* 2006, **174:**119-125.
36. Kreuter J, Gelperina S: **Use of nanoparticles for cerebral cancer.** *Tumori* 2008, **94:**271-277.
37. van Gelder W, Cleton-Soeteman MI, Huijskes-Heins MI, van Run PR, van Eijk HG: **Transcytosis of 6.6-nm gold-labeled transferrin: an ultrastructural study in cultured porcine blood-brain barrier endothelial cells.** *Brain Res* 1997, **746:**105-116.
38. Nighoghossian N, Wiart M, Cakmak S, Berthezene Y, Derex L, Cho TH, Nemoz C, Chapuis F, Tisserand GL, Pialat JB, *et al.*: **Inflammatory response after ischemic stroke: a USPIO-enhanced MRI study in patients.** *Stroke* 2007, **38:**303-307.
39. Saleh A, Schroeter M, Jonkmanns C, Hartung HP, Modder U, Jander S: **In vivo MRI of brain inflammation in human ischaemic stroke.** *Brain* 2004, **127:**1670-1677.
40. Taschner CA, Wetzel SG, Tolnay M, Froehlich J, Merlo A, Radue EW: **Characteristics of ultrasmall superparamagnetic iron oxides in patients with brain tumors.** *AJR Am J Roentgenol* 2005, **185:**1477-1486.
41. Taupitz M, Wagner S, Schnorr J, Kravec I, Pilgrimm H, Bergmann-Fritsch H, Hamm B: **Phase I clinical evaluation of citrate-coated monocrystalline very small superparamagnetic iron oxide particles as a new contrast medium for magnetic resonance imaging.** *Invest Radiol* 2004, **39:**394-405.

European Journal of Neuroscience, Vol. 26, pp. 1387–1398, 2007 doi:10.1111/j.1460-9568.2007.05792.x

CNS-irrelevant T-cells enter the brain, cause blood–brain barrier disruption but no glial pathology

Alina Smorodchenko,[1,*] Jens Wuerfel,[1,*] Elena E. Pohl,[2,*] Johannes Vogt,[2] Eva Tysiak,[1] Robert Glumm,[1] Sven Hendrix,[2] Robert Nitsch,[2] Frauke Zipp[1,†] and Carmen Infante-Duarte[1,†]
[1]Cecilie-Vogt-Clinic for Molecular Neurology, Charité-Universitaetsmedizin Berlin and Max-Delbrueck-Center for Molecular Medicine, Berlin, Germany
[2]Institute of Cell Biology and Neurobiology, Center for Anatomy, Charité-Universitaetsmedizin Berlin, Germany

Keywords: CNS, EAE, MRI, multiphoton microscopy, multiple sclerosis

Abstract

Invasion of autoreactive T-cells and alterations of the blood–brain barrier (BBB) represent early pathological manifestations of multiple sclerosis and its animal model experimental autoimmune encephalomyelitis (EAE). Non-CNS-specific T-cells are also capable of entering the CNS. However, studies investigating the spatial pattern of BBB alterations as well as the exact localization and neuropathological consequences of transferred non-CNS-specific cells have been thus far lacking. Here, we used magnetic resonance imaging and multiphoton microscopy, as well as histochemical and high-precision unbiased stereological analyses to compare T-cell transmigration, localization, persistence, relation to BBB disruption and subsequent effects on CNS tissue in a model of T-cell transfer of ovalbumin (OVA)- and proteolipid protein (PLP)-specific T-cells. BBB alterations were present in both EAE-mice and mice transferred with OVA-specific T-cells. In the latter case, BBB alterations were less pronounced, but the pattern of initial cell migration into the CNS was similar for both PLP- and OVA-specific cells [mean (SEM), 95×10^3 (7.6×10^3) and 88×10^3 (18×10^3), respectively]. Increased microglial cell density, astrogliosis and demyelination were, however, observed exclusively in the brain of EAE-mice. While mice transferred with non-neural-specific cells showed similar levels of rhodamine-dextran extravasation in susceptible brain regions, EAE-mice presented huge BBB disruption in brainstem and moderate leakage in cerebellum. This suggests that antigen specificity and not the absolute number of infiltrating cells determine the magnitude of BBB disruption and glial pathology.

Introduction

The blood–brain barrier (BBB) is a complex structure that consists of endothelial cells, pericytes, perivascular macrophages and astrocytic endfeet. The capillary brain endothelial cells are connected by tight junctions that contribute to the formation of an impermeable and electrically resistant barrier, which provides homeostasis and restricts the leucocyte traffic into the CNS (Engelhardt, 2006). Activated and possibly also inactivated lymphocytes, however, can cross the endothelial layer and make contact with the normal CNS even in the absence of inflammation. This immune surveillance is believed to be essential for the protection of the brain from pathogen-induced damage and does not appear to affect BBB integrity (Brabb *et al*., 2000; Hickey, 2001). In the case of antigen recognition, such as CNS infection or autoimmune attack, T-cells may initiate an inflammatory cascade that leads to BBB breakdown and the penetration of much higher numbers of activated leucocytes into brain parenchyma (Hickey *et al*., 1991; Bechmann *et al*., 2007). In multiple sclerosis (MS) and its animal model, experimental autoimmune encephalomyelitis (EAE), the invasion of encephalitogenic T-cells through the BBB (Wekerle *et al*., 1986) and leakage of brain capillaries (Kermode *et al*., 1990) are considered earlier manifestations of the autoimmune pathology. Moreover, using high-resolution magnetic resonance imaging (MRI), we have recently shown that BBB alterations in the murine brain frequently precede clinical development of EAE (Wuerfel *et al*., 2007).

The role of non-CNS-specific T-cells in BBB disruption and glial alterations is less well understood. It was shown *in vitro*, that ovalbumin (OVA)-specific activated T-cells are able to damage brain vascular endothelial cells (Sedgwick *et al*., 1990) and to alter the blood–retinal barrier (Hu *et al*., 2000). However, no study has so far been performed that systematically compares T-cell transmigration, localization, persistence, relation to BBB disruption and subsequent effects on CNS tissue in transfer models of labelled activated encephalitogenic vs non-CNS-specific T-cells *in vivo*. Therefore, we combined two imaging approaches, MRI and multiphoton microscopy (MPM), to monitor T-cell infiltration and CNS alterations in a model of T-cell transfer of OVA- and proteolipid protein (PLP)-specific T-cells *in vivo*.

Materials and methods

Animals

Female SJL/J mice (6–8 weeks old) were purchased from Charles River (Sulzfeld, Germany). C57BL/6 transgenic mice expressing green fluorescent protein (GFP) under the control of the β-actin

Correspondence: Professor Frauke Zipp, as above.
E-mail: frauke.zipp@charite.de
*A.S., J.W and E.P. contributed equally to this work.
†C.I.-D. and F.Z. contributed as senior authors to this work.

Received 12 May 2007, revised 25 July 2007, accepted 28 July 2007

promoter (Okabe *et al.*, 1997) were a gift from Dr Masura Okabe (Osaka University, Japan). Transgenic mice were backcrossed to SJL background for six generations in our animal facilities.

Models of adoptive transfer

For transfer of PLP- or OVA-specific T-cells, mice were immunized in the footpads with 250 mg murine PLP peptide p139–151 (Pepceuticals, Leicester, UK) or OVA (Sigma-Aldrich, Hamburg, Germany), as previously described (Aktas *et al.*, 2005). At Day 10, draining lymph node cells were isolated and restimulated with 12.5 μg/mL PLP or OVA for 4 days at 37 °C (Aktas *et al.*, 2005). Thereafter, T-cells were incubated with 50 μM carboxyfluorescein diacetate succinimidyl ester [5(6)-CFDA, Molecular Probes], as described previously (Gimsa *et al.*, 2001), and injected i.v. into syngeneic recipients (12×10^6 blasts per mouse; four mice received PLP- and eight mice received OVA-specific cells). Activation of T-cells was monitored via the expression of CD25, CD44 and CD69 (BD Biosciences, Heidelberg, Germany), using flow cytometry as described previously (Nitsch *et al.*, 2004).

To confirm the accuracy of the data obtained by transferring CFDA-labelled cells, three additional experiments were performed, as described for non-transgenic cells, using GFP-transgenic SJL mice as a source of PLP-specific GFP cells. Two mice received 12×10^6 GFP-PLP-specific blasts; one mouse received 18×10^6 blasts.

Mice were scored for EAE as follows: 0, no disease; 1, tail weakness; 2, paraparesis; 3, paraplegia; 4, paraplegia with forelimb weakness or paralysis; and 5, moribund or dead animals. All procedures were performed in accordance with protocols approved by the local animal welfare committee, LAGetSi (Landesamt fuer Arbeitsschutz, Gesundheitsschutz und technische Sicherheit), Berlin, Germany, all experiments conformed to the European Communities Council Directives (86/609/EEC).

MRI analysis

MRI was performed at Day 9 after induction of EAE (score 2.5–3.5) or transfer of OVA-specific T-cells on a 7 Tesla rodent scanner (Pharmascan 70/16AS, Bruker, Germany) applying a 20 mm RF-Quadratur-Volume head coil. Mice were placed on a heated circulating water blanket to ensure constant body temperature of 37 °C. During image acquisition, mice were anaesthetized with 1–1.5% Isofluran (Forene, Abbott, USA) under constant ventilation monitoring. Axial and coronal T1-weighted images (MSME; TE 10.5 ms, TR 322 ms, 0.5 mm slice thickness, Matrix 256 × 256, FOV 2.8 cm) were acquired before and after i.v. injection of 0.5 mmol/kg Gadopentate dimeglumine (Gd; Magnevist, Schering, Germany).

MPM and data analysis

One day after MRI investigation, animals were injected i.v. with 0.5 mg rhodamine-dextran (Sigma-Aldrich) and decapitated 5 min afterwards. Brains were removed and divided into brainstem, cerebellum and hemispheres. Cortexes were cut into 400-μm-thick slices with a Vibratome (NVSLM1; Motorized Advance Vibroslice). Brainstem, cerebellum and cortex slices containing the hippocampal formation were placed in a thermoregulated chamber and continuously perfused with aerated (95% O_2, 5% CO_2) artificial cerebrospinal fluid. T-cells and brain vessels, stained with CFDA and rhodamine-dextran, respectively, were visualized by a multiphoton confocal laser-scanning microscope (Leica, Heidelberg, Germany) equipped with a 20 × water-immersion objective (numerical aperture 0.95; Olympus). Both fluorescent dyes were excited at a wavelength of 840 nm. Fluorescence from green (CFDA or GFP) and red (rhodamine-dextran) channels was collected with two external non-descanned detectors using 525/50 and 610/75 nm filters, respectively. Three- or four-dimensional (*x–y* plane, *t*, or *x–y–z* plane, *t*) images were acquired at depth range 50–200 μm. Z-stacks were rendered in 3D using Volocity Visualization (Improvision, England).

Immunohistochemistry and fluorescence microscopy

After MPM analysis, slices were collected and fixed in 4% paraformaldehyde (PFA) and incubated in phosphate-buffered sucrose solution (0.8–1.4 M) for 1 week before horizontal cutting into 20-μm sections at −31 °C (Cambridge Instruments, Nussloch, Germany). For light microscopy, sections were incubated with 3% H_2O_2 for blocking of endogenous peroxidase, washed three times with phosphate-buffered saline (PBS), and soaked in 10% normal goat serum to block non-specific binding. Thereafter, sections were incubated overnight at 4 °C with one of the following antibodies: rat-anti-rat RTIBu/mouse H-2IA (1 : 4; Serotec, UK/International), rabbit anti-IBA-1 (1 : 1000; Wako Chemicals, Neuss, Germany), rabbit anti-glial fibrillary acidic protein (GFAP; 1 : 750; DAKO Deutschland GmbH, Germany) or rat anti-CD3 antibody (1 : 100; Serotec UK/International). As secondary antibodies, biotinylated anti-rat Ig (1 : 250; Linaris Biologische Produkte, Wertheim, Germany) and anti-rabbit Ig antibodies (1 : 250; Vector Laboratories, Burlingame, CA, USA) were incubated for 2 h at room temperature. Next, sections were preincubated with ABC-solution (ABC-Elite; Vector Laboratories) and developed with 0.03% H_2O_2 and 1% 3,3′-diaminobenzidine tetrahydrochloride (DAB; Sigma-Aldrich).

For stereological analysis, mice were lethally anaesthetized (0.5% ketamine i.p.) and transcardially perfused with tyrode followed by 4% PFA containing 0.05% glutaraldehyde and 15% picric acid. Spinal cords were removed, postfixed (2 h in 4% PFA) and cryoprotected (30% sucrose in Tris-buffered saline) at 4 °C for 24 h. Next, tissue was frozen in tissue-freezing medium and stored at −80 °C. Tissue blocks were cut into entire series of 50-μm transverse sections on the cryostat. Every fourth section was selected (with a random start) and stained with a biotin-conjugated anti-CD3 antibody (BD Biosciences) for 2 h at room temperature. Sections were then washed and transferred to ABC solution for 1 h. After final washes in PBS, sections were stained with 0.07% DAB activated with 0.001% H_2O_2 in PB, mounted on gelatine-coated slides, dehydrated through an ascending series of ethanol, and coverslipped.

To assess demyelination, paraffin-embedded spinal cords were cut longitudinally in 10-μm sections. After rehydration, selected sections were used for CD3 staining using the microwave antigen retrieval technique. Anti-CD3 from Serotec (1 : 250) was used as primary antibody, and anti-rat biotin as secondary antibody. Sections were developed with the ABC-DAB method described above. After several rinses in PBS, counterstaining with Luxol Fast Blue was performed as described elsewhere (Kluver & Barrera, 1953). Finally, sections were dehydrated with ascending alcohol and coverslipped. Selected sections were examined under light microscopy and digitally photographed (Olympus BX-51, Hamburg, Germany).

For fluorescence microscopy, slides stained with primary anti-CD3 and anti-IBA-1 antibodies were further incubated with an anti-rat Ig Alexa 488 and anti-rabbit Ig Alexa 568 (Molecular Probes, Eugene, OR, USA) for 2 h at room temperature. Finally, the sections were washed three times with PBS for 15 min and coversealed with immumount (Thermo Electron Corporation, Pittsburgh, PA, USA). Images were taken with a filter U-MNIBA using an Olympus digital camera.

Stereological analysis and counting procedure

Total numbers of CD3-positive cells were quantified in a defined region of interest in the ventral horn of the spinal cord, levels L3–L5. This region of interest was determined by characteristic anatomical formations of α-motor neurons within the grey matter, with a typical posterolateral cluster at L5 defining the lower boundary and an anterolateral cluster at L3 defining the upper boundary (Nicolopoulos-Stournaras & Iles, 1983). Five sections were chosen for stereological analysis of each mouse (four mice per group).

High-precision design-based stereological assessments were performed with a stereology workstation, consisting of a modified light microscope (Zeiss Axioplan with Plan-Neofluar objectives: 10 × for delineation of the investigated area; 40 × for CD3 counting in mice spinal cord transverse sections), motorized specimen stage for automatic sampling (Ludl Electronics, Hawthorne, NY, USA), video camera (Microfire, Optronics, CA, USA) and software (StereoInvestigator, MicroBrightField, Williston, VT, USA). The investigator was blinded to the experimental conditions. Total numbers of CD3-positive cells were determined with the optical fractionator, identified by CD3 staining and morphology, and were calculated from the numbers of counted CD3 cells and the corresponding sampling probabilities.

Statistical analysis

Comparisons between mouse groups were performed by one-way analysis of variance for independent measures. To determine which means were significantly different from the mean of the corresponding control group *post hoc*, Bonferroni's multiple comparison tests for pairwise comparisons were performed. All calculations were performed with GraphPad Prism version 4.00 for Windows (GraphPad Software, San Diego, CA, USA).

Results

BBB permeability in models of encephalitogenic and non-CNS-specific T-cell transfer

EAE was induced by adoptive transfer of activated PLP-specific T-cells into SJL syngeneic mice. Mice developed clinical signs from Day 10 to 14 after transfer (score 2.5–3.5), coinciding with about 20% bodyweight loss. Similarly, SJL mice were transferred with the same amount of OVA-specific T-cells (OVA-mice). These mice did not develop any clinical signs and did not lose bodyweight during the examination period. Before transfer, both PLP- and OVA-specific cells were activated (data not shown). Naive mice served as controls.

All EAE-mice showed Gd-enhancing lesions at Day 9 after cell transfer. Lesions were confined to brainstem, cerebellum and periventricular areas (Fig. 1A–C), and were absent in control animals. None of the OVA-mice developed distinctive parenchymal lesions equivalent to EAE animals (Fig. 1D–F). However, pronounced vascular/perivascular enhancement also appeared in OVA-animals in comparison with naïve mice, especially in the cerebellar, brainstem and periventricular area (Fig. 1F). Immunohistochemical examination of brain regions presenting Gd-enhancement demonstrated inflammatory foci with T-cell infiltrations at all sites of lesions, which is indicative of the accuracy of our MRI measurements (Fig. 2). Prior to immunohistochemical analysis, brains were removed 1 day after MRI, divided into brainstem, cerebellum and cortex region containing the hippocampal formation, and examined on MPM, as described in Materials and methods. Furthermore, BBB alterations shown on MRI were validated by using MPM to examine leakage of rhodamine-dextran (Fig. 3). BBB disruptions were observed in both EAE and OVA-mice. However, BBB alterations were less pronounced in mice transferred with CNS-irrelevant T-cells (Fig. 3D–F). In line with the BBB alteration detected by MRI, leakage of rhodamine-dextran – in both models of T-cell transfer – was predominantly confined to cerebellar blood vessels and to brainstem vessels adjacent to the cerebellum (Fig. 3A and B, and D and E), but was absent in any of the cortical regions analysed (Fig. 3C and F). Control naïve animals showed no rhodamine-dextran extravasation or Gd-enhancement (Figs 1G–I and 3G–I).

Brain localization of infiltrating encephalitogenic and non-CNS-specific T-cells

We further aimed to monitor the routes of T-cell infiltration into the brain in both T-cell-transfer models. Using MPM, we examined the infiltration of CFDA-labelled T-cells into three different brain regions (brainstem, cerebellum and cortex region containing hippocampal formation) at onset of EAE or 10 days after transferring OVA-specific T-cells. Vessels were visualized by injecting rhodamine-dextran (see Materials and methods).

In EAE-mice, CFDA-positive encephalitogenic T-cells were predominantly distributed in perivascular cuffs and adjacent parenchyma of brainstem and cerebellum, as well as in areas of dense capillary networks within neuronal cell layers of the ammons horn and dentate gyrus of the hippocampus, although no extravasation was visible in this region (Fig. 4A). CFDA-positive activated OVA-specific T-cells were also detected, widely distributed in all brain regions examined at Day 10 after cell transfer (Fig. 4B).

To exclude the possibility that instability of CFDA-labelling during the period of experimentation influenced our results, we performed a series of EAE-transferring PLP-specific green T-cell blasts from GFP-transgenic SJL mice (Okabe *et al*., 1997) in three different SJL recipients. Two mice were transferred with the standard amount of 12×10^6 blasts; the third mouse received an overload of blasts (18×10^6) in order to visualize better invading T-cells. In mice transferred with 12×10^6 blasts, GFP-transgenic cells accumulated in brain parenchyma to the same extent and with the same distribution as CFDA-labelled T-cells (data not shown). In the mouse injected with 18×10^6 cells, a larger amount of infiltrated T-cells was detected, although this mouse developed similar clinical signs to mice injected with 12×10^6 blasts. The large amount of cells infiltrating the brainstem coincided with massive disruption of the BBB in this region, whereas hippocampal vessels remained intact despite the huge number of cells infiltrating this area (Fig. 4C).

In addition, we performed experiments to demonstrate that OVA-specific CFDA-labelled cells that were detected 10 days post-injection were indeed T-cells and not microglia/macrophages that could have incorporated the dyes by phagocytosis. Figure 4D shows that T-cells (green) and IBA-1-positive phagocytes (red) were not colocalized, confirming the stable presence for at least 10 days of non-CNS-specific T-cells inside the brain.

Stereological quantification of neural- and non-neural-specific T-cells within the CNS

The data shown above demonstrate that OVA-specific T-cells were able to transmigrate into the CNS and promote BBB alterations. We

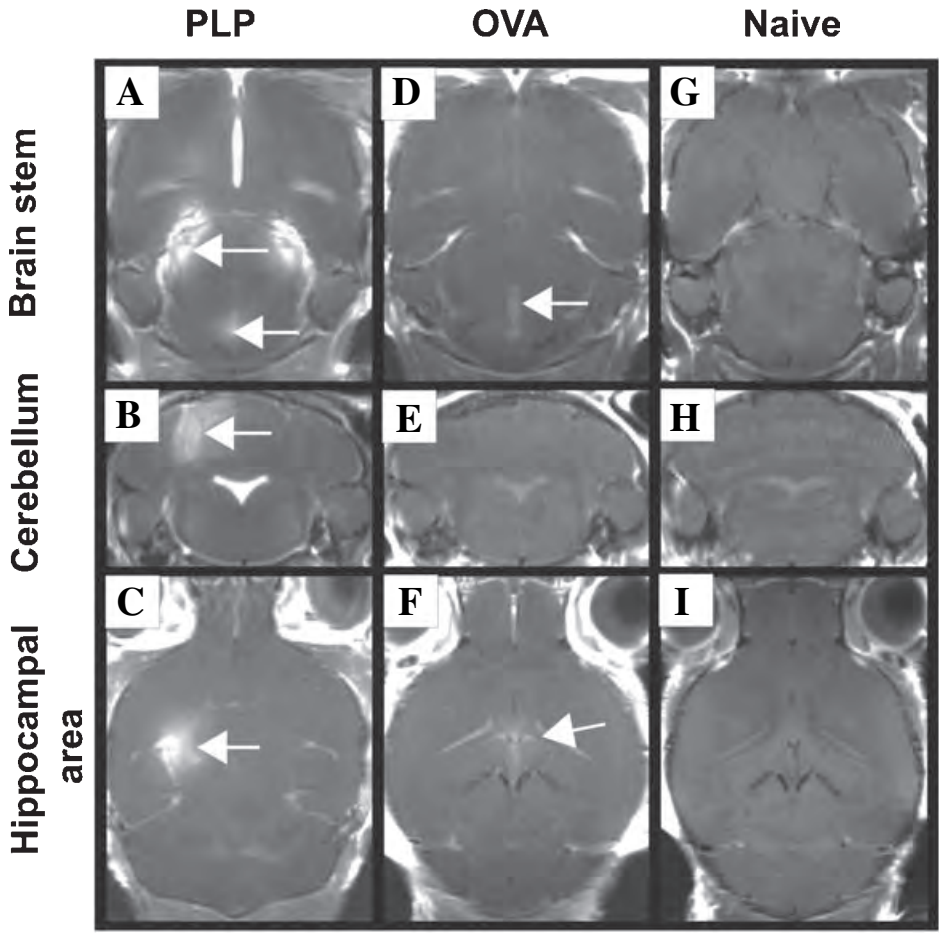

FIG. 1. Vascular extravasation and lesions in MRI of encephalitogenic vs CNS-irrelevant T-cell transfer models. MR images at Day 9 post-injection of proteolipid protein (PLP; A–C)- or ovalbumin (OVA; D–F)-specific T-cells and control naïve SJL/J mice (G–I). Images are representative of four mice transferred with PLP-specific cells, four mice transferred with OVA-specific T-cells and three control mice. The images show the enhancement of T1-weighted signal intensity after i.v. administration of 0.5 mmol/kg Gd. (A–C) In all mice transferred with PLP-specific T-cells, Gd lesions were detectable in the brainstem, the cerebellum and/or in the periventricular area (arrows), but were absent in the hippocampal area. (D–F) Fifty percent of mice transferred with non-CNS-(OVA)-specific T-cells showed perivascular signal increase, predominantly in the periventricular area (arrows) and in the brainstem and cerebellar region, but not in the hippocampus. (G–I) In none of the control mice was BBB leakage detectable.

asked whether the increased perivascular enhancement in MRI correlated with the infiltration of OVA-specific cells. To compare amounts of CNS-infiltrating T-cells in PLP and OVA transfer models, we performed high-precision unbiased stereological analysis. This design-based stereological assessment was carried out in representative small areas of the CNS, in which all structures are in close proximity, i.e. lumbar spinal cord transverse sections (L3–L5). Quantification was performed on Days 7, 10 and 23 after cell transfer. Naïve mice served as controls. Figure 5A shows an example of T-cell infiltration in the spinal cord at Day 10 post-transfer of OVA- and PLP-specific T-cells. Figure 5B shows that similar amounts of both PLP- and OVA-specific T-cells were indeed able to penetrate the CNS [mean (SEM), 95×10^3 (7.6×10^3) and 88×10^3 (18×10^3), respectively]. Interestingly, while PLP-specific T-cells were detectable in the same frequency in the first 2 weeks and slightly decreased thereafter, the presence of OVA-specific T-cells in spinal cord was transient and the amount of infiltrating cells returned to control values after 3 weeks [mean (SEM), control = 13×10^3 (2.4×10^3); PLP = 66×10^3 (8.6×10^3); OVA = 17×10^3 (3.2×10^3)]. This indicates that equal numbers of PLP- and OVA-specific T-cells infiltrated the CNS, but only the encephalitogenic T-cells persisted (Fig. 5B).

Glial pathology in the transfer models with encephalitogenic and CNS-irrelevant T-cells

Because activated non-neural-specific T-cells are capable of transmigrating through the BBB, persist for a short time and alter BBB, we wondered to what extent the different T-cell populations interact with and affect glial cells. Brain slices from EAE- and OVA-mice were analysed immunohistochemically. Increased microglial cell density (IBA-1 staining, Fig. 6A) and astrogliosis (GFAP staining, Fig. 6B) were both observed exclusively in the brain of EAE-mice, but not in brain areas of OVA-mice or in control animals at Day 10 post-injection. Gliosis was detected in all brain regions investigated, i.e. brainstem, cerebellum and hippocampal area. However, more accentuated astrogliosis was observed in brainstem and cerebellal areas (Fig. 6B). In addition, we monitored, in both transfer models spinal cord demyelination by Luxol Fast Blue staining (Fig. 7A), and activation of antigen-presenting cells by analysing the brain expression of MHC class II (Fig. 7B). In concordance with the data on gliosis, demyelinated axons and MHC class II-positive cells were detected exclusively in CNS regions of EAE-mice (Fig. 7A and B, respectively). Thus, in the absence of antigen-recognition, activated

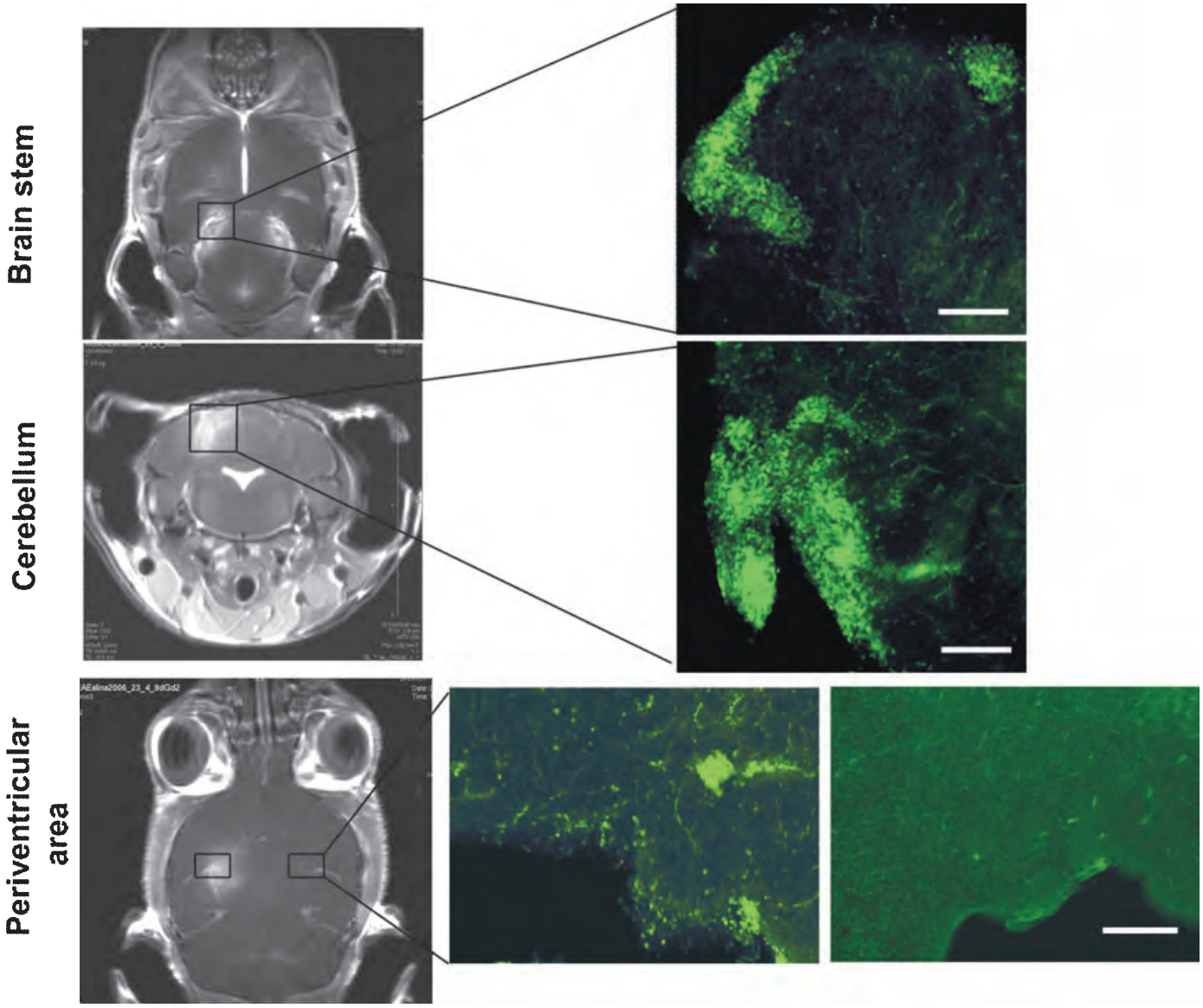

FIG. 2. Immunohistochemical examination of brain regions presenting with Gd enhancement. Brain sections of mice transferred with PLP-specific cells showing Gd-enhancing lesions (left panels) at Day 10 post-injection were analysed immunohistochemically for the presence of CD3-positive cell infiltrations (right panels). One day after MRI, brainstem, cerebellum and cortex slices containing the hippocampal formation were examined by MPM prior to preparation of cryosections and CD3 staining. CD3-positive PLP-specific T-cells (green) were distributed in the parenchyma of all brain regions in which BBB leakage was found (scale bar: 100 μm). Results are representative of EAE-mice.

T-cells, i.e. OVA-specific T-cells, were able to penetrate the CNS but did not promote alterations in cellular architecture.

Discussion

In the present study we compared in a murine model of adoptive transfer the ability of CNS- and non-CNS specific T-cells to alter BBB integrity, penetrate the CNS and affect glial cell activity. To monitor accurately BBB integrity, we used both MRI *in vivo* and MPM *ex vivo*. Additionally, MPM enabled us not only to monitor BBB alteration but also to localize strictly those T-cells that were transferred and to distinguish them from endogenous T-cells of unknown specificity.

Both T-cell groups, those specific for the myelin antigen PLP and those for the non-neural antigen OVA, caused microscopic BBB alterations. Although MRI revealed only slight perivascular signal intensity changes (potentially by Gd-DTPA leakage into the Virchow-Robin-spaces) in susceptible regions of the brain, we clearly demonstrated BBB breakdown by extravasation of rhodamine-dextran in MPM. BBB leakage occurred in the absence of any form of antigen presentation inside the brain, as, in contrast to an earlier report, we did not administer OVA into the mouse CNS before or during T-cell transfer (Westland *et al*., 1999). Previous studies showed that the cerebellum (Tonra *et al*., 2001; Muller *et al*., 2005; Silwedel & Forster, 2006), certain regions of the periventricular area (Ueno *et al*., 2000) and the brainstem (Muller *et al*., 2005) are particularly susceptible to alterations of BBB integrity under inflammatory conditions. Our MRI

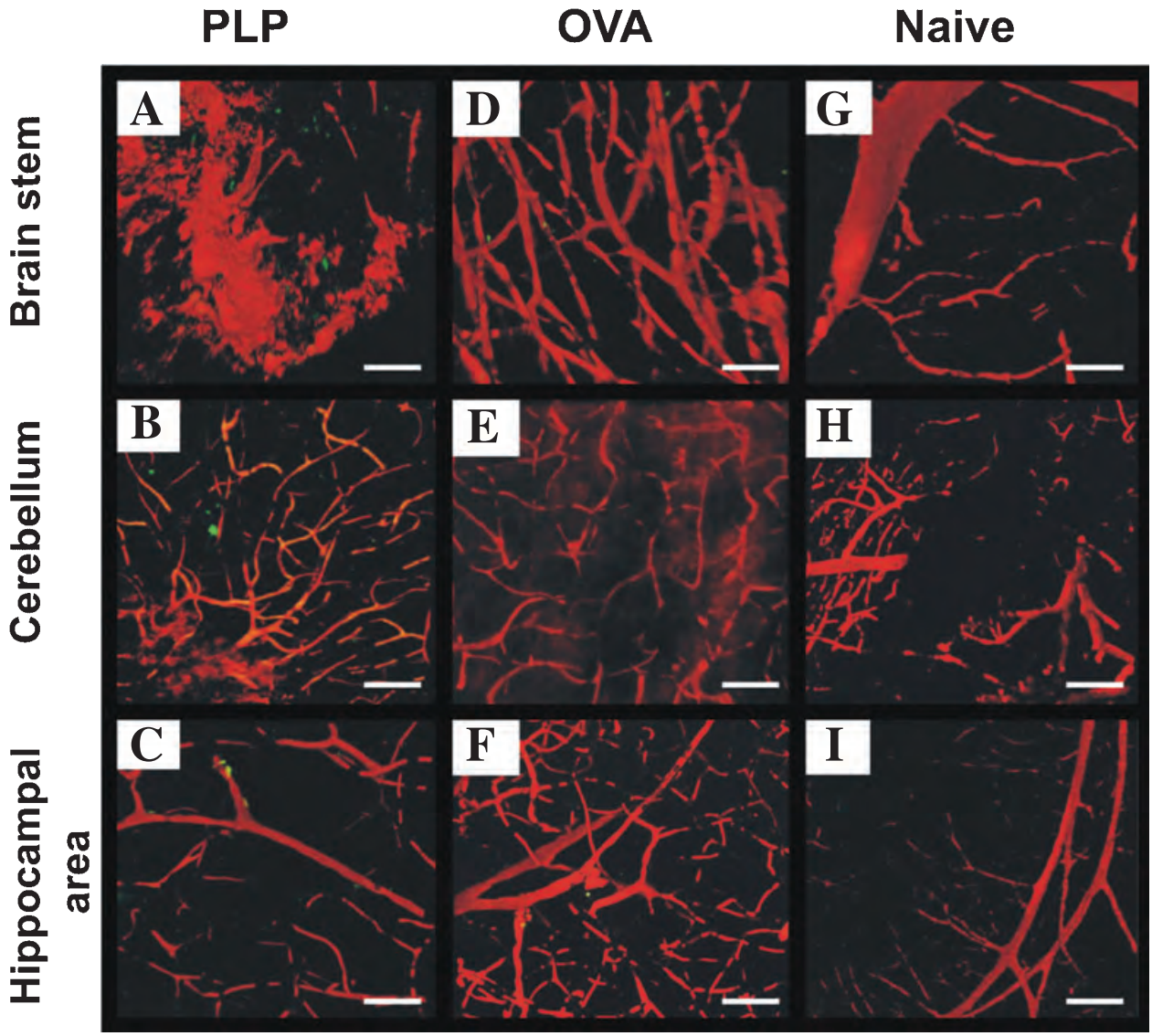

FIG. 3. Multiphoton images in models of encephalitogenic vs CNS-irrelevant T-cell transfer. Three-dimensional MPM imaging of vessels in brain parenchyma of mice transferred either with CFDA-SE-labelled proteolipid protein (PLP)-specific (A–C) or ovalbumin (OVA)-specific T-cells (D–F). Naïve mice served as control (G–I). Brain vessels were visualized *in vivo* at Day 10–12 post-transfer by i.v. injecting 0.5 mg rhodamine-dextran 5 min before decapitation. (A–C) Massive extravasation of rhodamine-dextran in brainstem (A) of all EAE-mice compared with moderate leakage in the cerebellum (B). No leakage was detected in hippocampal areas (C). (D–F) Moderate leakage was observed in both the brainstem (D) and cerebellum (E), and was absent in the hippocampal area (F) of all mice transferred with OVA-specific T-cells. (G–I) Vessels of naïve SJL mice were intact. Images are representative of four mice transferred with PLP-specific cells, four mice transferred with OVA-specific T-cells and two control mice. Scale bar: 100 μm.

and MPM data go beyond these observations, as we showed an increased susceptibility of cerebellar and periventricular vessels even in the absence of the inflammatory cascade, i.e. in the context of CNS-irrelevant T-cell transfer. Furthermore, we detected an increased BBB disruption in brainstem regions adjacent to the cerebellum. Anatomical peculiarities of cerebellar vessels, also vascularizing the adjacent area of the brainstem, indicate a susceptibility of this region for BBB alterations (Silwedel & Forster, 2006). Although BBB disruption was more pronounced in mice transferred with CNS-specific cells, the pattern of initial cell migration into the brain parenchyma was similar for both PLP- and OVA-specific cells. This finding contradicts a recent murine study reporting that activated non-CNS-specific cells failed to migrate into the CNS (Archambault *et al*., 2005), but is in line with data in rats reported as early as the beginning of the 1990s (Hickey

FIG. 4. Multiphoton imaging of CFDA-labelled proteolipid protein (PLP)- and ovalbumin (OVA)-specific infiltrating T-cells. Infiltrating T-cells were visualized at the onset of EAE or 10 days after transferring non-neural-specific T-cells. Vessels were labelled with rhodamine-dextran as described for Fig. 3. (A and B) Infiltrating T-cells were detected in all brain regions analysed in both PLP and OVA transfer models. Cell numbers are not provided as these multiphoton images are not suitable for quantification. (C) Multiphoton imaging of brainstem and cortex of SJL/J mice after adoptive transfer of GFP-transgenic PLP-specific cells (18×10^6) from SJL mice. Large numbers of specific transgenic T-cells invaded both brainstem and hippocampal areas of mouse brain, although in the cortical area no BBB leakage was observed. Scale bar: 50 μm. (D) Multiphoton confocal 3D imaging of IBA-positive cells and CFDA-positive T-cells. Immunohistochemical analysis of IBA-1 expression in cerebellar tissue was performed at Day 10 post-injection of CFDA-labelled OVA-specific T-cells. The 3D picture was reconstructed from 16 images (z-stack, 0–17 μm death) using Volocity Visualization software (Improvision). T-cells (green) were not colocalized with IBA-1-positive cells (red). Scale bar: 50 μm.

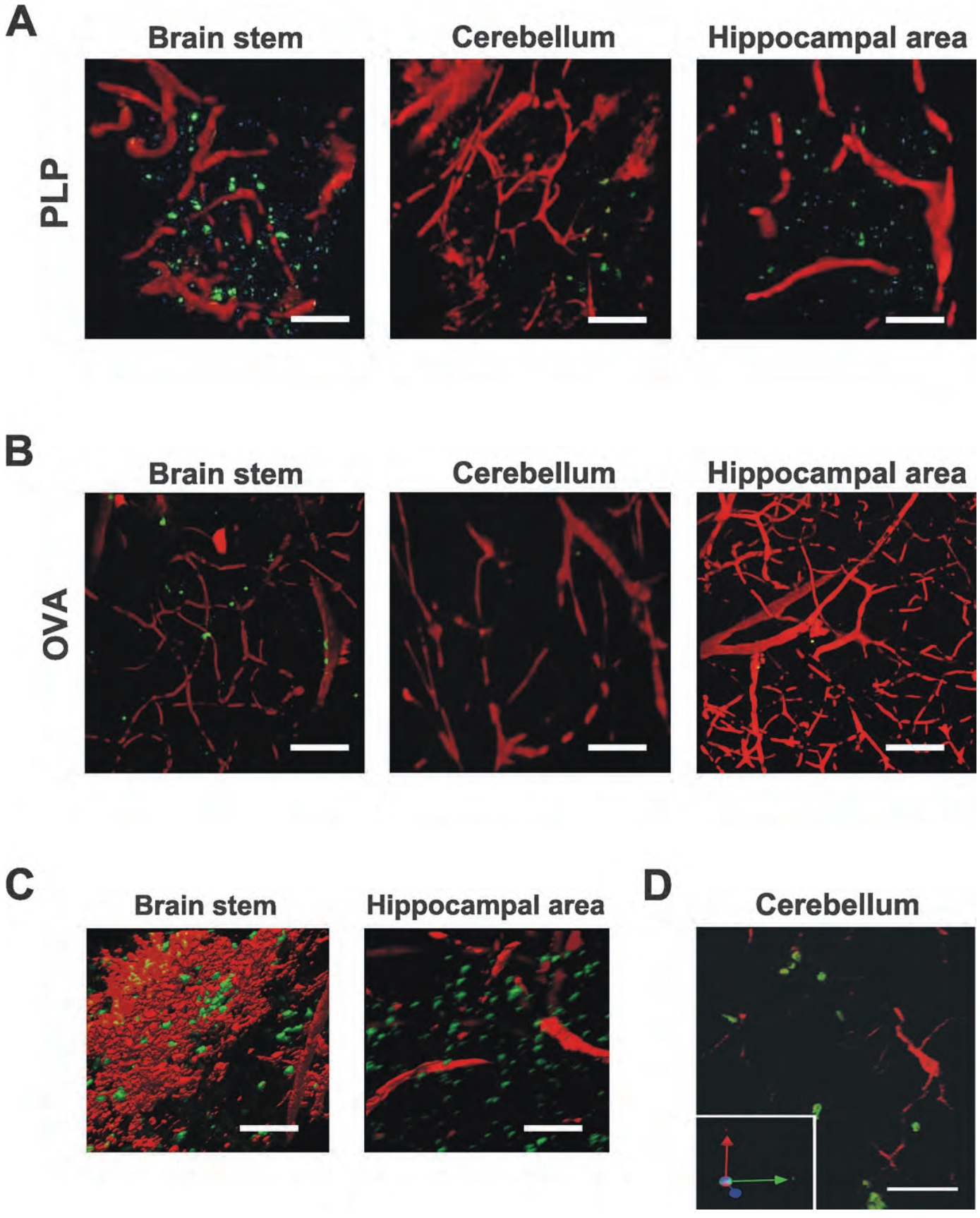

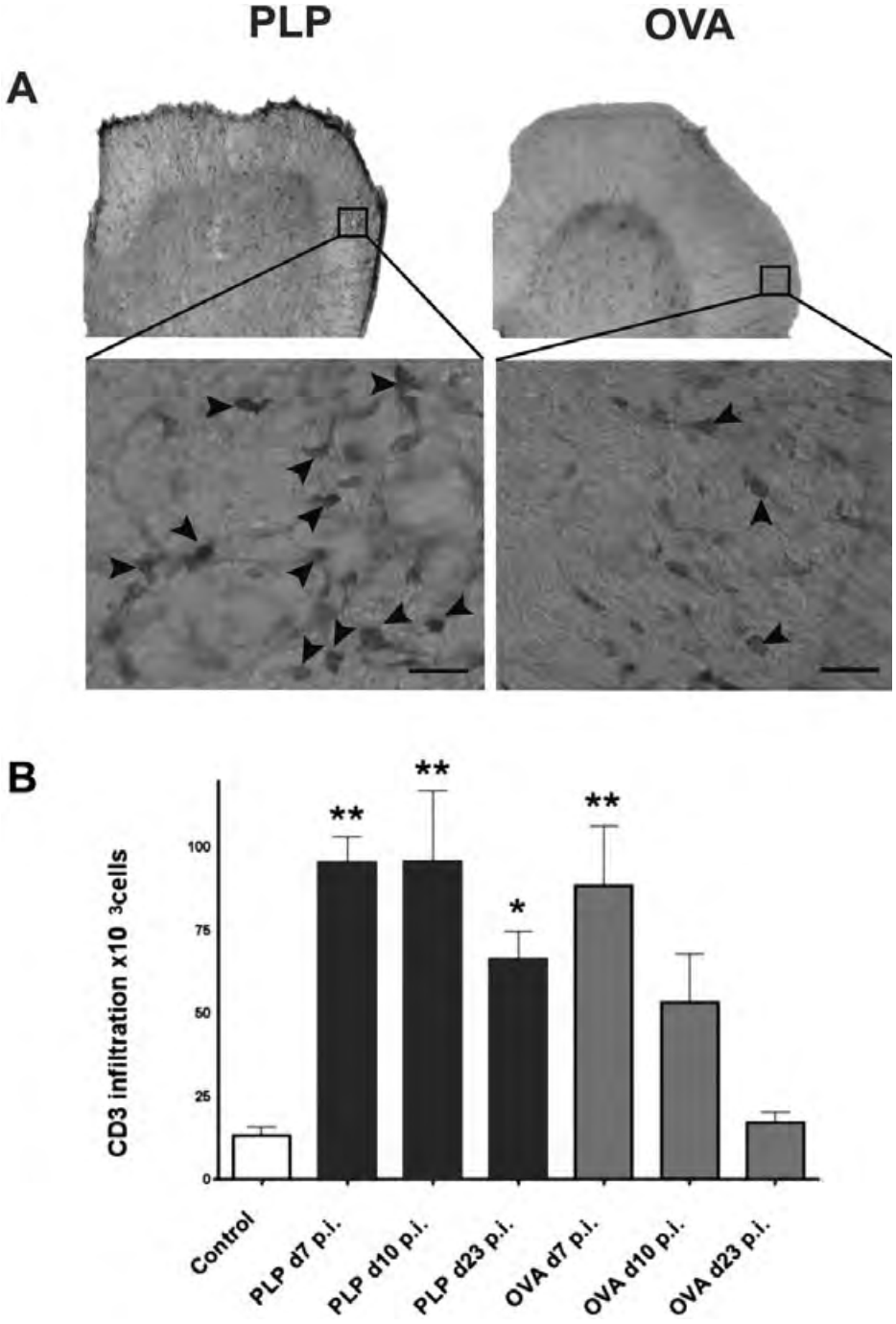

FIG. 5. Dynamic of T-cell permanence in the CNS in the model of ovalbumin (OVA)-specific T-cell transfer. (A) Example of infiltration of CD3-positive cells (arrows) into the lumbar spinal cord at Day 10 post-injection (p.i.) of proteolipid protein (PLP)-specific (left panels) and OVA-specific cells (right panels). An overview of the ventral horn and a section in higher magnification are depicted. Scale bar: 20 μm. (B) Stereological quantification of CD3-positive cells in transverse sections of lumbar spinal cord (levels L3–L5) from mice transferred with either PLP- (black bars) or OVA-specific (grey bars) T-cells. Analyses were performed at Day 7, 10 and 23 p.i., and show that although the same numbers of PLP- and OVA-specific T-cells were able to infiltrate the CNS, the amount of infiltrating OVA-specific T-cells decreased over time and returned to control values after 3 weeks. Mice per group = 4; mean number of sections counted per mouse = 5.1; base of counting spaces = 50 × 50 μm; height of counting spaces = 6 μm; guard zone from top of section = 1 μm; mean section thickness = 13.01 μm; mean number of counting spaces per sample = 469; mean number of counted T-cells per sample = 815; average predicted coefficient of error of estimated total number of T-cells = 0.0468. Date represent mean ± SD. *$P < 0.05$; **$P < 0.01$.

et al., 1991) and confirmed many years later in a study on rat blood–retinal barrier (Hu *et al*., 2000). More recently, Kawakami *et al*. showed that OVA-specific T-cells were able to enter the CNS and move through the parenchyma. However, only cells encountering their antigen persisted and interacted with neural cells (Kawakami *et al*., 2005). Using MPM in living brain slice cultures, we previously showed that OVA-specific T-cells can directly contact neurons once they are activated (Nitsch *et al*., 2004). Here we show that *in vivo*, OVA-specific T-cells infiltrate the CNS and induce transient disruption of the BBB, but do not lead to a tissue response.

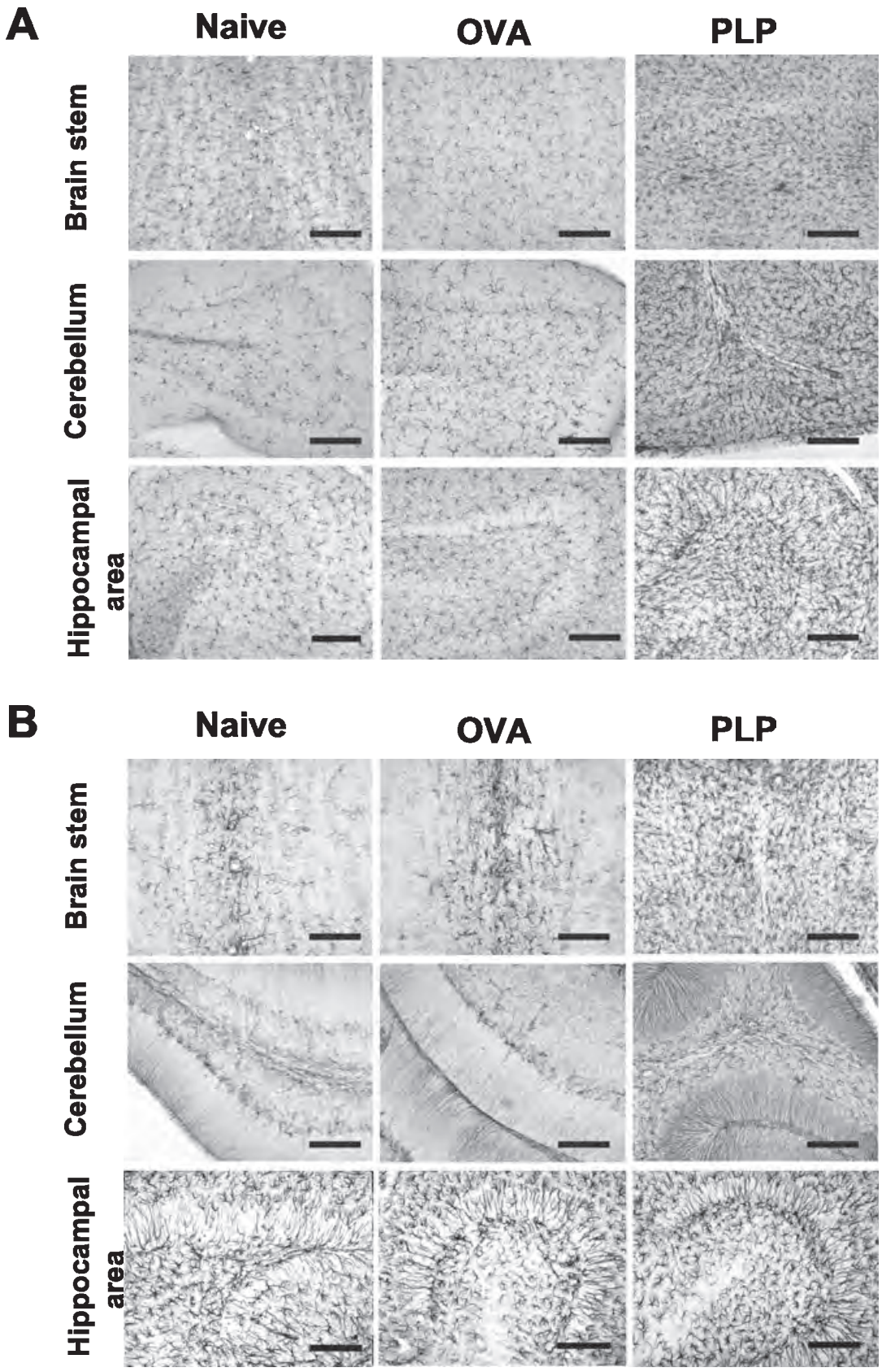

FIG. 6. Cellular composition in brain sections of mice transferred with proteolipid protein (PLP)- and ovalbumin (OVA)-specific T-cells or naïve control animals. Cryosections of brainstem, cerebellum and hippocampal area were stained with antibodies against IBA-1 (A) and GFAP (B) at Day 10 after adoptive transfer. Enhanced microglial cell density (A) and astrogliosis (B) were detected exclusively in brain regions of mice transferred with CNS-specific T-cells (right panels), but not in mice that received non-CNS-specific T-cells (middle panels) or control animals (left panels). Scale bar: 50 μm.

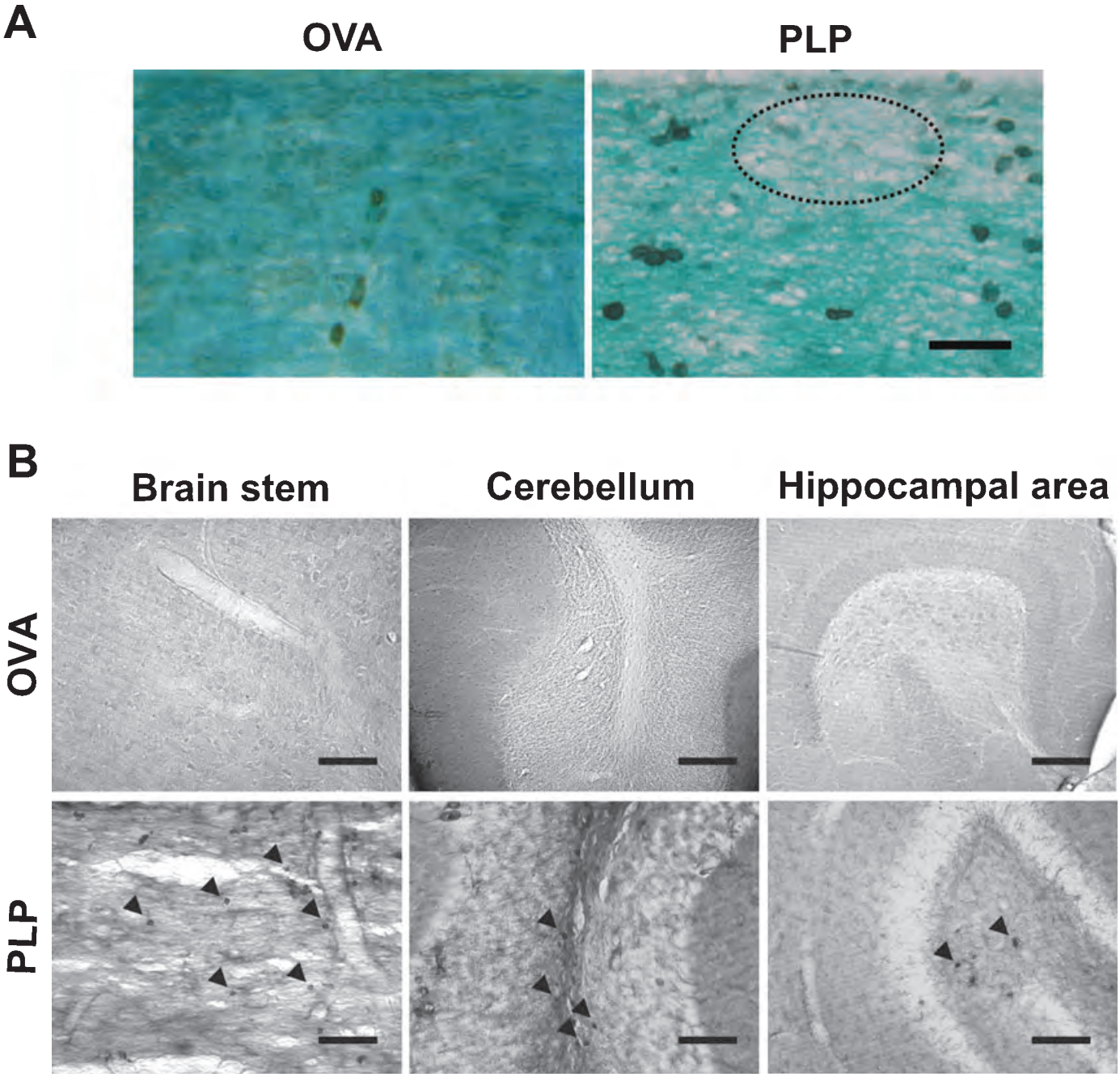

FIG. 7. Assessment of demyelination and activation of antigen-presenting cells in the CNS of mice transferred with proteolipid protein (PLP)- and ovalbumin (OVA)-specific T-cells. (A) Luxol Fast Blue and CD3 staining (dark cells) of longitudinal spinal cord sections of mice transferred with PLP- and OVA-specific T-cells. Areas of white matter demyelination (ringed area) were only observed in the vicinity of encephalitogenic T-cells (right), and not in the CNS of mice transferred with OVA-specific cells (left). Scale bar: 25 μm. (B) Distribution of MHC class II-positive cells (arrows). Activated class II-positive cells were only detected in the brain regions of mice injected with PLP-specific cells (lower panels). No MHC class II expression was detected in mice transferred with OVA-specific T-cells (upper panels). Scale bar: 50 μm with the exception of brainstem section of a PLP-transferred mouse, in which the scale bar is 100 μm.

Interestingly, we discovered T-cells in areas of the brain in which leakage neither of rhodamine-dextran nor of Gd was detectable, indicating that BBB disruption is the consequence of rather than the prerequisite for T-cell penetration, a conception that is in agreement with a previous study on BBB alterations based on electron microscopy (Claudio *et al*., 1990), and with other reports on cellular infiltration based on histological (Koh *et al*., 1993; Muller *et al*., 2005) or MRI investigations (Rausch *et al*., 2003; Floris *et al*., 2004). Furthermore, our stereological cell quantification revealed the same number of encephalitogenic and CNS-irrelevant T-cells during the initial phase of invasion – 1 week post-injection. Thus, cell activation, not antigen-specificity, determines the ability of T-cells to migrate into the CNS.

On the other hand, antigen-specificity and not the absolute number of infiltrating cells seems to determine the magnitude and distribution of BBB disruption. In the OVA model, we observed similar levels of rhodamine-dextran extravasation in susceptible brain regions compared with EAE. In contrast, in mice transferred with CNS-specific T-cells, broad BBB disruption could be detected in the brainstem, moderate leakage in the cerebellum, and no alterations of

BBB in the cortical areas. The pattern of BBB alterations corresponded to the presence of myelin proteins in these regions. We hypothesize that the myelin-antigen concentration determines the local antigen presentation and, consequently, the extent and the type of effector function of reactivated T-cells (Abbas *et al*., 1996).

Importantly, only encephalitogenic T-cells but not non-CNS-specific T-cells promoted perturbations in cellular architecture, as revealed by enhanced microglial cell density, astrogliosis and demyelination, detected in all EAE brain regions analysed. Thus, although activated T-cells have the potential to alter microglia phenotype and function in an antigen-independent way (review in Carson, 2002), *in vivo* microglia proliferation was triggered exclusively by CNS-specific T-cells and was probably antigen dependent. It is also conceivable that only encephalitogenic T-cells are activated by perivascular dendritic cells (Becher *et al*., 2006) and may then interact with microglial cells in an antigen-independent manner. In fact, only brain regions of EAE-mice showed MHC class II-positive cells, indicative of activation upon antigen presentation. Microglial proliferation and activation as well as the presence of reactive astrocytes have been widely described in EAE (Goldmuntz *et al*., 1986; Smith & Eng, 1987; Matsumoto *et al*., 1992). In our study, increased density of microglial cells was observed equally in brainstem, cerebellum and hippocampal area. In contrast, astrocytic reactivity corresponded with distribution of lesions and BBB alteration, and was much more marked in the brainstem and the cerebellum compared with the hippocampi.

Taken together, our results demonstrate that, in the 'healthy' brain, antigen recognition and interaction of activated T-cells with glial cells are prerequisites for initiating an inflammatory cascade leading to gliosis and demyelination. Previously, we reported an increased flow in vessels followed by BBB disruption in patients with MS (Wuerfel *et al*., 2004). Here, we found that activated CNS-irrelevant T-cells recognizing non-mammalian antigen, too, have the capacity not only to enter the CNS but also to promote alterations in the permeability of cerebral blood vessels without promoting any glial pathology. However, in a compromised BBB, such as in MS (Kwon & Prineas, 1994; Minagar & Alexander, 2003), bystander perturbations of the barrier caused by non-specific effector cells may have further pathological consequences. Enhanced BBB leakage may promote not only distended oedema and consequent local hypoxic damage, but also decreased mitochondrial content of brain endothelial cells (Claudio *et al*., 1989) and related alterations of brain homeostasis. This, in concert with leakage of pro-inflammatory mediators, may induce disease exacerbation, e.g. in patients with MS suffering from a common infection.

Acknowledgements

We thank Alistair Noon and Andrew Mason for reading the manuscript as native English speakers. This work was supported by the Institute for Multiple Sclerosis Research (IMSF) Goettingen/Gemeinnuetzige Hertie Foundation (to F.Z.), a grant from the Charité (Rahel-Hirsch Stipend to C.I.-D.), the German Research Council (SFB 507, to F.Z. and R.N.), and the German Ministry of Science (BMBF, to F.Z. and R.N.).

Abbreviations

BBB, blood brain barrier; CFDA, carboxyfluorescein diacetate succinimidyl ester; DAB, 3,3′-diaminobenzidine tetrahydrochloride; EAE, experimental autoimmune encephalomyelitis; Gd, Gadopentate dimeglumine; GFAP, glial fibrillary acidic protein; GFP, green fluorescent protein; MPM, multiphoton microscopy; MRI, magnetic resonance imaging; MS, multiple sclerosis; OVA, ovalbumin; PBS, phosphate-buffered saline; PFA, paraformaldehyde; PLP, proteolipid protein.

References

Abbas, A.K., Murphy, K.M. & Sher, A. (1996) Functional diversity of helper T lymphocytes. *Nature*, **383**, 787–793.

Aktas, O., Smorodchenko, A., Brocke, S., Infante-Duarte, C., Topphoff, U.S., Vogt, J., Prozorovski, T., Meier, S., Osmanova, V., Pohl, E., Bechmann, I., Nitsch, R. & Zipp, F. (2005) Neuronal damage in autoimmune neuroinflammation mediated by the death ligand TRAIL. *Neuron*, **46**, 421–432.

Archambault, A.S., Sim, J., Gimenez, M.A. & Russell, J.H. (2005) Defining antigen-dependent stages of T cell migration from the blood to the central nervous system parenchyma. *Eur. J. Immunol.*, **35**, 1076–1085.

Becher, B., Bechmann, I. & Greter, M. (2006) Antigen presentation in autoimmunity and CNS inflammation: how T lymphocytes recognize the brain. *J. Mol. Med.*, **84**, 532–543.

Bechmann, I., Galea, I. & Perry, V.H. (2007) What is the blood–brain barrier (not)? *Trends Immunol.*, **28**, 5–11.

Brabb, T., von Dassow, P., Ordonez, N., Schnabel, B., Duke, B. & Goverman, J. (2000) In situ tolerance within the central nervous system as a mechanism for preventing autoimmunity. *J. Exp. Med.*, **192**, 871–880.

Carson, M.J. (2002) Microglia as liaisons between the immune and central nervous systems: functional implications for multiple sclerosis. *Glia*, **40**, 218–231.

Claudio, L., Kress, Y., Factor, J. & Brosnan, C.F. (1990) Mechanisms of edema formation in experimental autoimmune encephalomyelitis. The contribution of inflammatory cells. *Am. J. Pathol.*, **137**, 1033–1045.

Claudio, L., Kress, Y., Norton, W.T. & Brosnan, C.F. (1989) Increased vesicular transport and decreased mitochondrial content in blood–brain barrier endothelial cells during experimental autoimmune encephalomyelitis. *Am. J. Pathol.*, **135**, 1157–1168.

Engelhardt, B. (2006) Molecular mechanisms involved in T cell migration across the blood–brain barrier. *J. Neural Transm.*, **113**, 477–485.

Floris, S., Blezer, E.L., Schreibelt, G., Dopp, E., van der Pol, S.M., Schadee-Eestermans, I.L., Nicolay, K., Dijkstra, C.D. & de Vries, H.E. (2004) Blood–brain barrier permeability and monocyte infiltration in experimental allergic encephalomyelitis: a quantitative MRI study. *Brain*, **127**, 616–627.

Gimsa, U., Wolf, S.A., Haas, D., Bechmann, I. & Nitsch, R. (2001) Th2 cells support intrinsic anti-inflammatory properties of the brain. *J. Neuroimmunol.*, **119**, 73–80.

Goldmuntz, E.A., Brosnan, C.F., Chiu, F.C. & Norton, W.T. (1986) Astrocytic reactivity and intermediate filament metabolism in experimental autoimmune encephalomyelitis: the effect of suppression with prazosin. *Brain Res.*, **397**, 16–26.

Hickey, W.F. (2001) Basic principles of immunological surveillance of the normal central nervous system. *Glia*, **36**, 118–124.

Hickey, W.F., Hsu, B.L. & Kimura, H. (1991) T-lymphocyte entry into the central nervous system. *J. Neurosci. Res.*, **28**, 254–260.

Hu, P., Pollard, J.D. & Chan-Ling, T. (2000) Breakdown of the blood–retinal barrier induced by activated T cells of nonneural specificity. *Am. J. Pathol.*, **156**, 1139–1149.

Kawakami, N., Nagerl, U.V., Odoardi, F., Bonhoeffer, T., Wekerle, H. & Flugel, A. (2005) Live imaging of effector cell trafficking and autoantigen recognition within the unfolding autoimmune encephalomyelitis lesion. *J. Exp. Med.*, **201**, 1805–1814.

Kermode, A.G., Thompson, A.J., Tofts, P., MacManus, D.G., Kendall, B.E., Kingsley, D.P., Moseley, I.F., Rudge, P. & McDonald, W.I. (1990) Breakdown of the blood–brain barrier precedes symptoms and other MRI signs of new lesions in multiple sclerosis. Pathogenetic and clinical implications. *Brain*, **113**, 1477–1489.

Kluver, H. & Barrera, E. (1953) A method for the combined staining of cells and fibers in the nervous system. *J. Neuropathol. Exp. Neurol.*, **12**, 400–403.

Koh, C.S., Gausas, J. & Paterson, P.Y. (1993) Neurovascular permeability and fibrin deposition in the central neuraxis of Lewis rats with cell-transferred experimental allergic encephalomyelitis in relationship to clinical and histopathological features of the disease. *J. Neuroimmunol.*, **47**, 141–145.

Kwon, E.E. & Prineas, J.W. (1994) Blood–brain barrier abnormalities in longstanding multiple sclerosis lesions. An immunohistochemical study. *J. Neuropathol. Exp. Neurol.*, **53**, 625–636.

Matsumoto, Y., Ohmori, K. & Fujiwara, M. (1992) Microglial and astroglial reactions to inflammatory lesions of experimental autoimmune encephalomyelitis in the rat central nervous system. *J. Neuroimmunol.*, **37**, 23–33.

Minagar, A. & Alexander, J.S. (2003) Blood–brain barrier disruption in multiple sclerosis. *Mult. Scler.*, **9**, 540–549.

Muller, D.M., Pender, M.P. & Greer, J.M. (2005) Blood–brain barrier disruption and lesion localisation in experimental autoimmune encephalomyelitis with predominant cerebellar and brainstem involvement. *J. Neuroimmunol.*, **160**, 162–169.

Nicolopoulos-Stournaras, S. & Iles, J.F. (1983) Motor neuron columns in the lumbar spinal cord of the rat. *J. Comp. Neurol.*, **217**, 75–85.

Nitsch, R., Pohl, E.E., Smorodchenko, A., Infante-Duarte, C., Aktas, O. & Zipp, F. (2004) Direct impact of T cells on neurons revealed by two-photon microscopy in living brain tissue. *J. Neurosci.*, **24**, 2458–2464.

Okabe, M., Ikawa, M., Kominami, K., Nakanishi, T. & Nishimune, Y. (1997) 'Green mice' as a source of ubiquitous green cells. *FEBS Lett.*, **407**, 313–319.

Rausch, M., Hiestand, P., Baumann, D., Cannet, C. & Rudin, M. (2003) MRI-based monitoring of inflammation and tissue damage in acute and chronic relapsing EAE. *Magn. Reson. Med.*, **50**, 309–314.

Sedgwick, J.D., Hughes, C.C., Male, D.K., MacPhee, I.A. & ter Meulen, V. (1990) Antigen-specific damage to brain vascular endothelial cells mediated by encephalitogenic and nonencephalitogenic CD4+ T cell lines in vitro. *J. Immunol.*, **145**, 2474–2481.

Silwedel, C. & Forster, C. (2006) Differential susceptibility of cerebral and cerebellar murine brain microvascular endothelial cells to loss of barrier properties in response to inflammatory stimuli. *J. Neuroimmunol.*, **179**, 37–45.

Smith, M.E. & Eng, L.F. (1987) Glial fibrillary acidic protein in chronic relapsing experimental allergic encephalomyelitis in SJL/J mice. *J. Neurosci. Res.*, **18**, 203–208.

Tonra, J.R., Reiseter, B.S., Kolbeck, R., Nagashima, K., Robertson, R., Keyt, B. & Lindsay, R.M. (2001) Comparison of the timing of acute blood–brain barrier breakdown to rabbit immunoglobulin G in the cerebellum and spinal cord of mice with experimental autoimmune encephalomyelitis. *J. Comp. Neurol.*, **430**, 131–144.

Ueno, M., Akiguchi, I., Hosokawa, M., Kotani, H., Kanenishi, K. & Sakamoto, H. (2000) Blood–brain barrier permeability in the periventricular areas of the normal mouse brain. *Acta Neuropathol. (Berl.)*, **99**, 385–392.

Wekerle, H., Linington, C., Lassmann, H. & Meyermann, R. (1986) Cellular immune reactivity within the CNS. *Trends Neurosci.*, **9**, 271–277.

Westland, K.W., Pollard, J.D., Sander, S., Bonner, J.G., Linington, C. & McLeod, J.G. (1999) Activated non-neural specific T cells open the blood–brain barrier to circulating antibodies. *Brain*, **122**, 1283–1291.

Wuerfel, J., Bellmann-Strobl, J., Brunecker, P., Aktas, O., McFarland, H., Villringer, A. & Zipp, F. (2004) Changes in cerebral perfusion precede plaque formation in multiple sclerosis: a longitudinal perfusion MRI study. *Brain*, **127**, 111–119.

Wuerfel, J., Tysiak, E., Prozorovski, T., Smyth, M., Mueller, S., Schnorr, J., Taupitz, M. & Zipp, F. (2007) Mouse model mimics multiple sclerosis in the clinico-radiological paradox. *Eur. J. Neurosci.*, **26**, 190–198.

Mein Lebenslauf wird aus datenschutzrechtlichen Gründen in der elektronischen Version meiner Arbeit nicht veröffentlicht.

Publikationsliste

Abgeschlossene Publikationen:

E. Tysiak, J. Wuerfel, T. Prozorowski, M. Smyth, S. Mueller, J. Schnorr, M. Taupitz, F. Zipp. Mouse model mimics multiple sclerosis in the clinico-radiological paradox.
EUROPEAN JOURNAL OF NEUROSCIENCE 2007, Jul; 26(1):190-198.

J. Wuerfel, A. Smorodchenko, E. Pohl, J. Vogt, **E. Tysiak**, R. Glumm, S. Hendrix, R. Nitsch, F. Zipp, C. Infante-Duarte. CNS-irrelevant T cells enter the brain, cause blood-brain barrier disruption but no glial pathology.
EUROPEAN JOURNAL OF NEUROSCIENCE 2007, Sept; 26(6):1387-98.

J. Wuerfel, M. Haertle, H. Waiczies, **E. Tysiak**, I. Bechmann, K.D. Wernicke, F. Zipp, F. Paul. Perivascular spaces – MRI marker of inflammatory activity in the brain?
BRAIN 2008, Sep;131(Pt 9):2332-40.

A. Mundt, C. Winter, S. Mueller, J. Wuerfel, **E. Tysiak**, J. Schnorr, M. Taupitz, A. Heinz, G. Juckel. Targeting activated microglia in Alzheimer´s pathology by intraventricular delivery of a phagocytosable MRI contrast agent in APP23 transgenic mice.
NEUROIMAGE 2009, Jun;46(2):367-72.

E. Tysiak, P. Asbach, O. Aktas, H. Waiczies, M. Smyth, J. Schnorr, M. Taupitz, J. Wuerfel. Beyond blood brain barrier breakdown – in vivo detection of occult neuroinflammatory foci by magnetic nanoparticles.
JOURNAL OF NEUROINFLAMMATION 2009, Aug 6;6:20.

Publikationen in Vorbereitung:

E. Tysiak, J. Wuerfel, R. Glumm, F. Zipp, C. Infante-Duarte. In vivo MRI evidence for circumventricular organ involvement in CNS inflammation.

E. Tysiak, M. Smyth, E. Schellenberger, T. Prozorowski, O. Aktas, U. Schulze-Topphoff, J. Schnorr, S. Wagner, M. Taupitz, F. Zipp, and J. Wuerfel. Electrostatically Stabilized Magnetic Nanoparticles - a New Strategy for T cell Labeling.

E. Tysiak, J. Gärtner, E. Wilichowski. Recurrent Steven Johnson Syndrome in a boy with Chlamydia pneumoniae infection.

Posterpräsentationen

E. Tysiak, S. Zurborg, P. Ritter, M. Moosmann, T. Wüstenberg, A. Villringer. Automatic Classification of Vigilance Stages in Wakeful Subjects - A First Step towards Finding fMRI - Correlates of Vigilance.
BNF 2004, Luckenwalde, Deutschland

J. Wuerfel, P. Asbach, **E. Tysiak**, M. Taupitz, O. Aktas, F. Zipp. Diffuse Blut-Hirn-Schrankenstörung in MRT-Verlaufsuntersuchungen eines Mausmodells der Multiplen Sklerose (aktive experimentelle autoimmune Enzephaomyelitis, EAE) – mögliche Abweichung von Eintrittspforte und Entzündungsherd.
DGN 2005, Wiesbaden, Deutschland

E. Tysiak, J. Wuerfel, O. Aktas, T. Prozorowski, A. Smorodchenko, S. Mueller, J. Schnorr, M. Taupitz, F. Zipp. In vivo MRImaging of trigeminal nerve root inflammation in a mouse model of multiple sclerosis.
BNF 2006, Luckenwalde, Deutschland

J. Wuerfel, A. Smorodchenko, E. Pohl, J. Vogt, **E. Tysiak**, R. Glumm, S. Hendrix, F. Zipp, C. Infante-Duarte. CNS-irrelevant T cells enter the brain, cause blood-brain barrier disruption but no glial pathology.
DGfI 2007, Heidelberg, Deutschland

E. Tysiak, J. Wuerfel. Gadofluorine M enhanced MRI: Circumventricular organs show neuroinflammatory activity in vivo.
ISMRM 2009, Honolulu, Hawaii, USA

Selbstständigkeitserklärung

Erklärung

„Ich, Eva-Kristin Würfel, geb. Tysiak, erkläre, dass ich die vorgelegte Dissertation mit dem Thema „Magnetresonanztomographische Darstellung neuroinflammatorischer Prozesse in einem Mausmodell der Multiplen Sklerose“ selbst verfasst und keine anderen als die angegebenen Quellen und Hilfsmittel benutzt, ohne die (unzulässige) Hilfe Dritter verfasst und auch in Teilen keine Kopien anderer Arbeiten dargestellt habe.“

01.03.2010

Danksagung

Ich möchte mich bei Prof. Dr. Karl Max Einhäupl, Prof. Dr. Ulrich Dirnagl und Prof. Dr. Helmut Maxeiner bedanken für ihren begleitenden Rat und die außerordentliche Unterstützung meines Promotionsvorhabens.

Ich danke Prof. Dr. Orhan Aktas und Dr. Jens Würfel für die hervorragende Anleitung und Betreuung während der experimentellen Arbeit. Weiter danke ich Dr. Timour Prozorovski, Dr. Ulf Schulze-Topphoff, Dr. Carmen Infante-Duarte und Alina Smorodchenko für die Hilfestellung bei der Erlernung spezieller zell- und immunbiologischer Techniken. Ich danke Nancy Nowakowski und Susan Pikol für die fachkundige Anleitung und Unterstützung in der praktischen Ausführung der Experimente.